ABSTRACT

Title of Document:	BRIDGING THE BIOLOGY-ELECTRONICS COMMUNICATION GAP WITH REDOX SIGNALING
	Tanya Gordonov, Doctor of Philosophy, 2015
Directed By:	Professor William E. Bentley, Fischell Department of Bioengineering

Electronic and biological systems both have the ability to sense, respond to, and communicate relevant data. This dissertation aims to facilitate communication between the two and create bio-hybrid devices that can process the breadths of both electronic and biological information. We describe the development of novel methods that bridge this bi-directional communication gap through the use of electronically and biologically relevant redox molecules for controlled and quantitative information transfer. Additionally, we demonstrate that the incorporation of biological components onto microelectronic systems can open doors for improved capabilities in a variety of fields.

First, we describe the original use of redox molecules to electronically control the activity of an enzyme on a chip. Using biofabrication techniques, we assembled HLPT, a fusion protein which generates the quorum sensing molecule autoinducer-2,

on an electrodeposited chitosan film on top of an electrode. This allows the electrode to controllably oxidize the enzyme *in situ* through a redox mediator, acetosyringone. We successfully showed that activity decrease and bacterial quorum sensing response are proportional to the input charge.

To engineer bio-electronic communication with cells, we first aimed for better characterizing an electronic method for measuring cell response. We engineered *Escherichia coli* (*E.coli*) cells to respond to autoinducer-2 by producing the β-galactosidase enzyme. We then investigated an existing electrochemical method for detecting β-galactosidase activity by measuring a redox-active product of the cleavage of the added substrate molecule PAPG. In our novel findings, the product, PAP, was found to be produced at a rate that correlated with the standard spectrophotometric method for measuring β-galactosidase, the Miller assay, in both whole live and lysed cells. Conversely, to translate electronic signals to something cells can understand, we used pyocyanin, a redox drug which oxidizes the *E.coli* SoxR protein and allows transcription from the *soxS* promoter. We utilized electronic control of ferricyanide, an electron acceptor, to amplify the production of a reporter from *soxS*. With this novel method, we show that production of reporter depends on the frequency and amplitude of electronic signals, and investigate the method's metabolic effects. Overall, the work in this dissertation makes strides towards the greater goal of creating multi-functional bio-hybrid devices.

BRIDGING THE BIOLOGY-ELECTRONICS COMMUNICATION GAP WITH REDOX SIGNALING

By

Tanya Gordonov

Dissertation submitted to the Faculty of the Graduate School of the
University of Maryland, College Park, in partial fulfillment
of the requirements for the degree of
Doctor of Philosophy
2015

Advisory Committee:
Professor William E. Bentley, Chair
Professor Gregory F. Payne
Associate Professor Ian White
Professor Reza Ghodssi
Assistant Professor Rohan Fernandes

Dedication

I dedicate this work to my late father, Boris Gordonov, who first sparked my love of science and taught me the value of education and pursuing my goals.

Acknowledgements

I would like to acknowledge the members of my doctoral committee for their time, advice, and support throughout my years of doing research. I would especially like to thank my advisor, Dr. William Bentley, for providing me with the necessary guidance and environment for turning into a successful independent researcher. I would also like to acknowledge my labmates, all of whom were instrumental in my day-to-day functioning in the lab, and without whose wise words and example I would not be anywhere near where I am today. I would like to thank my family for always supporting my pursuit of a higher education degree, especially my parents for instilling in me the importance of education and love for science from an early age. I'd like to thank my friends, who, despite not always understanding the scientific details behind my work, encouraged me by saying that my lay-man descriptions sounded "cool". Lastly, I'd like to thank my husband Paul, for being not only as supportive as a husband can be, but also for being helpful and understanding as only another graduate student going through similar processes can be.

Table of Contents

Chapter 1: Motivation and Introduction

This chapter provides a brief introduction to the fields and concepts that span the whole dissertation, and the motivation and research context for the work. Chapters 2-4 can each stand alone and provides their own abstracts, relevant background, methodology sections, results and discussion, and conclusions. Overall summary, contributions, and future work are detailed in Chapter 5.

Motivation

Efficient, programmable, and meaningful communication and information transfer between biology and electronics is a highly sought-after functionality with many applications in clinical and research settings. These applications range from biosensors for detection of biomolecules in blood samples, implantable devices, devices for study of cellular signaling cascades and function, to autonomous cell-on-chip devices with remote sensing and control. If we are to make the best predictions and analyses of diseases as well as study and manipulate the biological environment, it is necessary to explore and improve upon both aspects of this bi-directional bio-electronic communication path.

While there are a variety of examples and goals of the biology-to-electronics communication route, one of the overarching objectives is to be able to gather as much biological information as possible and to best interpret it using electronics. Biology is expert at detecting biomolecules (be it through enzymes or cells) that are undetectable otherwise, and translation of this information to electronic form allows for fast measurement, interpretation, representation, and manipulation of data, along

with easy storage. Better translation of biological to electronic information would allow for more efficient and relevant diagnoses and studies, as would better understanding and interpretation of the phenomena. The additional possibility of real-time *in situ* measurements that electronic sensing presents greatly increases the technology's benefits and desirability.

Conversely, granting cells the ability to readily interpret signals originating from electronics into pre-programmed functions would allow us to manipulate and study cellular behavior with an unprecedented degree of precision. For this, we would need direct control of cell behavior that can elicit a desired amplitude of response at a desired time and at a pre-programmed location. On top of their programmability, electronic devices can sense electric, magnetic, thermal, and acoustic changes with speed and precision that biological entities cannot. Translating this information to cells would allow for a much wider range of studies and behaviors. In addition to cells, wiring functional proteins to respond to electronic signals in meaningful ways would further biochemical studies where precise control cannot otherwise be easily achieved.

Thus, it can be seen why a bridging of the communication gap between biology and electronics would benefit advancement in a variety of applications and fields. This gap derives from the fact that biological entities communicate with proteins, small molecules, and ions, whereas electronics does so with electrons. Redox molecules seem to fit the bill as a candidate for intermediate translators because they are electron carriers that can interact with an electrode and can also be biologically relevant[1]. In this dissertation, we show that our ability to manipulate

redox molecules' interactions with both cells and electronics and our knowledge of what governs those interactions allows us to use them for electrically-driven enzyme-activity attenuation, electrochemical cell-based gene reporter analysis, and as live-cell gene activators.

Research goals

The overarching aim of this work is to facilitate meaningful information transfer and communication between biology (cells and proteins) and electronics (electrodes). In order to accomplish this, we aimed to work on three different developments:

1. A method to use electronic signals to attenuate enzyme activity, described in Chapter 2
2. An analysis to enhance use of a method for electronic measurement of reporter protein expression from live cells, described in Chapter 3
3. A method to allow electronic signals to modulate gene expression, described in Chapter 4

All the above aims use various redox molecules to translate either the electronic signals to biological or vice versa.

Research background

Redox molecules and electrochemistry

In this work, it is our ambition to utilize redox molecules as the intermediaries between biology and electronics, as they can interact in meaningful ways with cells and proteins as well as with electrodes. Redox stands for reduction and oxidation –

which are processes of gain or loss of electrons, respectively - as shown in Figure 1.1 a. This loss or gain of electrons depends on the standard potential of the molecules interacting and on the states of the molecules. The standard electric potential (E_0) of a molecule is a number that can be used to determine whether it will draw electrons from or donate electrons to another molecule with a known E_0. When two molecules interact, typically the one with a more positive E_0 will draw electrons from a molecule with a more negative one – as demonstrated in Figure 1.1 b. For this to work, the molecules have to also be in the correct form (i.e. have the electrons to donate in the first place or have "space" to accept electrons) – in the reduced form to donate electrons, and in the oxidized form to accept them. The molecules also have to interact with each other closely enough in space for the transfer to take place.

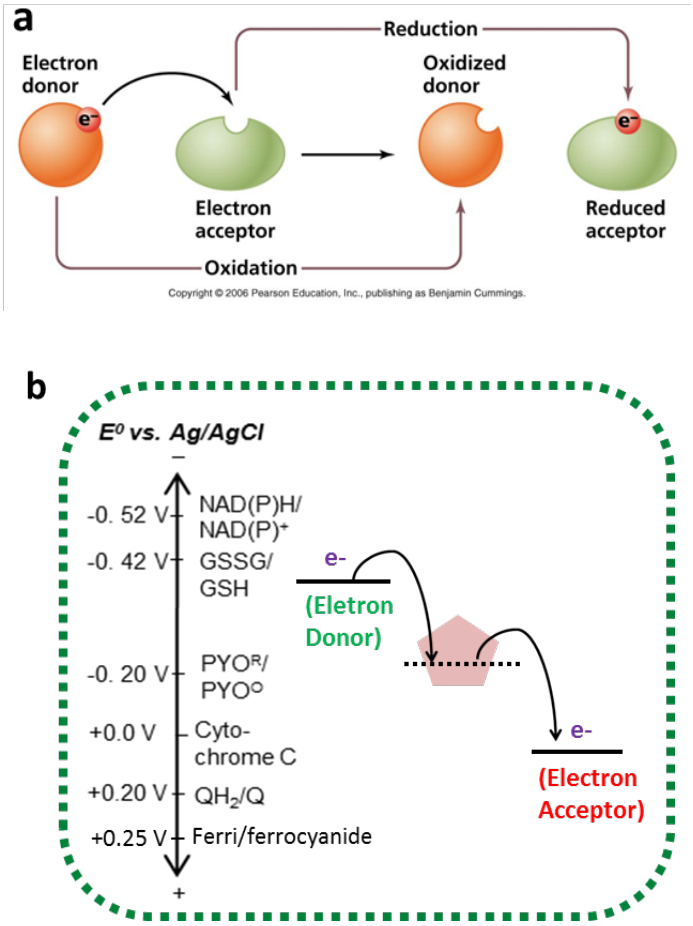

Figure 1.1: Redox principles. a, The participants and interactions in a typical redox reaction (image taken from http://academic.pgcc.edu/~kroberts/Lecture/Chapter%205/redox.html). **b,** A potential profile based on E_0 vs. an Ag/AgCl electrode of several biologically-relevant molecules. In an interaction, electron donors possess a more negative E_0 and acceptors a more positive.

An electrode can be biased at a potential such that it interacts with the redox molecule in a similar manner – donating or drawing electrons. The amount of electrons that are exchanged at the electrode is measured as the current at the device (an electrochemical analyzer), which is connected to a computer. This current is

measured at a working electrode, is balanced for the solution as a whole at the counter electrode, and is compared to the current at the reference electrode where the electrochemical reactions are well-characterized - example of a setup can be seen in Figure 1.2 a [2]. In this way, a three electrode system can be used to not only precisely measure the amount of a redox molecule, but can give information as to the relative amounts of the forms (oxidized or reduced) and, importantly, can be used to change a molecule's form by applying the relevant potential.

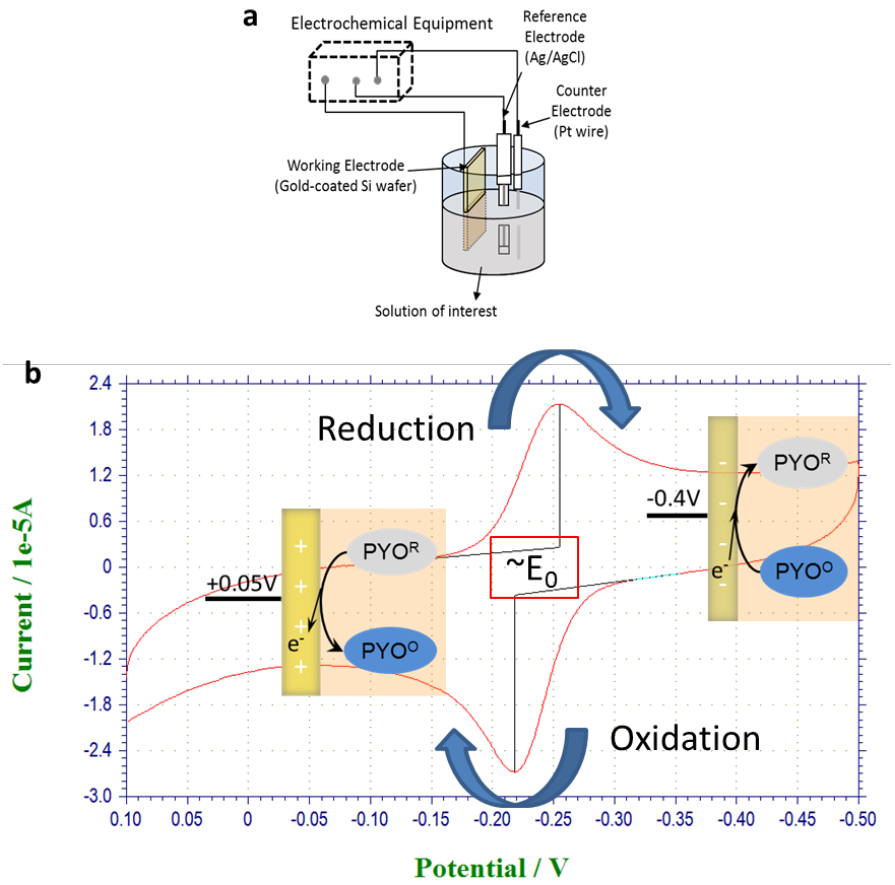

Figure 1.2: Electrochemical setup and CV analysis. a, Schematic of the general electrochemical setup that is used in the experiments in this work, with the solution of interest containing mediator and/or cells. **b,** A cyclic voltammogram of 40µM pyocyanin, with an apparent E_0 around -0.22V. The upper peak indicates the reduction and the lower peak the

oxidation. At an electrode biased at -0.4V, the pyocyanin will be reduced and the current will measure the amount of oxidized pyocyanin (which will tend to the negative as oxidized pyocyanin is depleted). At an electrode biased at +0.05V the pyocyanin will be oxidized and the current will measure the amount of reduced pyocyanin (which will tend to the positive as reduced pyocyanin is depleted).

Electrochemistry techniques that are relevant to this dissertation include cyclic voltammetry, chronoamperometry, and bulk electrolysis. Cyclic voltammetry (CV) involves the cycling of the voltage at the working electrode between two limits at a specified speed and measuring the resulting current. CV is useful for investigating the solution of interest for redox-active components, where peaks or increases in current can be measured and compared to controls. CV's allow for the finding of the E_0 as well as the reduction and oxidation currents of redox molecules in the given system. Additionally, the calculated current or charge can allow one to measure the concentration of the redox analyte. In this dissertation, we used CV's to both determine the oxidation and reduction currents for bulk electrolysis and to construct a charge vs. analyte concentration graph for further measurement. Determining charge, which is current over time, from a CV and correlating that to analyte concentrations allows more robust measurements when the solution conditions may change slightly and result in a change in the potential of the peak current.

Chronoamperometry (CA) involves the selection of one or more potentials, and their application to the solution for set amounts of time. The readout of a CA is again the current. CA's applied for short amounts of time can be used to measure the concentration of an analyte which is either oxidized or reduced at the set potential.

CAs applied for longer periods of time, such as in bulk electrolysis, can be used to change the redox state of a molecule in solution. For bulk electrolysis, the counter and working electrodes must be separated by a salt bridge (this allows only charge to pass through between the two compartments). Additionally, stirring and a large electrode surface area speed up the process. In this dissertation, we use bulk electrolysis to change back and forth the redox state of redox molecules.

As an example, the redox molecule pyocyanin has an E_0 around -0.34 vs. an Ag/AgCl electrode, with the exact value depending on the conditions of the system[3]. In order to determine the E_0 for a setup, CV can be used. If the E_0 of a redox molecule of interest lies within that potential range, one will see reduction and/or oxidation peaks as the molecule changes forms (this of course depends on the reversibility of the reactions). For pyocyanin we can see in Figure 1.2 b that the E_0 of a 40μM solution was around -0.22V in the given conditions. When the potential was more negative than this number, reduction of pyocyanin takes place (upper right inset), and when the potential was more positive oxidation takes place (lower left inset).

Electrochemical effects on cells

An important concern when designing a system where electricity is going to be used in the vicinity of cells is the negative effect that this current may have on the cells or proteins. To our knowledge, the potential range in which we worked has not been shown to cause significant cellular damage, by itself or through the generation of byproducts, ions, or reactive oxygen species in significant quantities – especially for the time scales that we intend on using (minutes-hours). Our CV measurements

were run in the 0.6 to -0.5V range. In either LB, defined minimal media, or phosphate buffer of pH ~7, we have not observed the formation of significant amounts of the above-mentioned species.

Hydrogen peroxide formation ($O_2 + 2H^+ + 2e^- \leftrightarrow H_2O_2$) occurs in the presence of oxygen around -0.2V. This could have potentially affected our system when we performed bulk electrolysis at -0.3V, but because we were working in an anaerobic system there was minimal oxygen for the hydrogen peroxide to form from. Around +0.6V the reverse reaction occurs ($H_2O_2 \leftrightarrow O_2 + 2H^+ + 2e^-$), but we did not stay at the +0.6V potential for more than a few seconds when performing cyclic voltammetry and therefore saw no problems[2,4]. It is certainly hard to say what exactly happens in the system because, for example, the precise content of LB media is unknown and there could be possible unforeseen cellular byproducts- but thorough testing gave us an idea of what phenomena were taking place. More relevant in-depth information on redox molecules in biological context is presented in the Introductions of the following chapters.

Biochips and bio-hybrid devices

Part of the larger aim of this work is to build novel bio-hybrid devices and to advance their overall functionality. This is also the aim of the Maryland Biochip Collaborative, whose insights and work inspired much of what we accomplished here. Bio-hybrid devices, as described here, are a class of devices that contain living and non-living components and usually involve an intimate interaction between the two that allows for or increases their functionality. The goal is to harness the advantages

of each to accomplish or enhance either a bio-measurement or bio-actuation goal. For example, bio-hybrid devices involving proteins immobilized on surfaces can allow for less bio-component use, faster process, and more precise measurements whereas immobilized cells allow for more fine-tuned environmental control and easier cell tracking[5-9].

Synthetic biology

Synthetic biology is a discipline that aims to modulate cells by engineering novel functionality through the rewiring of existing or the engineering of novel genetic circuits. It focuses on rational design of constructs from standardized parts (which would ideally work similarly in a variety of cellular environments) and provides a different perspective than traditional genetic engineering. Substantial progress has been achieved in many areas of research, including biomaterials, chemicals, energy production, bio-computation, and biosensors[10-17]. Additionally, studies have demonstrated the potential use of synthetic biology in biomedical applications such as drug development, tissue engineering, and cancer therapeutics[18-23]. Synthetic biology constructs have even been proposed for recycling and generation of valuable materials for space travel[24].

This work focuses on utilizing the tools of synthetic biology and on improving the capabilities of engineered constructs by allowing easier genetic response measurement and easing the load of engineered factors in the cells. Specifically – in Chapter 3 we show that the reporter protein β-galactosidase can be quantitatively measured in live cells by electrochemical means in a manner comparable to the standard Miller Assay. The enzyme is a commonly-used reporter in the synthetic biology community and its electrochemical measurement from live cells is an advancement that

goes well with the trend towards real-time miniaturized measurements in the community. In Chapter 4, we introduce a novel method for using electrochemical signals to turn on specific gene expression in a programmable manner. This also is an advancement that allows for the tuning production of a desired gene without the need for extra “clock” or “oscillator” genetic elements so often found in systems engineered for these purposes. We thus lessen the genetic burden of the control elements inside the engineered cells without sacrificing response capabilities. This development also works well with the trend towards miniaturization and may greatly enhance capabilities of engineered cell-based biohybrid devices.

Chapter 2: Electronic modulation of biochemical signal generation

The majority of this section is adapted from the following publication: Gordonov, T et al. “Electronic modulation of biochemical signal generation”. Nat Nanotechnol. 2014 Aug;9(8):605-10 with permission[25].

Chapter abstract

The goal of this work is to use electrical signals to assemble and “tune” an enzymatic pathway on a gold electrode chip, thereby creating a “programmable” biohybrid device containing both biological and electronic components. Our hypothesis is that the electric signals control both the amount of assembled enzymes and their activity, the latter by oxidation through a diffusible redox mediator. Our desire is that this process be stable, predictable, and that a generalized method for controlling biological activity is obtained.

Introduction

Microelectronic devices embedded with biological components often facilitate the interrogation of biology[26,27] as opposed to controlling biological function. Patterned protein and cell assemblies, for example, offer the potential for “in vitro” metabolic engineering[28-31], wherein coordinated biochemical pathways enable on-chip characterization of cell metabolism and possibly control of cell-based systems[32]. Considered among the animal- or human-on-a-chip technologies[33], such devices are envisioned to revolutionize drug development[34,35]. These ambitious goals will require

new biofabrication methodologies that expand bio-device interconnectivity[36] – enabling new modes of device assembly and of communication. Here we demonstrate electrically-mediated assembly, interrogation, and control of a multi-domain fusion protein that produces a bacterial signaling molecule. The biological system is electrically "tuned" using a natural redox molecule and its biochemical response is shown to provide the signaling cues to drive bacterial population behavior. We show that the biochemical output correlates with the electric input charge – suggesting the potential for employing electrical inputs to control complex on-chip biological processes.

As pictured in Fig. 2.1 a, the biohybrid device assembly process is electrically guided via electrodeposition[37,38]. As our model enzyme, the multi-domain fusion protein HLPT[32] (Fig. 2.1 b) is covalently grafted onto the chitosan scaffold electrodeposited on a gold electrode chip (Fig. 2.1 c). In this way the chitosan film serves as a template for protein incorporation onto the device surface. HLPT consists of an N-terminal pentahistidine tag and the bacterial enzymes LuxS and Pfs, which are the two terminal synthases of bacterial autoinducer-2 (AI-2). This quorum sensing (QS) signal molecule is normally secreted from cells to mediate a transition from individual cell to collective behavior within bacterial populations, and promotes the establishment of biofilms[39-41], among other phenotypes. In our work, we use electric signals to thus mediate bacterial responses. HLPT also contains a C-terminal pentatyrosine tag that allows covalent attachment to chitosan's primary amines via the enzyme tyrosinase[42]. These biofabrication assembly methods have proven reliable in retaining enzymatic activity on-chip and in providing an even protein coating [29,43].

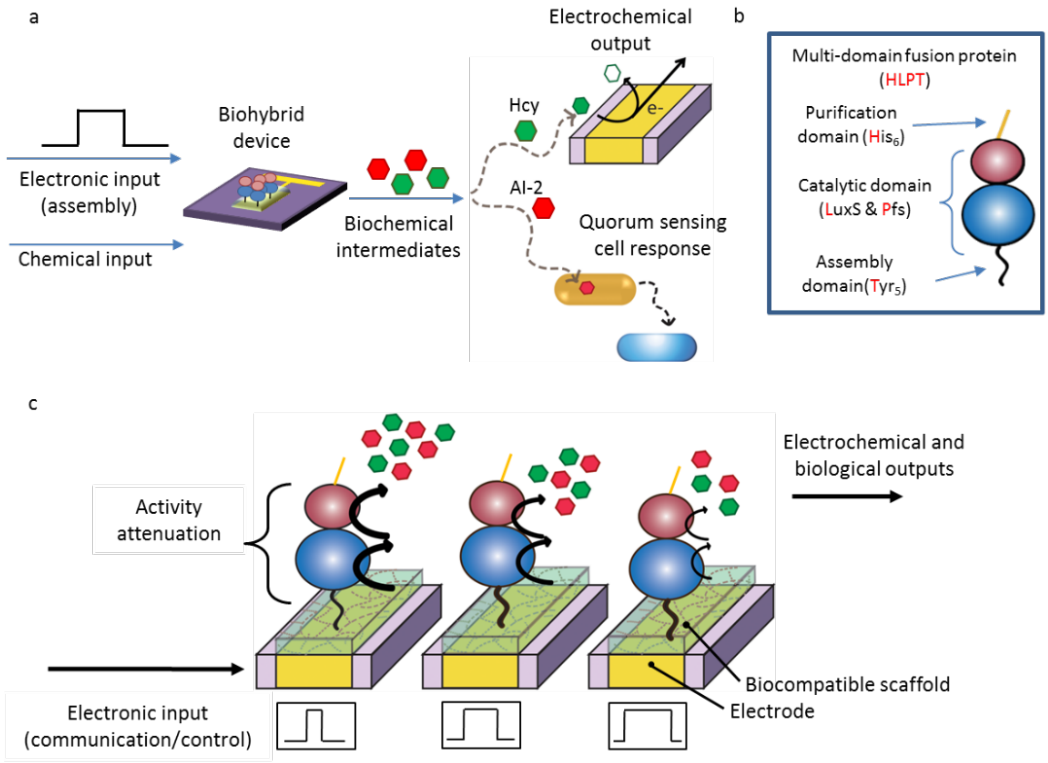

Figure 2.1: Schematic of biohybrid device controlled by electronic signals. a, Schematic diagram representing the biohybrid device receiving both chemical (enzyme reaction precursor) and electronic inputs, and through biochemical intermediates, translating them to both electrochemical signals and biological cells response. **b,** A representation of the components of the multi-domain fusion protein (HLPT) used in this study. **c**, The concept of the experiments is that by varying the electronic inputs through the electrodes on which HLPT is attached, we can vary the attenuation of HLPT activity and thus affect the electrochemical and biological responses in proportion to the input. Purple rectangles represent the silicon wafer, gold rectangles are patterned gold electrodes, semi-transparent turquoise rectangles are the biocompatible chitosan scaffold. Hcy is homocysteine, AI-2 is autoinducer-2. His stands for histidine and Tyr for tyrosine. LuxS and Pfs are enzymes making up HLPT.

Materials and methods

Chemicals and Reagents

DL-homocysteine, potassium hexachloroiridate(IV) (K_2IrCl_6), potassium hexachloroiridate(III) (K_3IrCl_6), 3′,5′-dimethoxy-4′-hydroxyacetophenone (acetosyringone, AS), S-(5′-adenosyl)-L-homocysteine (SAH), CBZ-Gln-Gly, glutathione (reduced form), phosphate buffered saline (PBS) tablets at pH 7.4, Trizma hydrochloride, chitosan of medium molecular weight, parafolmaldehyde powder, β-galactosidase enzyme from *E.coli* grade VIII, and tyrosinase enzyme from mushroom were purchased from Sigma Aldrich. Ellman's reagent (also known as DTNB or 5-(3-Carboxy-4-nitrophenyl) disulfanyl-2-nitrobenzoic acid) is from Uptima, Interchim. Tris-HCl pH 8.0 was from Quality Biological Inc. Sodium acetate, ampicillin sodium salt (Ap), monobasic and dibasic sodium phosphates, trichloroacetic acid, and LB Broth (Miller) were from Fischer Scientific. Kanamycin (Km) was from Genlantis. Calcium Chloride was from J.T.Baker. $FeCl_3$ was from Arcos Organics. DyLight antibody labeling kit, 405 (Thermo Fischer Scientific Inc.) was used for labeling the HLPT protein. Red fluorescent chitosan was labeled with 5-(and-6)-carboxyrhodamine 6G succinimidyl ester (Invitrogen) as per Wu *et al*. [44] Chelex-100 resin was from Bio-Rad. Microbial transglutaminase (mTG) was from Ajinomoto (Chicago, IL).

Biohybrid Device Assembly

A thin layer of chitosan was deposited on a gold-coated silicon chip (electrode fabricated as indicated in Methods) (cathode) by immersing it with a platinum counter

electrode (anode) into a 0.8 % chitosan solution (prepared as described[45]) and applying a current for 2.5 minutes at 4 A/m^2. After rinsing the chitosan film with distilled water, tyrosinase at 300U/µL was mixed with tyrosine-tagged HLPT (10 µM in PBS) and incubated at RT for 1 hour with the chitosan-coated electrodes. Afterwards, each electrode was briefly rinsed with PBS and kept in PBS until use. After appropriate treatments (see below) two similarly-treated electrodes, facing away from each other, were diagonally immersed in a 300 µl solution of 1 mM SAH in 0.1 M pH 7 Phosphate Buffer in a standard semi-micro cuvette (Cole Parmer). The cuvette was stoppered and incubated at 37 °C with 100rpm shaking for the indicated amount of time to let the enzymatic reaction take place (3-3.5 hours). See Figure 2.2 for setup.

On-Chip Biohybrid Device Electrical Attenuation

For *in situ* attenuation with acetosyringone, the gold chip with HLPT (assembled as above) was used as the working electrode in a 3 electrode system with a 0.5 mm diameter, 4 cm-long platinum counter electrode (Alfa Aesar), and Ag/AgCl reference electrode (BASi). These were put in a 250 µM AS solution and the working electrode biased at +0.55 V using a CH Instruments workstation (CHI 6273c) for the designated amount of time (10-1000 sec). The chip was then rinsed gently with PBS, and allowed to react with SAH as indicated above.

Electrochemical Homocysteine Detection

For measuring the homocysteine generated from an on-chip HLPT, the reaction solution is removed at the end of the incubation with SAH, allowing Hcy measurement. Cyclic voltammetry was used to detect homocysteine. A three electrode setup was used, with a 2 mm diameter gold working electrode (CH Instruments) and counter and reference electrodes same as in the attenuation method above. The potential was swept from 0 V to +0.7 V and back at 50 mV/sec (approximately 28 sec). Electrodes were cleaned briefly with Piranha solution (70 % H_2SO_4 and 30 % H_2O_2) before start of experiment. Between every measurement the working electrode was polished for 1 min with 0.05 micron alumina powder on a felt polishing pad (CH Instruments) and rinsed with distilled water, except during real-time measurement experiments. Integration of the output current yields the output charge in Coulombs ($Q=\int i dt$). In our experiments, the total accumulated charge at +0.7V is recorded and used as a measure of homocysteine.

Electrode Fabrication

A 4 inch silicon wafer (100 P/Doped, 1-100 ohm/cm resistivity with thermally grown oxide, from University Wafers) was coated by thermal evaporation with 20 nm of chromium (Cr) and 120 nm of gold (Au). Standard photolithography and subsequent etching of Cr and Au were performed to define electrodes of 7 mm diameter (Fig. 2.2). Each circular electrode is connected to a contact pad via a thin contact lead (0.2 mm in width). Electrodes were physically separated using a

microdicing saw. Fabrication steps were performed at the University of Maryland Nanocenter.

Setup for *in situ* Oxidation and Biohybrid Device Attenuation

Once the biohybrid device is assembled (see below), *in situ* attenuation using AS was achieved using the setup seen in Fig. 2.2 c. A 10 mL beaker filled with the mediator solution was positioned so that the electrodes were all immersed in the solution.

Setup for Biohybrid Device Enzymatic Reaction

For incubation of the assembled biohybrid device with the SAH substrate for subsequent Hcy and AI-2 generation, two chips, facing outward, were inserted diagonally and incubated in standard polystyrene semi-micro cuvettes (Cole Parmer) (Fig. 2.2 d). The chip was immersed so that the liquid (300 µl) reached to the top of the HLPT-immobilized portion (circular pattern) of the chip and not further.

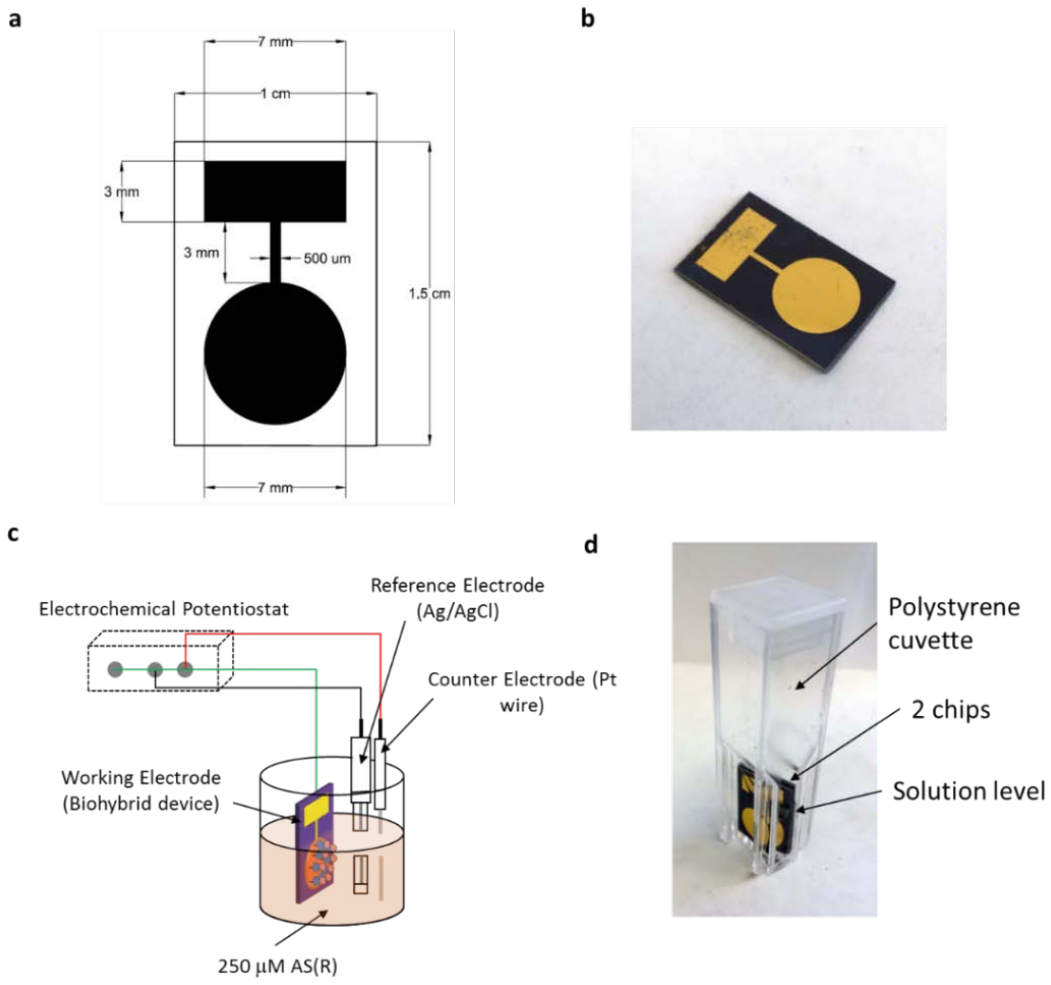

Figure 2.2: Chip and test system setup. a, The AutoCAD drawing and dimensions of one electrode for the mask used for fabrication of electrodes used in the biohybrid device assembly. **b**, A photo of the electrode chip on which HLPT was immobilized. **c**, A diagram of the setup used for *in situ* attenuation of the biohybrid device, in this case with 250 µM AS(R). **d**, A photo taken of the setup in which two electrodes, inserted diagonally and facing out, were incubated in 300µl of the substrate to allow enzymatic reaction (electrodes in photo do NOT have chitosan or HLPT on surface). AS(R) is the reduced acetosyringone redox mediator.

Electrodeposition of Chitosan Film and Enzymatic Assembly of HLPT

The thin film of the pH-responsive polysaccharide chitosan was electrodeposited onto the chip (Fig. 2.3 a,b)[45, 46]. Mushroom-derived tyrosinase was then used to oxidize HLPT's pentatyrosine tag, creating an active quinone, which grafts onto chitosan's primary amines via a Michael's adduct (Fig. 2.3 c). These methods have proven reliable in retaining enzymatic activity and in providing an even protein coating [29,47, 43].

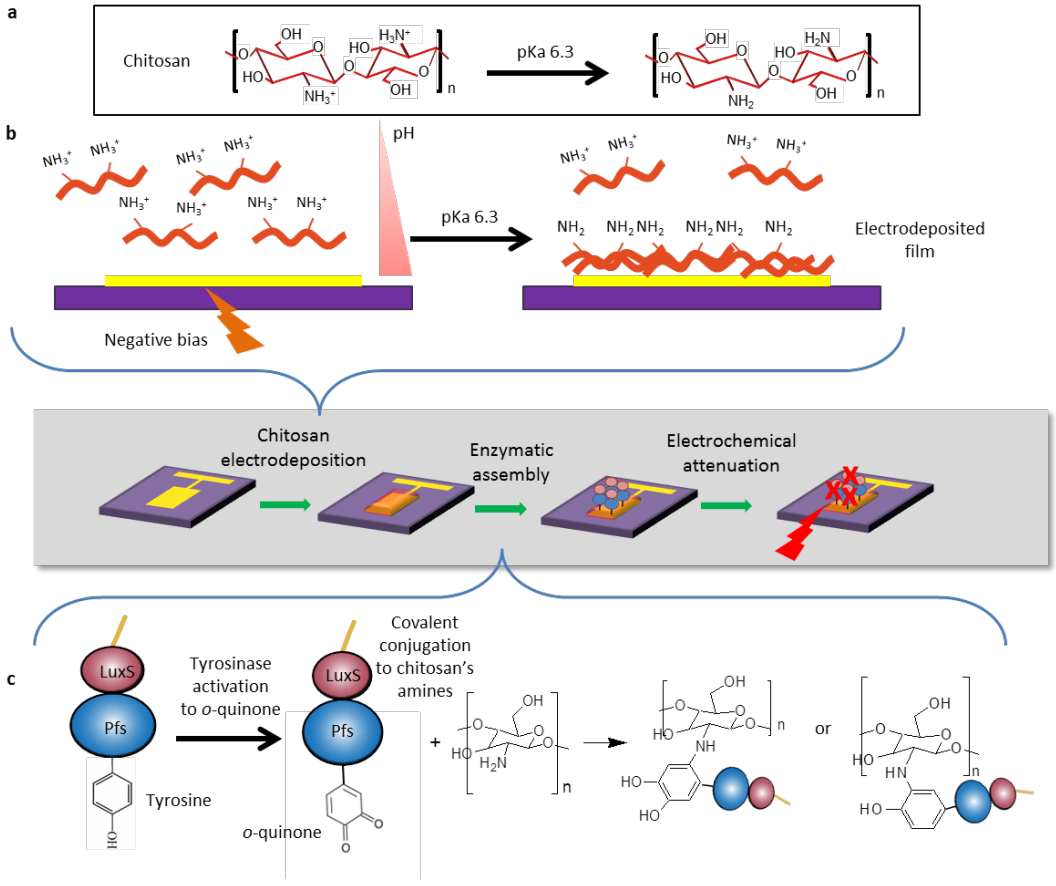

Figure 2.3: Biofabrication: Chitosan electrodeposition and tyrosinase-based enzyme conjugation. Middle schematic represents the biofabrication processes used in this paper, with the electrochemical attenuation being introduced in this work. **a**, The structure of

chitosan and its' amine groups below and above its pKa of 6.3. **b**, Immersion of a negatively-biased electrode into a solution of chitosan results in a pH gradient (higher pH at the surface) that promotes the electrodeposition of a chitosan film on the surface as well as the exposure of amine groups. **c**, Tyrosinase-mediated conversion of tyrosine residues to *o*-quinones results in the covalent attachment of HLPT protein to chitosan's amines.

Ellman's method: Homocysteine Measurement

The "Ellman's Test" was done according to manufacturer's instruction (Uptima, Interchim). Briefly, a DTNB stock solution is made with 50 mM sodium acetate and 2 mM DTNB in water. The Tris buffer is 1 M Tris at pH 8.0. Per each 1 mL total volume, 50 µL of the DTNB stock, 100 µL of the Tris solution, and 850 µL total distilled water and sample solution are added. In some experiments, these were scaled down by a factor of 10. DL- homocysteine standard solution was prepared in 0.1 M phosphate buffer pH 7.0. The contents are mixed and incubated at room temperature for 5 minutes. Optical absorbance is then read at 412 nm and the SH content is calculated by dividing the OD at 412 nm by 13600 $M^{-1}cm^{-1}$ to get the molarity in the assay, and multiplied by the total volume/sample volume ratio for the estimated original concentration.

AI-2 Reporter Cells and Cell Culture

Cells used for detection of AI-2 from HLPT were CT104 *Escherichia coli* (*E. coli*) (W3110-derived *luxS lsrFG* double mutant strain from lab stock) with the plasmids pCT6 (pFZY1 derivative, containing *lsrR* and *lsrR* promoter region fused

with *T7RPol*, Ap^r) [48] and pET200-EBFP2 (pET200 derivative, containing *EBFP2*, Km^r, from lab stocks). Cells were inoculated at 2 % from an LB overnight culture and Ampicillin and Kanamycin were added at 50 µg/mL. After an OD600 of about 0.4 was reached, cells were spun down in 300 µL volumes at 8000 rpm for 3 minutes, and re-suspended in PBS, 10 % LB and HLPT reaction mixture with homocysteine and AI-2. Reaction mixture, when incubated with the cells, was therefore at 90 % of original concentration or, in the cases where the concentration was higher than 50 µM, at 10%. All compared samples were similarly diluted. The cells were incubated for 4 hours at 37 °C at 250 rpm with aeration. After this, the cells were fixed with 2% paraformaldehyde in PBS for 30 minutes at room temperature and stored in 4 °C until measurement. Blue DAPI fluorescence was recorded by FACS (FACSARIA, BD Biosciences). To ensure sample consistency, 50,000 cells were collected for each sample and consistently gated by forward scatter (FSC) and side scatter (SSC). The mean blue DAPI fluorescence levels are based on the means from one or two different samples.

Enzymatic Activity Calculations

Enzyme activity was calculated in either nmol HCY/(min*mg protein) or as nmol HCY/(min*cm^2 of electrode). For both cases, the concentration of homocysteine measured in µM was calculated from the equations from the standard graph in Fig. 2.4 d. This concentration was then used to calculate the nanomolar amount of homocysteine present. The minutes for the formula were taken from the

recorded time of the reaction. The amount of protein was known in the solution-based experiments, as was the surface area of the electrodes in cm^2.

Oxidation with Strong Oxidant Ir(IV): Solution-Based Attenuation

Enzymes (Pfs, LuxS, or HLPT) were diluted in phosphate buffer pH 7.0 to the indicated concentration. Mediators were added and the samples incubated at room temperature for the indicated times. Solutions were then filtered using a 0.5 mL centrifugal filter (MWCO: 10 k, Millipore) and washed three times (5 minutes at 14,000 g) with 0.5 mL of phosphate buffer to wash out the mediator. The substrate used for HLPT or Pfs was 1 mM SAH. For LuxS the substrate, SRH, was produced by boiling 1 mM SAH in HCl[39]. The enzyme and substrate were reacted in the conditions indicated. For Pfs activity, the solution was incubated with both the attenuated Pfs and un-attenuated LuxS in equimolar concentrations, after which homocysteine was measured. The amount of generated homocysteine was detected using Ellman's reagent and/or via electrochemical method (see above). Absorbance measurements were performed with the addition of one of the enzymes to Ir(III) or Ir(IV) solutions.

Ellman's Method for Protein Sulfhydryl Measurement

The Ellman's Test was used for measuring accessible sulfhydryls present on proteins. The test was done according to manufacturer's instruction (Uptima, Interchim). The solutions were prepared the same as in the "Ellman's method" paragraph in Section 4 of this Supplementary material. Instead of a total of 1mL of

testing solution, all components were scaled down by a factor of 10 so that a total of 100 µl was tested in a 96-well clear plate. First, the proteins were treated with AS(O) or AS(R) for 500 sec at a ratio of 0.1 µM protein: 1 µM AS in PBS. These were then filtered as described in "solution-based attenuation" in above. Treated proteins were added at the indicated concentrations to PBS, 5 µl DTNB and 10 µl Tris. The contents were mixed and incubated at room temperature for 5 minutes. Optical absorbance was read at 412 nm and the SH content is calculated by dividing the OD at 412 nm by 13600 $M^{-1}cm^{-1}$ to get the molarity in the assay, and multiplied by the total volume/sample volume ratio for the estimated original concentration.

Protein Preparation for Electron Paramagnetic Resonance (EPR)

The protein HLPT was used at a final concentration of 20 µM. Samples were treated with Ir(IV) at 300 µM or AS at 200 µM as described above in "solution-based attenuation". For filtering and washing out the Ir and AS, Chelex 100 resin-treated deionized water was used. The Chelex treatment of water or PBS (which removes copper, iron, and other heavy metals) was done according to manufacturer's instructions – 2.5 grams of the resin was mixed with 50mL of either MilliQ-filtered di-H_2O or PBS for 1 hour. After a brief centrifugation, the liquid was decanted for use in EPR.

EPR Specifications/Measurements

CPH hydrochloride (known as 1-Hydroxy-3-carboxy-2,2,5,5-tetramethylpyrrolidine – HCl and abbreviated as CPH, from Enzo Life Sciences) at a

final concentration of 1 mM was used for all samples, for a 50 µL total sample. Measurements were taken at 2 minutes and 5 minutes after CPH addition. Also, a 16-run average was done for each sample. The intensities were normalized and averaged. All EPR measurements were carried out using a Bruker EMX ESR spectrometer (Billerica, MA) at ambient temperature. The settings were as follows: 1 G field modulation, 100 G scan range, and 20 mW microwave power, 80 s/scan for single scans, 40s/scan for 16-scan runs.

Inductively Coupled Plasma Optical Emission Spectrometry (ICP-EOS)

ICP EOS experiments were run on a Perkin Elmer Optima 4300DV. Samples were 200 µg/ml of HLPT diluted into diH_20 from 2.5 mg/ml in PBS (5 mL total). Samples of 2.33 mg/ml HLPT were incubated with 1.33 mM Ir(IV) or AS(O) for 1 hour and filtered as indicated above.

Bulk Acetosyringone Electrical Oxidation

Acetosyringone was dissolved in pH 7.0 phosphate buffer. The solution, in the indicated concentration, was put in a 10 mL beaker. Nitrogen was continuously bubbled through the solution to prevent oxygen interference. A three electrode system was set up and immersed in the solution - gold-coated silicon working electrode (area about 2 cm^2), platinum foil counter electrode with a glass salt bridge, and silver/silver chloride reference electrode. The working electrode was biased at +0.55 V and the output current was measured over time until it was <5 % of the starting current (about

1-2 hours). HLPT was then treated with the AS as in “solution-based attenuation” above.

On-chip HLPT attenuation: Control Reactions

Control reactions with non-oxidizing voltage (+0.22 V) in AS solution, as well as the oxidizing voltage (+0.55 V) in a solution of phosphate buffer alone were run and showed significantly lower currents than the experimental samples (Supplementary Fig. S2.4 a). Enzymatic activities (as calculated in Supplementary Information and seen in Supplementary Fig. S2.4 b) were correspondingly unaffected.

Real Time HLPT Activity Measurement On-Chip

For real time *in situ* measurements, the same general procedure for device assembly, *in situ* attenuation, and homocysteine electrochemical measurement as previously were followed. In these experiments though, CV’s were taken using a CHI Multiplexer from 8 samples one after the other, 3 minutes apart. A bare chlorinated Ag wire was used as the reference electrode, and electrodes remained in the test solution throughout, which was kept at room temperature.

Statistical Analysis

Statistical analysis with calculation of p-values was performed by using two-tailed, unequal variance Student t-tests. * indicates $p < 0.05$, ** $p < 0.01$, *** $p < 0.001$, ****$p < 0.0001$.

Results and discussion

After assembly, the desired biohybrid device will modulate the activity of HLPT for the guided synthesis of AI-2 and a byproduct, homocysteine (Hcy) (made in a 1:1 stoichiometric ratio). On-chip enzyme activity is assayed via three modalities - optically, electrochemically and biologically. Our experiments are carried out at physiologically relevant concentrations and importantly, our methods are linear in these ranges including a near real-time electrochemical method for Hcy. Applications that require real-time assessment and with no sampling (direct *in situ* measurement) may thus be feasible (Supplementary Fig. S2.5).

Homocysteine (Hcy) can be measured optically (Ellman's assay based on SH groups[49]) or electrochemically by sulfhydryl oxidation at a gold electrode (as discussed in Methods). A linear relationship between these methods (Fig. 2.4 a) yields quantification of biochemical flux through HLPT (Fig. 2.4 b) and allows measurement of HLPT activity over time without sample consumption (Fig. 2.7 c). AI-2 produced in a 1:1 ratio to Hcy assayed with a cell-based method is linearly correlated with Hcy in the same solution (Fig. 2.4 d).

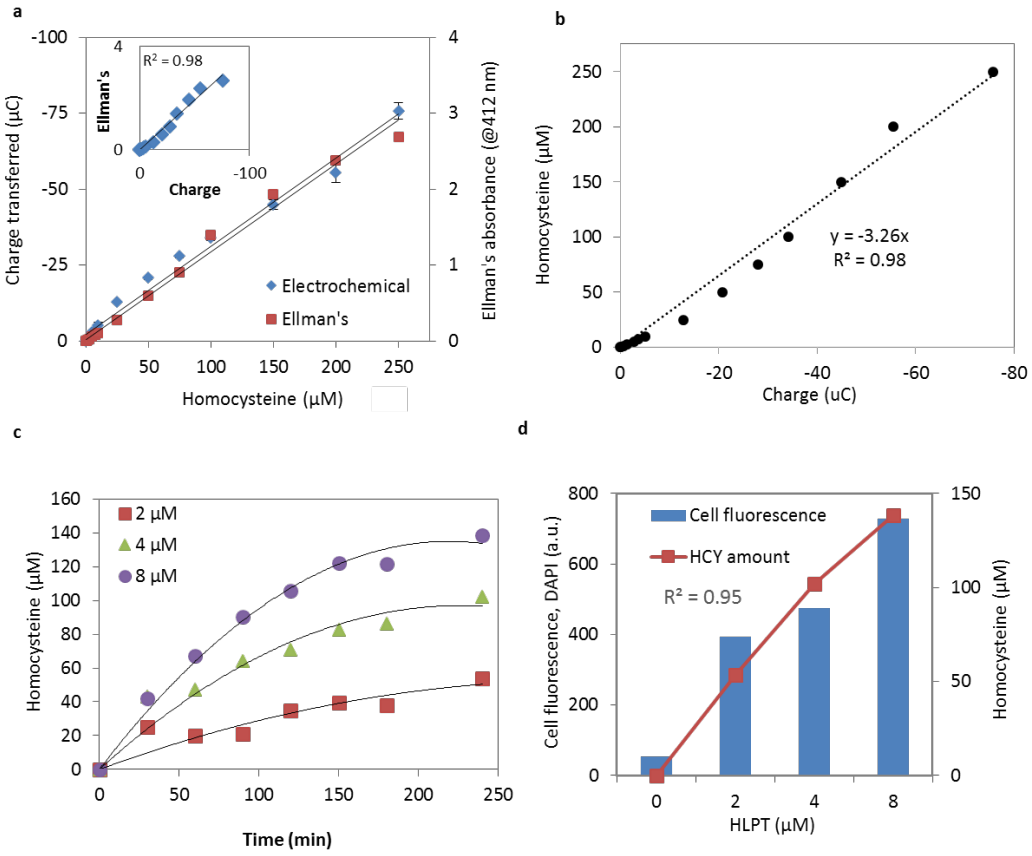

Figure 2.4: Detection of Hcy and AI-2. a, Comparison of the electrochemical detection method used in this chapter to the standard Ellman's assay. The Pearson correlation coefficient for linearity was calculated between the charge transferred and the Ellman's absorbance value, yielding an R^2 value of 0.98. Seven measurements were taken for each averaged data point. **b**, Graph of the same values as in **a** of the electrochemical data with the axes reversed. The fitted line was used throughout the chapter to convert charge to homocysteine concentration, and the R^2 value shown is the Pearson correlation coefficient for linearity. **c**, Different concentrations of HLPT were reacted with 1 mM SAH over the course of 4 hours at 37 °C. Electrochemical measurements were taken throughout. The fitted polynomial curves are used to convey trends. **d**, The products from the reactions in **c**, after the final time-point, were added to AI-2 reporter cells at a 1:10 dilution, whose average blue fluorescence response (FACS) can be seen. The Pearson correlation coefficient for linearity

between the homocysteine measured and the cell fluorescence response was calculated and gave an R^2 value of 0.95 (it is not for the HCy vs HLPT relationship). HLPT is the fusion enzyme under study.

HLPT oxidation can be mediated in several ways. Our initial studies employed chemical oxidation via powerful protein oxidant K_2IrCl_6 (iridium, denoted Ir(IV))[50]. Our results indicate that oxidized iridium and not its reduced form (controls) decreased HLPT activity in a predictable concentration- and time-dependent manner (Fig. 2.5, Supplementary Fig. S2.1).

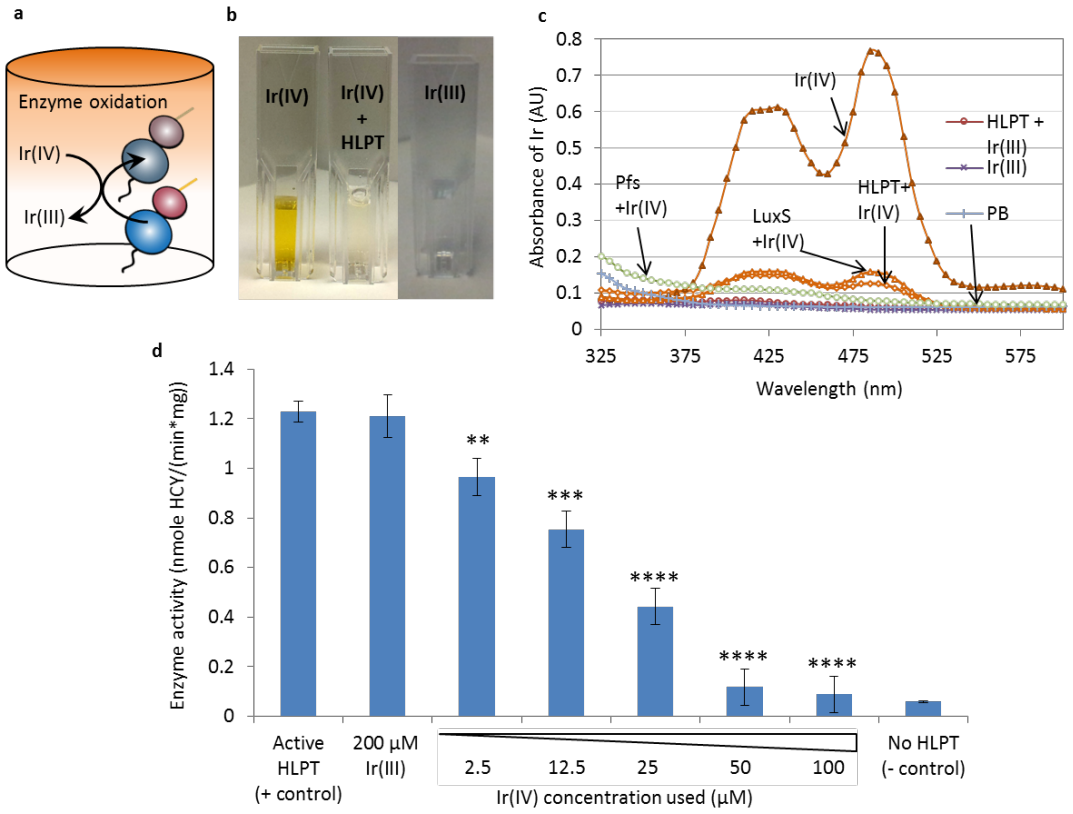

Figure 2.5: HLPT activity attenuation by strong oxidant Ir(IV) in solution. a, Proposed reaction of Ir(IV) with HLPT in solution, resulting in oxidation of HLPT and attenuation of enzymatic activity. **b,** Pictures showing the color change when Ir(IV) reacts with HLPT and

becomes reduced to Ir(III), losing its brownish color. **c**, Spectrophotometric measurements of Ir(IV) or Ir(III) after reacting with HLPT, Pfs, or LuxS for 40 minutes. All three proteins turn Ir(IV) to Ir(III) color. **d**, Activity of HLPT remaining after treatment of HLPT with different Ir(IV) amounts. All measurements done in triplicate and error bars indicate s.d. P values for samples were calculated using student's t-test (two tailed, unequal variance), compared to the active HLPT positive control. ** indicates $p < 0.01$, *** $p < 0.001$, **** $p < 0.0001$. Ir(III) and Ir(IV) are the reduced and oxidized forms of the redox mediator $IrCl_6$. HLPT is the fusion protein under study, and Pfs and LuxS are the two enzymes making up HLPT.

We predicted the reaction in Fig. 2.5 a to take place as the Ir(IV) oxidized HLPT, turning to Ir(III) in the process. Ir(IV) has a characteristic brownish color which diminishes as it is reduced to Ir(III) (Fig. 2.5 b). Incubating HLPT (as well as its constituents Pfs and LuxS, separately) with a solution of Ir(IV) shows a fall in absorbance, measured over the course of an hour (Fig. 2.5 c). In Fig. 2.5 d 1.5 µM HLPT was incubated for 1 hour with different Ir(IV) amounts. Hcy measurements were taken after filtering and further incubation with 1 mM SAH substrate for 3 hours at 37 °C.

Next, in order to test for electric actuation, we selected the natural plant-based redox mediator acetosyringone (AS) (E_0 of +0.5 V vs. Ag/AgCl). AS is generated during the innate plant immune response to pathogens, and then consumed in an oxidative burst [51]. It normally exists biologically in a reduced state (AS(R)). As can be seen in Fig. 2.6 b, we observed electric oxidation of AS by the simple evolution of a brownish-orange color change that is a characteristic of the oxidized form[52].

We next investigated whether electrically-oxidized AS could oxidize HLPT (Fig. 2.6 a), and the nature of that oxidation. LuxS has a divalent cation (Zn^{2+}, Fe^{2+}) at its active site, which could be a target for oxidation and attenuation of activity. Alternatively, sulfhydryl residues are more suitable targets for a generalized approach. AS(O) was added to HLPT, as well as LuxS and Pfs, after which the oxidation status of the protein was measured. Our results indicating ~4-fold reduction in –SH groups (Fig. 2.6 d) showed that AS(O) oxidized vulnerable sulfhydryl residues on all three proteins. These results are supported by electron paramagnetic resonance (EPR) spectroscopy, which yields a protein's more general oxidation state. That is, to detect general oxidation, we employed EPR probe, CPH (1-Hydroxy-3-carboxy-2,2,5,5-tetramethylpyrrolidine - HCl), which is oxidized by an oxidized HLPT so that its radical is revealed and detected. We measured a 2.5 fold increase in CPH radical from solutions where HLPT was treated with AS(O) (Fig. 2.6 c). Additionally, using inductively coupled plasma optical emission spectroscopy (ICP-EOS), we found Zn^{2+} was unaffected (Supplementary Fig. S2.2 b). In sum, our results demonstrate that HLPT activity is attenuated by oxidation of its sulfhydryl residues and not by oxidation of the active-site cation. Moreover, these results support the notion that on-chip reaction activity could be controlled by exposure to oxidized acetosyringone (AS(O)) and, further that the methodology might be predictable.

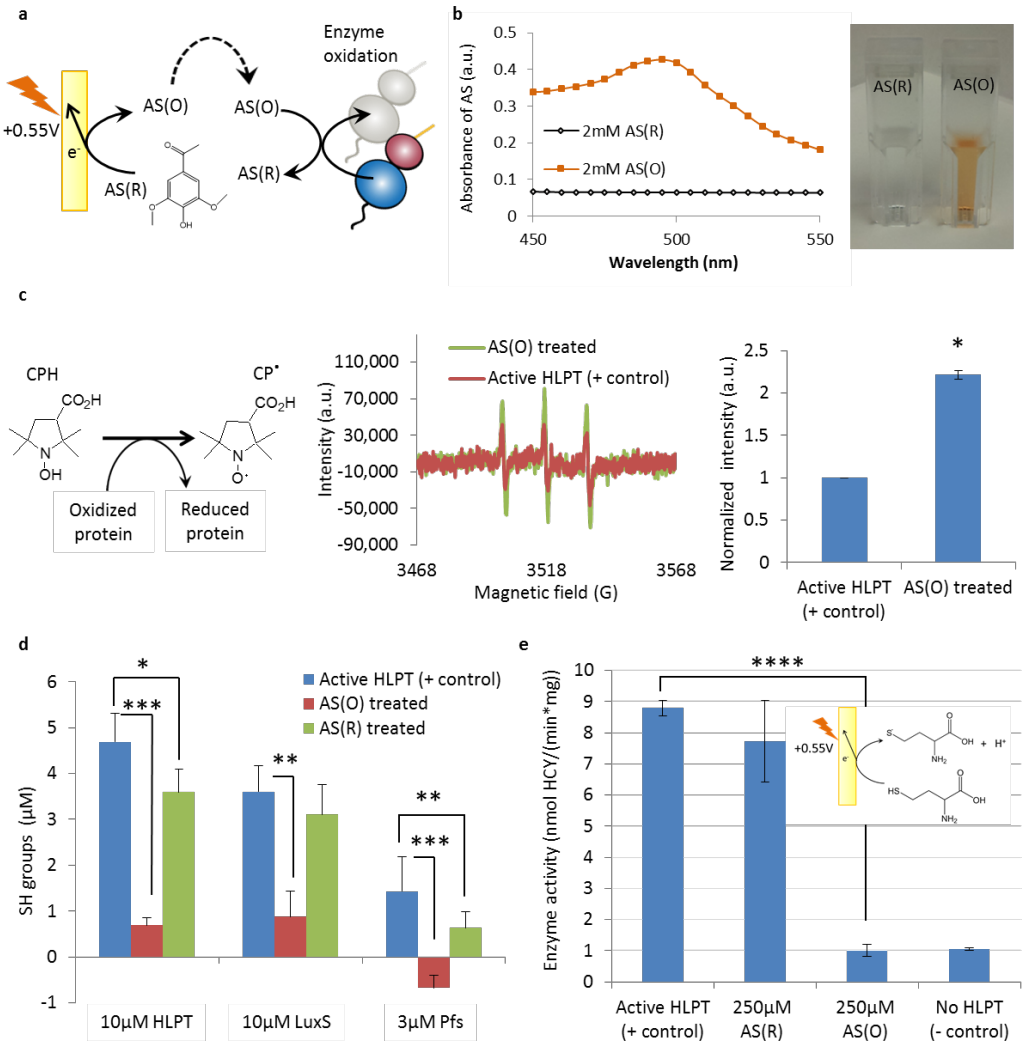

Figure 2.6: Electronically-driven HLPT attenuation by natural mediator AS.

a, Schematic of the electrochemical oxidation of AS(R) in solution is followed by its addition to HLPT, where it oxidizes and attenuates HLPT activity and is reduced back to AS(R) in the process. **b,** Spectrophotometric measurements of AS(R) and AS(O) – as AS is oxidized, it turns a brownish-orange color, detectable at 490nm. **c**, Oxidation of HLPT by AS(O) can be detected with the EPR probe CPH, which is oxidized by the AS(O)-oxidized protein. A higher EPR intensity is seen when the protein is treated with AS(O). The EPR spectra show samples measured after 2 minutes of CPH reaction with protein. The bar graph represents an average of several normalized measurements (see Supplementary Section 8). **d**, The

sulfhydryl groups detected through Ellman's assay after treatment of the proteins with AS(O) or AS(R). **e,** HLPT activity calculated from electrochemical measurements after incubation with AS(O) or AS(R). Inset shows the reaction of HCY as it is oxidized at the electrode. Measurements in **c** were done in duplicate. Measurements in **d** and **e** were done in triplicate. All error bars indicate s.d. Two-tailed, unequal variance student t-tests were run on c,d,e. * indicates $p<0.05$, ** $p<0.01$, *** $p<.001$, ****$p<0.0001$. AS(R) and AS(O) are reduced or oxidized acetosyringone, respectively. CPH is the electron paramagnetic resonance (EPR) spin probe 1-Hydroxy-3-carboxy-2,2,5,5-tetramethylpyrrolidine – HCl. HLPT is fusion protein. LuxS and Pfs are the catalytic enzymes within HLPT.

To test if AS(O)'s oxidation of HLPT affected activity, 1.5 µM HLPT was treated with AS(O) as above, then incubated with enzyme pathway precursor, S-adenosyl-homocysteine (SAH) (1 mM, 37 °C). At the end of the incubation (3-3.5 hours) the amount of Hcy produced was measured and HLPT activity was calculated. Our results show that HLPT activity decreased linearly with exposure time and proportionally to the AS(O)/HLPT ratio (Fig. 2.6 d and Supplementary Fig. S2.3). These demonstrate that HLPT activity is attenuated by AS(O) oxidation - an electronically-controlled process.

We next tested our main hypothesis – electric assembly of HLPT on a chip and *in situ* activity attenuation. For these on-chip experiments, the biohybrid device (assembled as described in Methods) was immersed in a solution of AS(R), where it served as the working electrode. In a one step process, the electrode was biased at +0.55 V, and the AS oxidized at the surface could react with the surface-bound HLPT

(Fig. 2.7 b). An amplified current output similar to that of solution-based oxidation was observed (Supplementary Fig. S2.4 a). To test our hypothesis that input charge correlates with decreased on-chip activity, both end-of-reaction and real-time measurements were performed. Enzyme-laden chips were biased at +0.55V for different times (10-1000 sec – resulting in different levels of accumulated input charge and oxidation of AS), after which they were incubated with the SAH substrate as before to allow Hcy and AI-2 generation. We calculated enzyme activity and found a linear decrease followed by a plateau at long exposure times (Fig. 2.7 c). Control reactions showed that both the oxidizing voltage (+0.55V) and the presence of AS were needed for attenuation (Supplementary Fig. S2.4 b). The observed linear decrease supports a conclusion that as more AS is oxidized at the surface, it reacts with and oxidizes more HLPT on the electrode – reducing its activity proportionally. Correspondingly, this was dependent on the amount of active HLPT present- as can be seen from the three different series of chips, each with different initial activities. Also, Hcy increased nearly linearly over time as indicated by our real time measurement. Finally, these measurements correlated with our “end-of-reaction” samples (Supplementary Fig. S2.5).

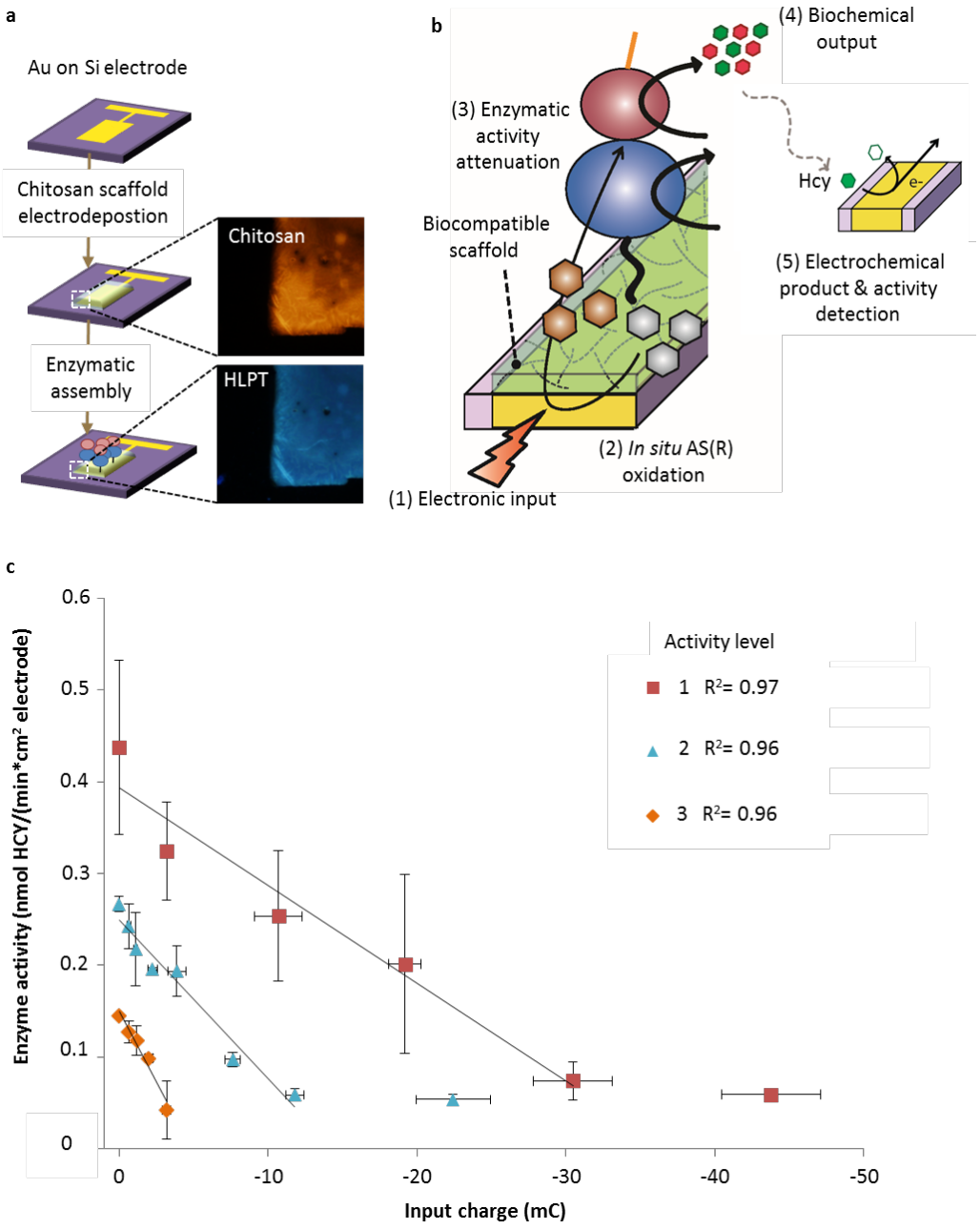

Figure 2.7: On-chip enzyme activity is linear with input charge. **a**, Immobilization of enzyme onto a silicon chip involves chitosan electrodeposition as a thin film followed by enzymatic assembly of HLPT. Fluorescent pictures of red-labeled chitosan and blue-labeled HLPT show film and enzyme co-localization onto the gold patterned electrode. **b**, Schematic depicting *in situ* enzyme attenuation. The same electrode on which the HLPT is attached is

used to oxidize the AS (grey to brown hexagons) in the vicinity of the protein and leads to activity attenuation. Activity is then measured by electrochemical detection of Hcy (green hexagon) as described in the text. **c**, Correlation between the input charge applied for *in situ* AS oxidation as in **b** and the Hcy measured from HLPT thusly attenuated at the end of 3.5 hours of incubation. Three series are depicted, with different initial enzymatic activities. There are two activity and four input charge measurements per data point. Error bars indicate s.d. R^2 values indicate Pearson correlation coefficients for linearity for the displayed averaged data. Values for Pearson and Spearman rank coefficients for monotonic correlation for all non-averaged data are, respectively- 0.81 and -0.91 for activity level 1, 0.92 and -0.93 for activity level 2, and 0.92 and -0.96 for series 3. Au is gold, Si is silicon. Hcy is homocysteine. mC is milliCoulombs. HLPT is fusion protein.

We then estimated the apparent numbers of electrons needed to deactivate one HLPT molecule for each on-chip reaction (see Supplementary Information for calculations and discussion). We found this number (30-90) to be of the same order of magnitude as the predicted number of target sulfhydryl residues that could be oxidized on the protein complex (based on crystal structures [53,54]).

We then asked whether we could predictably "tune" the activity of an assembled enzyme complex to a specific "setpoint". For these experiments, which are outlined and discussed in Supplementary Information, we utilized electronic signals to both load more than a sufficient amount of enzyme onto the chip and then "tune" the activity by calculating the needed charge and biasing the electrode for the estimated duration. In one envisioned application, this method might enable design and real-time feedback control of flux through a surface-assembled biochemical pathway.

Finally, the principal motivation of our concept was the ability of the biohybrid device to translate electrical signals to modulate complex biological behavior – including cell phenotype. We sought to demonstrate that on-chip modulation of HLPT affected generation of both Hcy and AI-2 and then, that AI-2 would affect the bacterial phenotype. In our case, this was the generation of a blue fluorescent protein among engineered *Escherichia coli* bacteria (Fig. 2.8 a). We prepared HLPT-immobilized electrode chips as before, and applied varied amounts of charge to attenuate enzymatic activity to various desired setpoints. As before, we let the enzymatic reaction take place, and electrochemically measured the amount of Hcy generated. Then, after exposing the cells to the solution containing AI-2, we used fluorescence-assisted cell sorting (FACS) to detect the blue fluorescent response. Figure 2.8 b shows FACS histogram plots of different fluorescence intensities resulting from HLPT-immobilized chips modulated using the indicated amounts of charge. Our results confirmed electrically-controlled generation of bacterial communication molecules (in the same proportion as Hcy) and similarly modulated biological signaling as indicated by cell fluorescence (Fig. 2.8 c) - meaning that we could predict and feedforward control biological behavior from our electrochemical Hcy measurements. Moreover, this first-ever finding shows that population-wide biological behavior was modulated electrically.

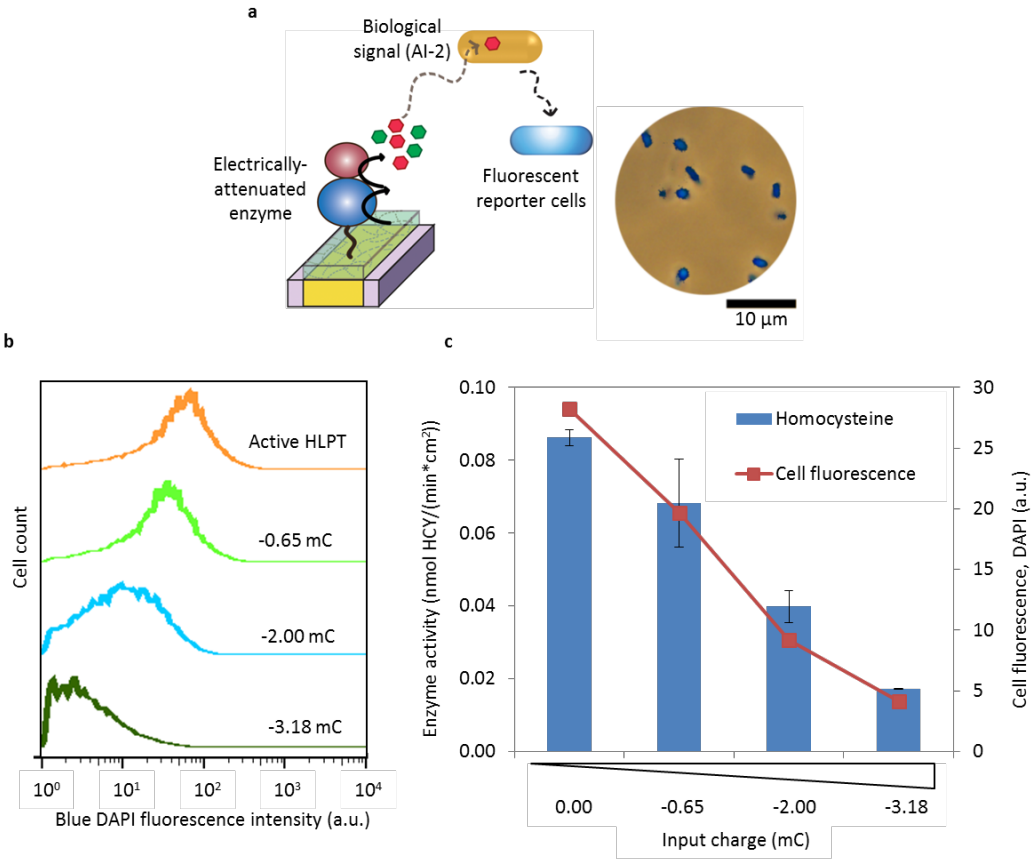

Figure 2.8: *In situ* enzyme attenuation mediates biological signaling. a, Schematic of experiment: HLPT is attenuated *in situ* as in Figure 2.7. The generated solution with AI-2 is added to reporter cells, which fluoresce blue. A bright field image of the cells is overlaid with the blue fluorescent image, showing co-localization of cells and fluorescence. **b**, Histograms from FACS (measuring blue DAPI fluorescence) run on AI-2 reporter cells to which the products of differentially-attenuated HLPT-immobilized electrodes were added. **c**, Comparison of the Hcy measured electrochemically and the average blue fluorescence of AI-2 reporter cells from HLPT immobilized on an electrode and attenuated with the indicated input charges. Cell fluorescence averages correspond to those in the histograms in **b**. Three measurements were taken for the activity in **c**, and error bars indicate s.d. The Pearson correlation coefficient for linearity calculated for cell fluorescence vs. enzyme activity

averages in **c** yielded an R^2 value of 0.98 (indicated). AI-2 is autoinducer-2. HCY is homocysteine. HLPT is the electrically-attenuated fusion enzyme. mC is milliCoulombs.

These combined results suggest that AS(O)-driven on-chip electronic attenuation may be a predictable process for our biohybrid device, and support our hypothesis that input charge correlates with both enzyme activity and the generation of two different biochemical products. Importantly, the assembly methods are biologically benign and device operation is enabled without the need for multiple liquid samples. This was envisioned for *in vitro* metabolic or pathway engineering[29,30]. We anticipate that our system and methods can easily be applied in microfluidic devices with embedded micro-scale electrodes. Indeed, our group has already demonstrated functional enzyme assembly on a chitosan layer, as well as electrochemical small-molecule measurement inside of microfluidic channels[29,55].

In the Supporting Information, we show generalized application of our method. We characterized chip actuated assembly and attenuation of two additional enzymes: (i) a common reporter, β-galactosidase and (ii) a microbial transglutaminase used in tissue engineering and other applications[56]. We found that AS(O) acted similarly in oxidizing these proteins and attenuating their activities (Supplementary Figures S2.7, S2.8, S2.9). We also used *in situ* electric oxidation of the alternative diffusible redox mediator $IrCl_6^{3-}$ to show attenuation of HLPT, β-galactosidase and microbial transglutaminase, with results similar to those obtained with AS (Supplementary Figures S2.7, S2.8, S2.9). These results demonstrate the wider applicability of our method, with possibility for further expansion.

Conclusions

This study provides the first evidence that direct electrical control of a diffusible redox mediator, at the surface of a gold electrode in the vicinity of an immobilized enzymatic pathway results in predictable protein oxidation, attenuation of activity, and biochemical signal generation. We envision that the novel suite of methodologies demonstrated here form the basis for targeting and controlling biochemical fluxes of other biohybrid devices. We therefore propose this methodology as a powerful addition to the biofabrication toolbox[57] that furthers the utilization of biologically inspired nano-scale processes by bridging the communications and fabrication gaps that exist between microelectronics and biological systems.

Acknowledgements

We thank the UMD Fischell Department of Bioengineering Core FACS Facility for assistance with FACS data collection and the UMD Nanocenter for providing workspace and tools for electrode fabrication and ICP-EOS measurements. We also Y. Zhou of the UMD Department of Nutrition and Food Science for help with EPR measurements. Financial support for this work was provided by the Defense Threat Reduction Agency (HDTRA1-13-0037), the National Science Foundation (no. 1160005 to WEB, no. 1264509 to HO Sintim) and the RWD Foundation.

Supplementary Information

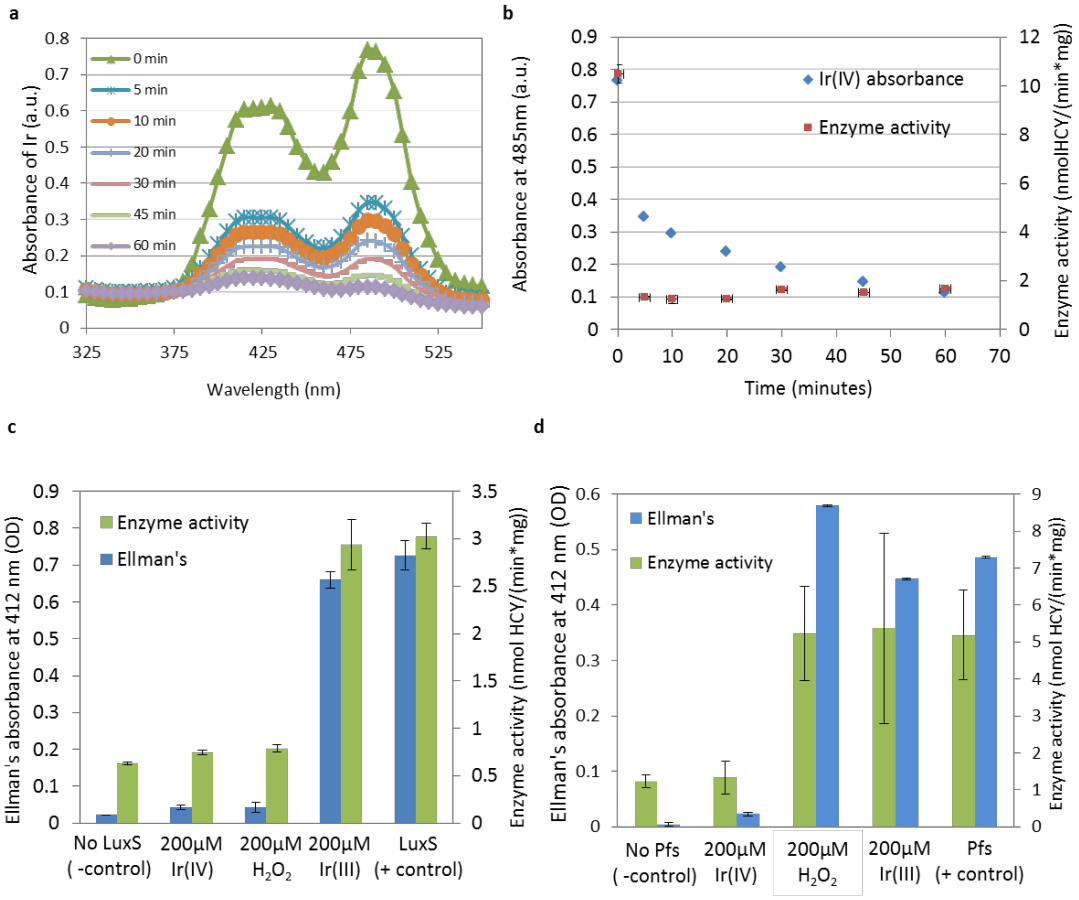

Supplementary Figure S2.1: Ir(IV) attenuation of HLPT, Pfs, and LuxS. a, Spectrum of Ir(IV) reacting with HLPT. **b**, Activity as measured electrochemically of samples taken from **a** over the course of an hour. **c**, LuxS activity remaining after treatment with the indicated mediators. **d**, Pfs activity after treatment similar to LuxS in **c**. Activity for **c** and **d** was measured using Ellman's assay and electrochemically (which was used to calculate the enzyme activity shown). Three samples were measured and averaged for each bar. Error bars represent s.d. Ir(III) and Ir(IV) are the reduced and oxidized forms of the redox mediator $IrCl_6$. HLPT is the fusion protein under study, and Pfs and Luxs are the two enzymes making up HLPT.

The absorbance falls more than 50 % in the first 5 minutes of the reaction and continues to decline steadily until it reaches values similar to those of Ir(III) (Supplementary Fig. S2.1 a, Figure 2.4 c). HLPT activity is completely reduced when 1.5 µM of HLPT is treated with 200 µM of Ir(IV) for one hour, and incubation of different HLPT to Ir(IV) ratios results in a predictable trend of activity decrease (Fig 2.5). Interestingly, the amount of fall in absorbance of Ir(IV) does not directly correlate with the same fall in activity, hinting that Ir(IV) may also oxidize residues on the protein that are not related to its activity (Supplementary Fig. S2.1 b).

Incubation of the enzymatic constituents of HLPT – LuxS and Pfs – separately with Ir(IV) for an hour also shows a significant decrease in activity, similarly to that of HLPT. 1.5 µM LuxS was incubated with SRH and 1.5 µM Pfs with both 1 mM SAH and then an active 4 µM LuxS for 3.5 hours. Interesting to note is the negligible effect on activity of Pfs from a hydrogen peroxide treatment – known to oxidize sulfhydryl groups on proteins[58]. This may be due to a lack of an SH group in the known reaction center of Pfs, as opposed to its presence in LuxS.

We wanted to investigate whether electrically-oxidized AS or Ir(IV) could oxidize HLPT residues, and the nature of that oxidation. AS(O), AS(R), Ir(IV) or Ir(III) were added to HLPT, after which the oxidation status of the protein was measured. As stated in the main sections, to detect general oxidation we employed EPR probe, CPH. When CPH is oxidized (by an oxidized HLPT, for example) its radical is revealed and detected. We measured a 5.5 fold increase in CPH radical from solutions where HLPT was treated with Ir(IV) (Supplementary Fig. S2.2 a), pointing to general oxidation of HLPT by Ir(IV) but not Ir(III).

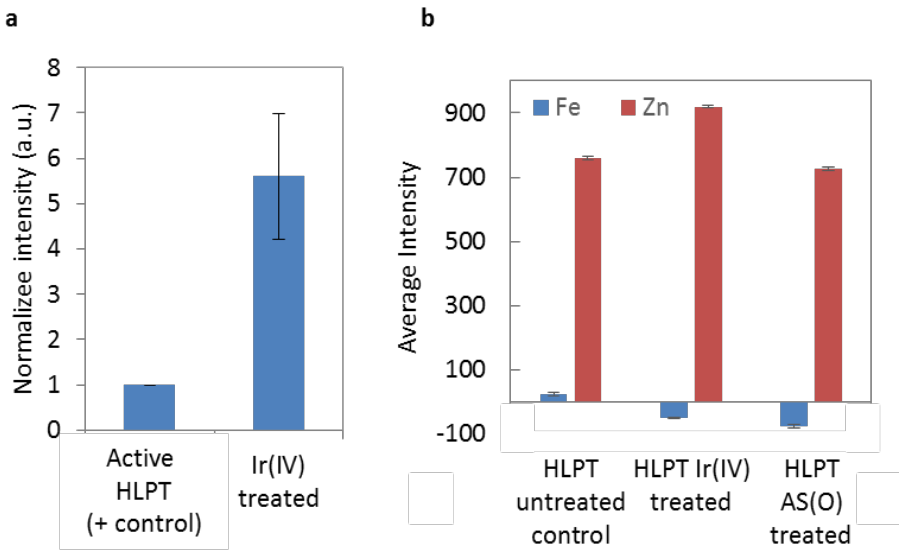

Supplementary Figure S2.2: Characterization of HLPT oxidation by Ir(IV) and AS. **a**, The bar graph of the average of several normalized measurements of EPR intensity of HLPT treated with Ir(IV). **b**, ICP EOS results before and after treatment of HLPT with either Ir(IV) or AS(O). Both Zn and Fe were recorded. One sample, with error bars indicating the s.d of three reads in **b**. CPH is the spin probe 1-Hydroxy-3-carboxy-2,2,5,5-tetramethylpyrrolidine – HCl. Ir(IV) is the oxidized form of the redox mediator $IrCl_6$. HLPT is the fusion protein under study. AS(O) is the oxidized form of the redox mediator acetosyringone.

We then explored whether AS(O) and Ir(IV) would oxidize amino acid residues or the divalent cation present in the active site. The cation, a Zn^{2+} or Fe^{2+} (depending on preparation methods) is necessary for LuxS function and has been said to leach out of the protein upon oxidation[59]. Since sulfhydryl residues can be easily oxidized by a variety of oxidants[60], and there are several present in HLPT, it was logical to test for this phenomenon. We found from 2 to 5-fold decreases in sulfhydryl levels of LuxS,

Pfs, and HLPT after treatment with AS(O) (Fig. 2.6 d). ICP-EOS determined there was no Zn loss from the LuxS active site (Supplementary Fig. S2.2 b). It also showed negligible quantities of iron (Fe). Thus, we were able to conclude that AS(O) oxidized sulfhydryl residues on Luxs, Pfs, and HLPT, as well as other likely targets, but did not seem to affect the presence of the divalent cation in the active site. Therefore, HLPT activity decrease due to oxidation by AS(O) may be due to amino acid residue oxidation and possible loss of active protein configuration rather than oxidation of the active-site Zn. This opens the doors for using AS(O) to potentially oxidize and attenuate the activities of other various enzymes, including those with sulfhydryl groups vulnerable to oxidation.

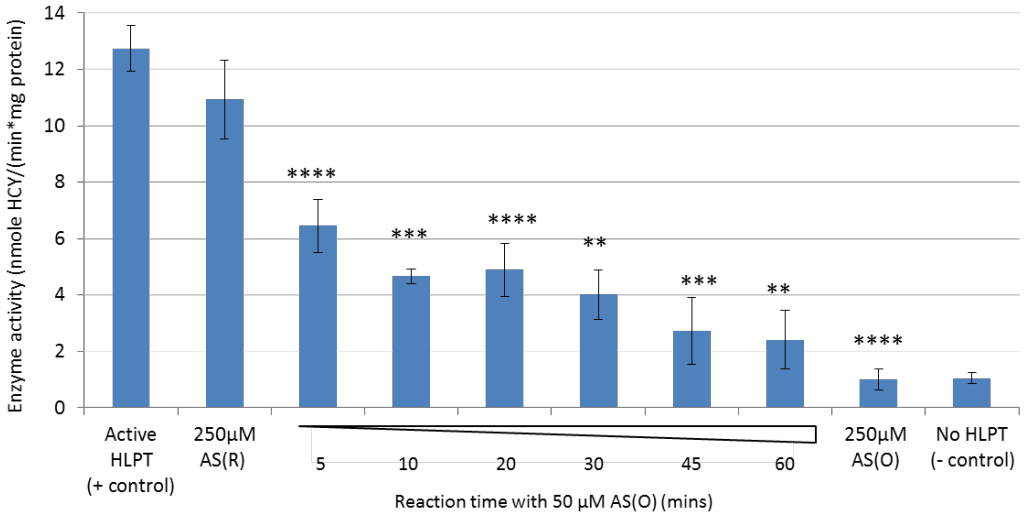

Supplementary Figure S2.3: Solution-based AS attenuation of HLPT activity. AS(R) or AS(O) at the indicated concentration was reacted with 1.5 µM HLPT for different amounts of time. 250µM AS(R) and AS(O) were reacted for 1 hour. Activity decrease shows a time-dependent response in the case of AS(O). Three samples were measured and averaged. Error bars represent s.d. P values were calculated using student's t-test (two tailed, unequal variance), compared to the active HLPT positive control. ** indicates $p < 0.01$, *** $p <$

0.001, **** $p < 0.0001$. AS(R) and AS(O) are the reduced and oxidized form of the redox mediator acetosyringone. HLPT is the fusion protein under study. HCY is homocysteine.

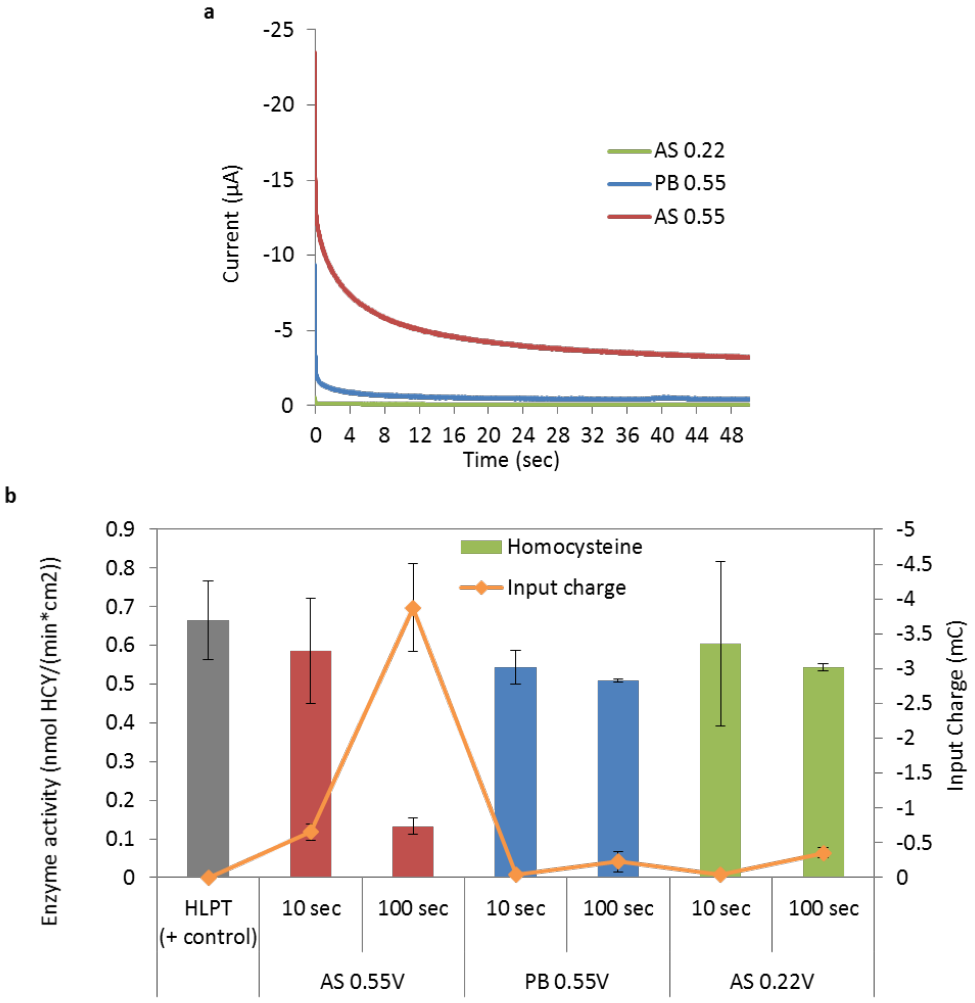

Supplementary Figure S2.4: *In situ* attenuation negative controls. a, Observed current of oxidizing (+0.55 V) or non-oxidizing (+0.22 V) voltages are applied to 250 µM AS and PB solutions with on-chip HLPT. **b**, Input charges and enzyme activity (homocysteine as measured electrochemically) after either 10 or 100 second treatments with the indicated mediator/voltage combinations. Three replicates were measured and error bars indicate s.d. AS indicates the redox mediator acetosyringone starting out in the reduced form. PB stands for phosphate buffer. HCY is homocysteine. HLPT is the fusion protein under study.

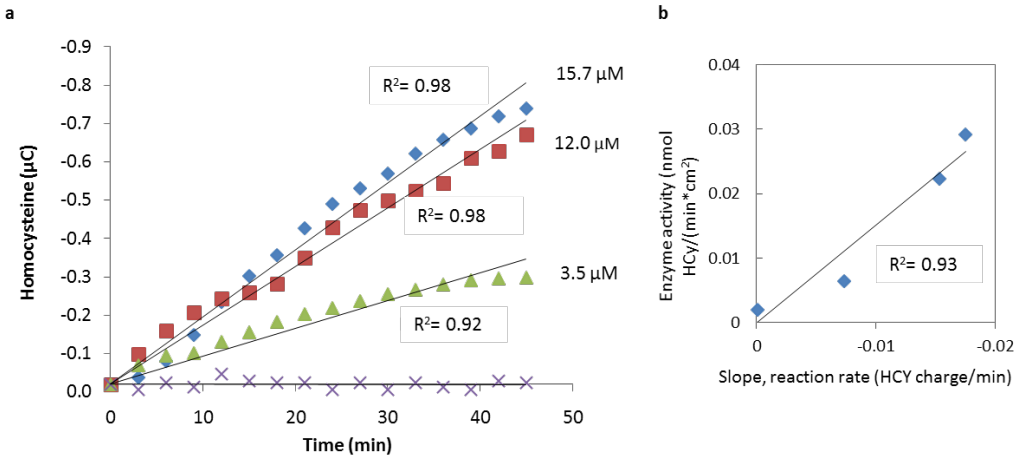

Supplementary Figure S2.5: Real-time activity measurement. **a**, *In situ* monitoring of Hcy evolution by HLPT immobilized and differentially-attenuated on-chip. Concentrations on the right side correspond to final measurements after 2 hours. **b**, Correlation between slopes of lines in **a** and final concentrations. R^2 value indicates the Pearson correlation coefficient for linearity in both **a** and **b**. HCY is homocysteine.

"Setpoint" Calculations and Procedure

The goal of these experiments was to test whether we could predictably "tune" the activity of an assembled enzyme complex to a specific "setpoint". These experiments would demonstrate that if we know the initial activity of the assembled biohybrid device, we may be able to calculate the charge that needs to be applied in order to reach a desired lower activity. In practical applications of our method, this would be the way to use feedback control for setting flux through the pathway and tuning the enzyme activity in real time.

First we used electronic signals to load a sufficient amount of the enzyme onto the chip using the biofabrication methodologies previously described. This was done

to a series of chips, all of which would have the same initial activity. This initial activity (tested by reacting only ONE set of chips in the series for 3 hours with SAH and measuring Hcy generation) (Step 1 in Supplementary Fig. S2.6) was then placed at point (0,y) with y being the calculated enzymatic activity. This point (0,y), was placed on the graph in Figure 2.7.

Our next step was to calculate the exposure line (similar to the trendlines in Fig. 2.7 c), which would allow us to predict the needed input charge to achieve a decrease in activity. We assumed that the slope of this line would be the average of the slopes of the two lines and that it would fall between on Fig. 2.7 c. The slope of our new line along with the point (0,y) allowed us to calculate the x-intercept and place the line on the graph (the equation of the line is given in Supplementary Fig. S2.6). We then decided on the decreased activity that we wanted to tune down to – in our example it was 0.15 nmol Hcy/(min*cm^2) (Step 2 in Supplementary Fig. S2.6).

We used the equation of this line to determine the needed exposure charge/time (-2.25 mC, about 81 sec) at +0.55 V to hit our desired activity level. We then biased several of the chips from the series at or near the calculated time (Step 3 in Supplementary Fig. S2.6). These additional chips were used for application of +/- 1mC of charge so that we could have additional values to test linearity and robustness. All attenuated chips were then incubated with SAH as before and their activity measured. Presumably, if the chips behaved as predicted, then their activities would fall on the line. Specifically, we expected the activity of the chips biased with -2.25mC to be 0.15 nmol Hcy/(min*cm^2). The error bars on both axes of the line in Supplementary Fig. S2.6 were calculated as the averages of those from the points on

the two adjacent lines on Fig. 2.7 c (the same lines as those used for the average slope calculation).

In Supplementary Figure S2.6 we can see that our results (red dot) after attenuation with the calculated charge are within the error range of the predicted values (lighter red dotted circle). The additional electrode chips (yellow dots) also followed the predicted trajectory. Overall, we conclude that electronic attenuation of HLPT using AS is predictable and a desired activity can be reached by performing the calculations above.

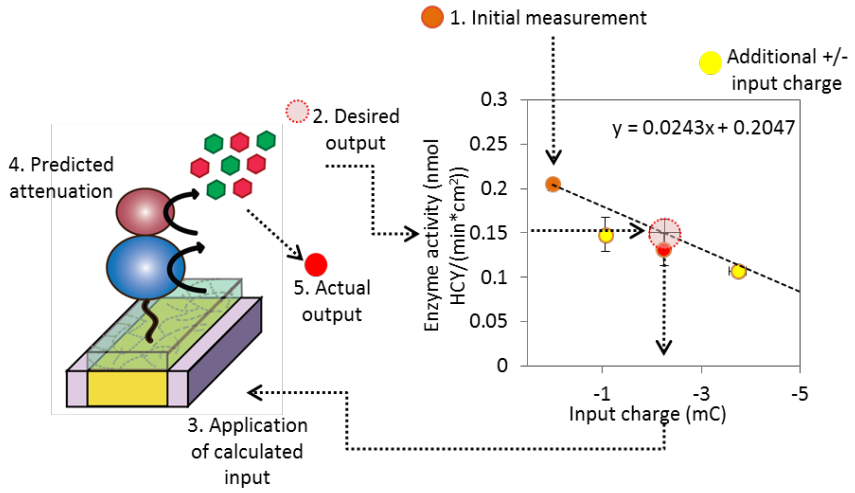

Supplementary Figure S2.6: Predictability of input charge and homocysteine generation. Three replicates were measured and error bars show s.d. The equation of the line was generated as described in the discussion. HCY is homocysteine.

Estimation of Electrons Used to Attenuate a Single Protein Molecule On-Chip

Our hypothesis is that the amount of input charge correlates to activity decrease through oxidation of a predictable amount of proteins – and more

specifically predictable amount of protein residues. These numbers were estimated for electrode-immobilized proteins.

First, the average specific activity in nmol HCY/(min*mg) was calculated from electrochemical measurements of known concentrations (and therefore amounts in mg) of the protein (1.5,2,4,8 μM). This average activity was then used to determine approximate amounts of protein that were immobilized on an electrode - assuming activity was similar to the average calculated for the solution-based protein.

The mg of protein present that were active on the chip were then converted to moles of protein based on molar mass (approximately 50 kDa), and finally to molecules of the protein. We thus had the number of active protein molecules on each attenuated and non-attenuated electrode. Again, this was calculated from the amount of Hcy generated from the chips.

To calculate the number of electrons that each molecule of protein was attenuated by, we first calculated the number of electrons that were used for each input current by dividing the total input charge by the charge of an electron. Then, we subtracted the molecules of protein for a specific sample from that of the positive control (which was not attenuated) to find the apparent decrease in the number of active protein molecules due to the input of current.

The number of electrons used to attenuate a particular sample was then divided by this decrease in number of active protein molecules. This yielded the average number of electrons that were needed in order to attenuate one molecule of protein for a particular data point. This number (30-90) was on the same order of magnitude at the number of easily-oxidized amino acid residues on HLPT. These

include primarily cysteine, but also methionine, lysine, arginine, proline, threonine, histidine, and tyrosine, which can be oxidized by a variety of oxidants, though of course not all of these residues would be accessible [61]. Additionally, electrons were probably used to alter the pH, the chitosan scaffold, and other environmental conditions. We believe that these numbers show that we do indeed have a quantifiable and predictable number of electrons that are used to attenuate each protein molecule. Furthermore, such a number would differ for different proteins and mediator combination and could be useful for determining the amount of current needed to attenuate a specific protein down to a desired activity level.

Electronic Attenuation with Additional Mediators and Proteins

The circular electrode chip described in Methods was used for all on-chip attenuation experiments in this section.

Attenuation of HLPT with the Mediator Ir on a Chip

HLPT was assembled on a chip using the same methods as previously described. Ir(III) was used as the mediator, at a concentration of 500 µM in phosphate buffer pH 7. A method identical to the one described in the methods section for on-chip attenuation was used to oxidize Ir(III) to Ir(IV) *in situ*, which would then oxidize the assembled HLPT and attenuate its activity. Above, we show that Ir(IV) is able to oxidize HLPT in a time and concentration-dependent manner in solution. Here we wanted to illustrate that on-chip attenuation of HLPT can also be done with *in situ* oxidation of Ir(III) to Ir(IV). Chips were incubated in the same manner as indicated in

the Methods section, and activity was measured and calculated again in the same way as before. The results below in Supplementary Figure S2.7 show that we saw a similar trend in activity attenuation by electronically-controlled oxidation of Ir(III) as we did with AS(R). When plotted on the same graph as in Figure 2.7 c, the leveling-off of activity decrease due to input charge is at a similar value to the other series, but the slope does seem to differ significantly.

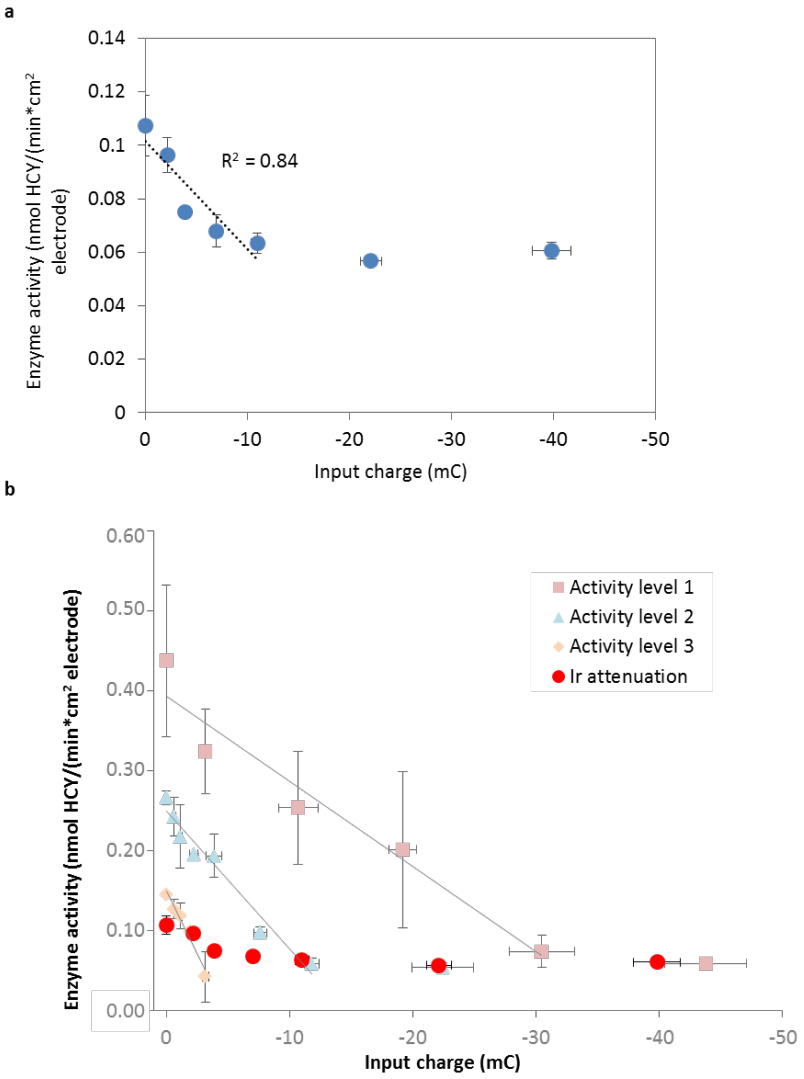

Supplementary Figure S2.7: On-chip attenuation of HLPT with Ir. **a**, The enzyme activity of HLPT is calculated from measured homocysteine product generated resulting from

attenuation of HLPT on-chip with the indicated input charges in a solution of 500 µM Ir(III). Three replicates for each data point were measured and error bars show s.d. The R^2 value was calculated from the Pearson coefficient for linearity. **b**, The same data as in **a**, only plotted on the same axes/graphs (lightened here) as in Figure 3c to show for comparison. Ir is the iridium redox mediator. HCY is homocysteine.

Attenuation of the Enzyme β-galactosidase On-Chip with Both AS and Ir

β-galactosidase is a commonly-used genetic reporter protein and an enzyme that hydrolyzes β -galactosides to monosaccharides. It is a well-studied sulfhydryl-containing enzyme with 19 cysteine residues per subunit [62]. These SH groups are believed to be important for maintaining the active conformation of the enzyme.

We first tested whether Ir(IV) and AS(O) can be used in solution to attenuate its activity. β -galactosidase was first diluted in 40 mM Tris HCl pH 7.5 to a concentration of 0.2 U/µl. Then, 5 µl (for Ir) or 1 µl of a 0.04 U/ µl stock (for AS) of this enzyme was incubated in 100 µl total with the indicated concentrations of Ir(III), Ir(IV), AS(R), and AS(O) in 40 mM Tris for 30 minutes (for Ir) or 2 hours (for AS). To measure the remaining activity, 10 µl of *o*-nitrophenyl β-D-galactopyranoside (ONPG) at 4 mg/ml was added. Another 30 minutes (for Ir) or 2 hours (for AS) were given for the reaction to take place at room temperature, during which the ONPG substrate is hydrolyzed by the enzyme to form *o*-nitrophenol (which is yellow) and galactose. The yellow product can be detected at 420 nm in a clear-bottomed 96-well plate in a standard plate reader. The results below in Supplementary Figure S2.8 indicate that Ir(IV) and AS(O) were able to attenuate β-galactosidase activity, whereas Ir(III) and AS(R) were not.

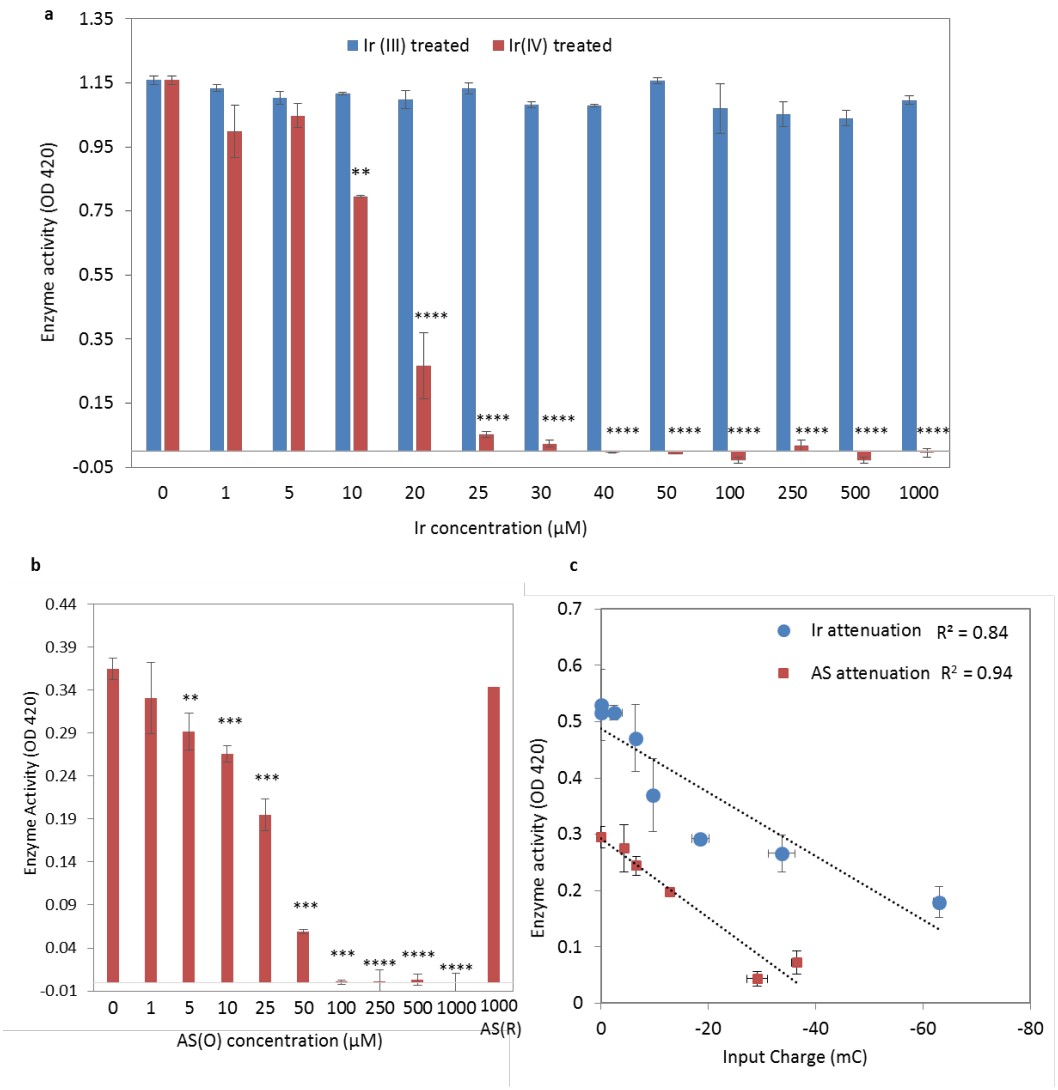

Supplementary Figure S2.8: Attenuation of β-galactosidase activity. a, Enzyme activity as indicated by the OD 420 measurement of the substrate evolution after treatment with either reduced (III) or oxidized (IV) Ir as indicated in the method. **b,** Enzyme activity as indicated by the OD420 measurement of the substrate evolution after treatment with either AS(R) at 1000 µM or the indicated concentration of AS(O). **c,** On-chip attenuation of β-galactosidase with either 500 µM Ir or 500 µM AS, as described in the method in this section. Enzyme activity is measured by the OD 420 of the substrate evolved. Error bars indicate s.d from three measurements for **a** and **b**, and three for the Ir series in **c** and four for AS series in **c**. The R^2 values were calculated from the Pearson correlation coefficient for

linearity for the linear portion indicated by the trendlines in **c**. For **a** and **b** two-tailed, unequal variance student's t-tests were performed for comparing against the 0 - concentration - treated positive control. ** indicates $p < 0.01$, *** $p<0.001$, and **** $p < 0.0001$. Ir(III) is the reduced form of the redox mediator $IrCl_6$, and Ir(IV) is the oxidized form. AS(R) and AS(O) are the reduced and oxidized forms of the redox mediator acetosyringone.

In order to apply our on-chip attenuation method for β-galactosidase we had to modify the steps required for assembling the protein onto the chitosan surface. Since we purchased the enzyme and it did not contain an engineered tyrosine tag for us to use for tyrosinase-mediated assembly, we used an alternative method developed by our group for use with such proteins. This method involves the mixing of the protein and the chitosan and the co-deposition of the protein within the chitosan film. It has been successfully applied to several enzymes [63-65]. Here we were able to successfully use this for β-galactosidase deposition, and retained activity of the enzyme within the chitosan scaffold on the electrode chips. We diluted the enzyme to 1 U/µl in 0.8% chitosan and co-deposited for 2 minutes at 4 A/m^2, after which the chip with the chitosan/enzyme film was gently washed and stored in 40 mM Tris HCl pH 7.5.

For on-chip attenuation, we again used the procedure outlined in the Methods and used either 250 µM AS(R) or 500µM Ir(III) in phosphate buffer, and biased the chips for various times and with a variety of input charges. After attenuation, each chip was incubated with 100 µl of 0.4 mg/ml ONPG at room temperature for 2 hours. These samples were collected and read in a plate reader at 420nm. We can see from the figure above that we were able to attenuate β-galactosidase activity with both Ir

and AS *in situ*, and the activity attenuation seems to correlate with the amount of charge that was used.

Attenuation of Microbial Transglutaminase with Ir and As

Microbial transglutaminase (mTG) is another commonly-used enzyme, and catalyzes the formation of a covalent bond between a free amine group (e.g., protein- or peptide-bound lysine) and the acyl group at the end of the side chain of protein- or peptide-bound glutamine.

To measure mTG activity, a reaction solution of 31 mM CBZ-Gln-Gly, 174 mM Tris pH 6, 87 mM hydroxylamine, 8.7 mM glutathione (reduced form) and 4mM calcium chloride was made. This reaction solution would then be added to the mTG in the indicated volume and incubated at 37 °C. Then a stop solution consisting of 5 % w/v $FeCl_3$ and 12 % v/v Trichloroacetic acid in deionized water was added at the indicated volume. This results in a brown color change, which can be measured at 525 nm in a plate reader. For measuring on-chip activity, the Tris pH was at 7 to prevent the dissolution of the chitosan membrane.

We first tested mTG for activity attenuation by exposure to Ir(IV) and AS(O) as with β-galactosidase above. mTG was from Ajinomoto (Chicago, IL), and was used at a stock concentration of 30 U/mg. To test attenuation of mTG in solution, Ir (III), Ir(IV), AS(R), and AS(O) at 1 mM stock concentrations in PBS were used. 1 µl of the mTG enzyme (at about 5 mg/ml) was incubated with the indicated concentrations in a total of 10 µl in PBS for 2 hours. For attenuation testing with AS(R) and AS(O), 50 µl of the reaction solution was then added for a half hour, with

37 °C incubation for 30 minutes. 50 µl of the stop solution was then added to the reaction, after which the OD at 525 nm was read on a plate reader. For Ir(III) and Ir(IV) attenuation, 1 µl was incubated with the indicated concentrations in a total of 10 µl in PBS for 30 minutes, after which the samples were washed with PBS as HLPT was previously, to dilute out the Ir. The same volumes of the reaction and stop solutions were added. The results below in Supplementary Figure S2.9 show that as with HLPT and β-galactosidase, mTG was attenuated with Ir(IV) and AS(O) but not Ir(III) or AS(R) in solution.

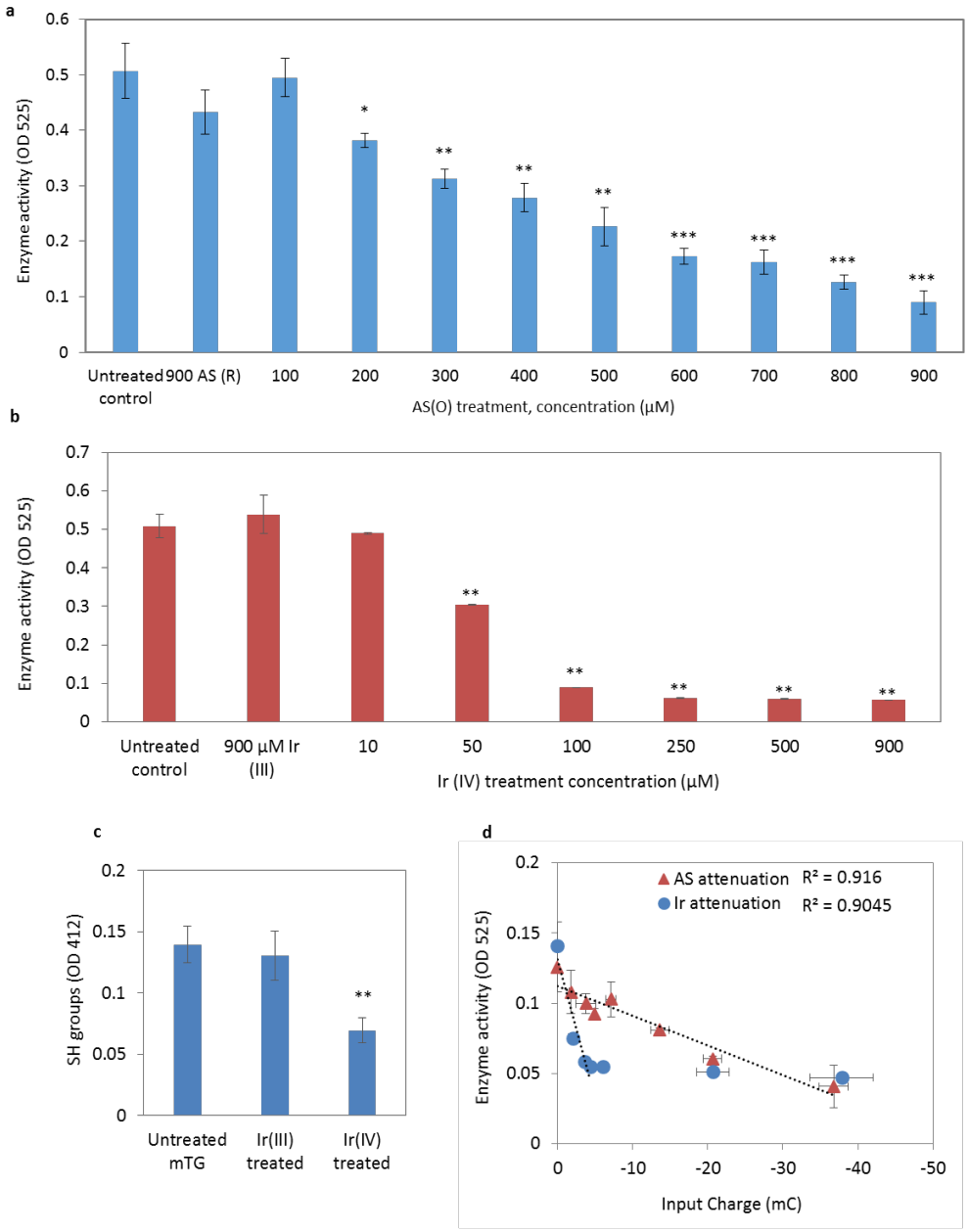

Supplementary Figure S2.9: Attenuation of mTG activity. a, Enzyme activity as indicated by the OD 525 measurement of the substrate reaction with the stop solution after treatment with either AS(R) at 900 µM or the indicated concentration of AS(O) as indicated in the method. **b,** Enzyme activity as indicated by the OD 525 measurement of the substrate reaction with the stop solution after treatment with either Ir(III) at 900 µM or the indicated concentration of Ir(IV). **c,** Sulfhydryl (SH) groups remaining non-oxidized after treatment of

mTG with either Ir(III) or Ir(IV), or untreated. **d,** On-chip attenuation of mTG with either 500 µM Ir or 250 µM AS, as described in the method in this section. Enzyme activity as in **a** and **b**. Error bars indicate s.d from three measurements for **a, b,** and **c**, and two to three for both series in c. The R^2 values were calculated from the Pearson correlation coefficient for linearity for the linear portion indicated by the trendlines. For **a** and **b** two-tailed, unequal variance student's t-tests were performed for comparing against the untreated positive control. * indicates $p < 0.05$, ** $p < 0.01$, and *** $p<0.001$. Ir(III) is the reduced form of the redox mediator $IrCl_6$, and Ir(IV) is the oxidized form. AS(R) and AS(O) are the reduced and oxidized forms of the redox mediator acetosyringone.

For on-chip attenuation, we again used the procedure outlined above for β-galactosidase to entrap mTG within the chitosan. A 3 U/mg mTG in 0.8% chitosan solution was used, after which the chips were stored in PBS. For *in situ* attenuation, 250 µM AS(R) or 500 µM Ir(III) in phosphate buffer were used, and the chips were again attenuated for various times and with a variety of input charges in the same manner as before. Each chip was then incubated with 75 µl of the reaction cocktail as above at pH 7, at 37 °C for 3 hours. These samples were collected, 50 µl of stop solution was added, and read in a plate reader at 525 nm. We can see from the figure above that we were able to attenuate mTG activity with both Ir and AS *in situ*, and the activity attenuation seems to correlate with the amount of charge that was used, as in our results in Figure 2.7, as well as above in Supplementary Figures S2.7 and S2.8.

We believe that the results in the above figures demonstrate that our method can be expanded beyond our model protein HLPT and the mediator acetosyringone. There are likely additional mediators and proteins to which this method could be

applied – and this might need to be determined on a case-by-case basis. We did not optimize the concentrations of the mediators nor the times of exposure or reaction in this section, but we do believe that further optimization could show more interesting trends. On the other hand, without optimization we found consistent results, demonstrating robustness. Additionally, perhaps proteins that are resistant to oxidation would be harder to oxidize using this method.

Chapter 3: Electrochemical measurement of the β-galactosidase reporter from live cells: a comparison to the Miller Assay

The majority of this section is adapted from a manuscript currently in review at *ACS Synthetic Biology* with the same title as the chapter.

Chapter abstract

With our ever-expanding abilities to construct complex synthetic biology systems, facile, real-time monitoring techniques to assess the performance and dynamics of these systems must be concomitantly developed and understood. Electrochemical monitoring offers the above advantages largely because signal transduction stems from direct electron transfer – allowing for potentially quicker and more integrated measurements. One of the most common genetic reporters, β-galactosidase, can be measured both spectrophotometrically (Miller assay) and electrochemically. However, since the relationship between the two is not well understood, the electrochemical method has not yet garnered the attention of biologists. With the aim of demonstrating the utility of the method to the synthetic biology community, we created a genetic construct that interprets and reports (with β-galactosidase) on the concentration of the bacterial quorum sensing molecule autoinducer-2. In this work, we provide for the first time a correlation between electrochemical measurements and Miller Units – enabling the meaningful interpretation of electrochemical signals by synthetic biologists. We show that the electrochemical assay works with both lysed and whole cells, allowing for the

prediction of one from the other, and for continuous monitoring of cell response. We further present a conceptually simple and generalized mathematical model for cell-based β-galactosidase reporter systems that could aid in building and predicting a variety of synthetic biology constructs. This first-ever in-depth comparison and analysis aims to shed light on and facilitate the use of electrochemical real-time monitoring in the synthetic biology field as well as open doors towards creating constructs that can more easily communicate information to electronic systems.

Introduction

Synthetic biology motivates the rewiring of biological systems for a myriad of applications, including sensing, directed feedback response to various inputs and the production of valuable products [66]. One of the aims of the field is to uncover the underlying design principles of biological systems through the rational design of gene and protein circuits[67,68]. Engineered biological systems have already contributed significantly to our understanding of how natural systems function and interact [69-71]. Complex genetic circuits and feedback loops have given us quantitative understanding of gene expression and signal transduction [72,73], insights into the diversity of behaviors that result from various control loops [74], and the ability to rationally control spatial organization and interactions between cells [75-77].

For ease of analysis and for developing designs, genetically engineered cells generally use a set of well-characterized reporters, typically fluorescent proteins such as green fluorescent protein (GFP) or enzymes such as β-galactosidase (β-gal)[78]. Fluorescent reporters, when engineered for short half-lives, allow nearly continuous

tracking of protein expression in live cells over time under varying conditions with intracellular resolution. In contrast, enzymatic reporters offer high sensitivity through signal amplification. Because the enzyme continually generates more detectable product over time, very small amounts of the enzyme can be measured. Requiring lower copy numbers of reporter in order to achieve a desired sensitivity eases the transcriptional/translational burden on the cell[79] so that the process of detection does not independently influence the system's biology.

The β-gal reporter enzyme is one of the most common genetic reporters, and its standard analysis using the Miller assay[80] is a textbook example of a well-quantified method for measuring protein expression and enzyme activity. Typically, cell samples are collected and lysed at specified time points, and the freed enzyme is allowed to react with the substrate, ortho-nitrophenyl- β –galactoside (ONPG). The yellow-colored product o-nitrophenyl (ONP) is produced by enzymatic cleavage and is quantified by measuring absorbance. The amount of product, the extent of the enzymatic reaction and the amount of cells in the sample are used to calculate Miller Units, which can be used to compare gene expression across samples taken under various conditions. Although reliable, the Miller assay has critical limitations. The assay requires cell lysis, which prevents continuous measurement or localization of the signal within a cell population. Diffusion and reaction of a different β-gal substrate, X-gal, provides an optical measure of LacZ localization but makes quantification more difficult. These constraints become more problematic as researchers move from traditional flask and well-plate formats towards microfluidic and lab-on-a-chip formats that better support rapid, highly sensitive and selective

measurements. As a result, recent influential papers in synthetic biology have mainly relied on fluorescent reporters[13,81,82].

Since one of the aims of synthetic biology is to progress towards analysis and control over natural circuits as well as the design and manipulation of synthetic parts, we must have measurement techniques that track closely with the dynamics of the synthetic system. Such techniques would further the construction of more predictive models of metabolic and cellular networks for both understanding existing and engineering novel circuits. This paper is largely motivated by the great work of the biosensor and biochip community, where researchers have used the redox molecule p-aminophenyl β-D-galactopyranoside (PAPG) as a substrate for electrochemically measuring β–gal activity both inside and outside of cells[83-91]. Many of these systems focus on the development of sensitive electrode and biochip systems that can provide real-time measurements on the microscale, are cost-efficient, and allow easy integration with electronic systems.

Electrochemical sensing uses electron exchanges between redox-active molecules and electrodes to generate measurable electrochemical signals. The fast kinetics of electrochemical methods make them promising for dynamically monitoring constructs of synthetic biology. Additionally, the electronic output provides quantitative data that can be easily analyzed and used in modeling the system. However, many such electrochemical devices for β-gal measurement are manufactured in-house, precluding their proliferation among synthetic biology laboratories. Moreover, there remains no direct comparison to a standard that is well understood by synthetic biologists - the Miller Unit. This disconnect motivated us to

investigate the relationship between the electrochemical (using PAPG) and spectrophotometric (using ONPG) methods of measurement of β–gal to better help those familiar with the Miller Unit understand how to take advantage of electrochemical sensing.

Here, we show for the first time that the electrochemical substrate PAPG can be used to detect β–gal in a manner comparable to when ONPG is used as a spectrophotometric substrate. We demonstrate the electrochemical method by quantifying the responses of both whole cells expressing β–gal and lysed cells, and correlate both responses to the Miller assay. We created a whole-cell biosensor that detects the quorum-sensing molecule autoinducer-2 (AI-2) and responds by producing β–gal in a concentration-dependent manner. The genetic circuitry is generalizable to any stimuli or molecular cue that evokes a cell response, contingent on a genetic link to a natural or synthetic promoter. We specifically chose to detect AI-2 because it is a molecule secreted by over 55 bacterial species and facilitates quorum sensing (QS)[92]. QS represents population dependent bacterial communication and response and mediates bacterial virulence and biofilm formation[93]. QS is particularly relevant as the problem of antibiotic resistance escalates[94]. Thus, in our example, we utilize synthetic biology constructs to transduce molecular signals that mediate biomolecular cell-to-cell communication into electrical output signals that can be further quantified, analyzed, and modeled.

We use both our electrochemical and spectrophotometric data to create a computational model of the biosensor under both lysed and whole cell conditions, and correlate the electrochemical sensor measurements to the genetic response through

the Miller assay. With this framework, researchers can measure whole cell response with all the advantages of electrochemical detection, without sacrificing understanding of the underlying genetic response. Overall, our in-depth analysis of the whole-cell electrochemical AI-2 biosensor and corresponding computational model furthers the use of electrochemical monitoring for synthetic biology.

Materials and Methods

Chemical Reagents and Biocomponents

4-aminophenyl β-D-galactopyranoside (PAPG), 4-aminophenol (PAP), β-galactosidase (β-gal) and ortho-Nitrophenyl-β-galactoside (ONPG) were from Sigma-Aldrich. PAPG was dissolved in diH2O and β-gal was dissolved in 40 mM Tris-HCl. PAP and ONPG were dissolved in 0.1 M phosphate buffer (PB). "*In vitro*" autoinducer-2 (AI-2) was produced through previously described biological nanofactories[95]. Briefly, the nanofactory fusion protein HGLPT (His_6-protein G-LuxS-Pfs-Tyr_5) was purified from *E. coli* BL21 *luxS*$^-$ and incubated with 1 mM of the substrate S-(f'-deoxyadenosin-5')-L-homocysteine (SAH) at 37° C with shaking at 250 rpm, resulting in AI-2 synthesis. The enzymatic reaction product was twice extracted by an equal volume of chloroform.

Electrochemical PAP Detection

PAP was detected electrochemically through cyclic voltammetry (CV). CVs were performed with a CHI Instruments 600-series electrochemical analyzer (CH

instruments, Inc.) using an Au working electrode (2 mm diameter, CH Instruments, Inc.), a 4 cm-long platinum counter electrode (Alfa Aesar), and Ag/AgCl reference electrode (BASi). CVs were run from -0.15 to 0.3 V at a scan rate of 50 mV/s. The current at the reduction peak was used to measure PAP concentration.

Bacterial Strains, Plasmids and Culture Conditions

In order to enhance the AI-2 responsiveness of *E. coli* ZK126[96], a double chromosomal knockout of *lsrFG* and *luxS* strain, CT108, was created using one-step inactivation method[97]. Briefly, pKD4 was PCR amplified using primers lsrFGHP1, ATGGCAGATTTAGACGATATTAAAGATGGTAAAGATTTTCGTGTAGGCTG GAGCTGCTTC, and lsrHP2[98]. The PCR product was electrically transformed into ZK126 pKD46 (to express the Red recombinase). *lsrFG:Kan*^{r} recombinants were screened with kanamycin and pKD46 plasmid was cured by growing at 37^{o}C. After confirming the gene replacement by PCR, the kanamycin resistant gene, *Kan*^{r}, was removed by transforming a helper plasmid, pFLPe-Tet (Gene Bridges), to express the FLP recombinase. Then *luxS* was knocked-out from ZK126 *ΔlsrFG* following the similar procedure published before[98]. CT108 was created after the removal of the kanamycin resistance gene similarly descripted as above. Plasmids pCT6[99] and then the commercially-available pET200/D/LacZ (Life Technologies) were introduced via standard heat-shock protocols of chemically-competent cells.

Miller Assay (Colorimetric β-gal Activity Detection)

Miller assay was performed according to standard protocols[80]. Briefly, cells were lysed with chloroform and sodium dodecyl sulfate (SDS) to release *β*-gal. The substrate ONPG was added and cleaved by *β*-gal into a yellow molecule, *o*-nitrophenol. Absorbance at 600 nm, 550nm, and 420 nm was quantified by a Molecular Systems plate reader. The OD at 600nm was measured from 250 µl of cells and the ODs at 420 nm and 550 nm were measured from 200 µl of cells.

AI-2 Detection with Bacterial Biosensor

E. coli CT108 pCT6/pETLacZ was grown in LB Broth, Miller (Fischer Scientific) at 37°C with aeration by shaking at 250 rpm, then reinoculated at 2% and grown to early log phase (OD600 0.2). Cells were incubated with AI-2 at 37 °C with shaking at 250 rpm, then spun down and resuspended in phosphate-buffered saline (PBS) at an OD600 of 2. 0.5 mg/mL PAPG was added and CVs were performed as described above. To validate the electrochemical results, the commonly used Miller assay was performed on lysed cells to quantify β-galactosidase activity.

Cell Lysis

10 % chloroform and 0.005 % SDS were added to cells resuspended in PBS. The reaction was vortexed and incubated at room temperature for 5 min. For absorbance measurements, the reaction was spun down for 4 minutes at 8000 rpm and the supernatant was removed for measurement. For electrochemical measurements,

the reaction was spun down for 1 minute at 14,000 rpm and the supernatant was removed for measurement.

Results and Discussion

Electrochemical characterization of *LacZ* expression

A generalized scheme of the electrochemical detection of PAP to characterize cellular *LacZ* expression is presented in Figure 3.1 a. Molecular cues signal intracellular synthetic biology controllers (represented in abstract form) to drive *LacZ* gene expression, which produces the β-gal enzyme as a surrogate for phenotypic output. To perform electrochemical enzyme activity measurements, PAPG is added, enters the cell, and is cleaved by β-gal into PAP (Figure 3.1 b), in an analogous manner as ONPG is cleaved into ONP for optical measurements. PAP can then exit the cell and be detected electrochemically by oxidation to *p*-iminoquinone using a three electrode system (Figure 3.1 b and c)[64]. The current readout, as can be seen in Figures 3.1 d (cyclic voltammetry scan) and e (peak current of the cyclic voltammograms), is linearly proportional to PAP concentration over a fairly wide range. See Supplementary Figure S3.4 for additional information on the oxidation vs. reduction current of PAP. This method allows the characterization of the amount of β-gal, whether in lysed cells or within an intact cellular environment. Since we foresee this measurement method being especially useful in miniaturized lab-on-a-chip systems, it is important to note that the sensitivity of smaller electrodes towards PAP should not decrease because sensitivity is measured as current/electrode area. Additionally, microelectrode edge effects resulting in enhanced diffusion of PAP to the electrode may actually increase sensitivity on the microscale.

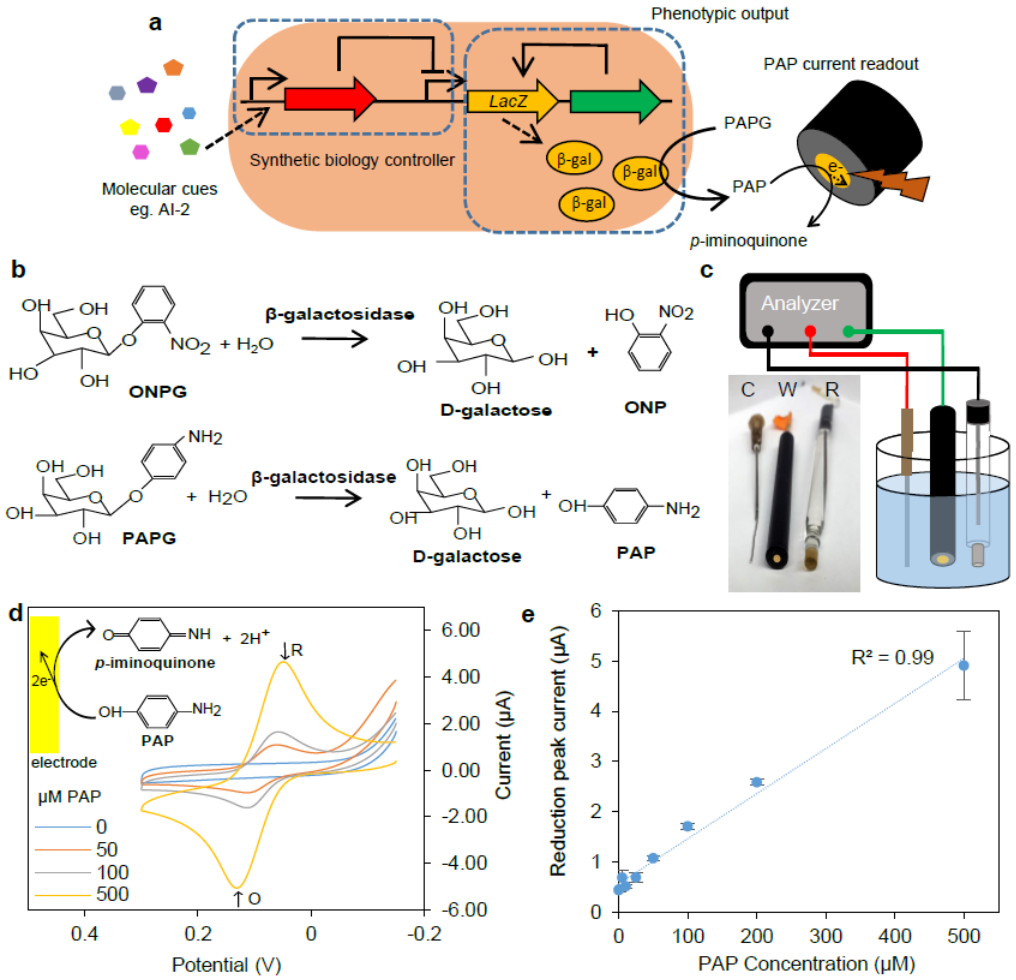

Figure 3.1: Overall goal schematic and PAP electrochemical characterization. a, A general electrochemical biosensing scheme for a cell producing β-galactosidase as a reporter (phenotypic output) from a promoter of choice or a combination of genetic elements (synthetic biology controller) in response to various molecular cues (AI-2 in this paper). Once β-galactosidase is produced, 4-aminophenyl β-D-galactopyranoside (PAPG) is added. PAPG enters the cell and is cleaved by β-gal into the redox active molecule p-aminophenol (PAP). PAP exits the cell and is quantified through cyclic voltammetry at the electrode. **b,** Molecular structures of the cleavage of ONPG to ONP and D-galactose and PAPG to PAP and D-galactose by β-gal. **c,** The counter (C), working (W), and reference (R) electrodes used in this work and a schematic of the electrochemical system setup. **d,** Sample cyclic voltammograms

of different concentrations of PAP using the setup in **c**. Inset showing reversible PAP oxidation to p-iminoquinone at the electrode. R and O indicate reduction and oxidation peaks, respectively. **e,** PAP standard curve shows correlation between PAP concentration and the reduction peak current, taken from **d**.

Characterization of β-gal produced by biosensor cells

To study the utility of electrochemical β-gal detection in cells, we constructed an *E. coli* sensor cell strain (*luxS-, lsrFG-, Δ(argF-lac)169*) that relies on native import and phosphorylation of AI-2 to de-repress expression of the lsr promoter (Figs. 3.2 a,b). Using a two-plasmid system we amplify the native signal strength (*lsr* promoter) by driving expression of T7 RNA polymerase (from pCT6). This, in turn, amplifies gene expression from a generic pET vector, engineered to produce β-gal. This two-plasmid expression system provides biological amplification that greatly increases the sensitivity of the strain to AI-2, as discussed by Tsao *et al.* (2010). As seen in Figure 3.2 c, the cells respond in a predictable, dose-dependent manner; that is, the β-gal response as measured by the Miller assay correlates with the concentration of added AI-2. These response trends correspond with our previous results for systems involving AI-2 uptake by cells[99]. Because the stoichiometry of the reaction using the electrochemical substrate (PAPG) is the same as that using the colorimetric Miller substrate (ONPG), we expect a direct correlation between the Miller and electrochemical assays. We selected cells at 3 hours post-AI-2 induction for further experiments since the responses were robust and the Miller response correlated most closely to the AI-2 concentration (Supplementary Figure S3.1).

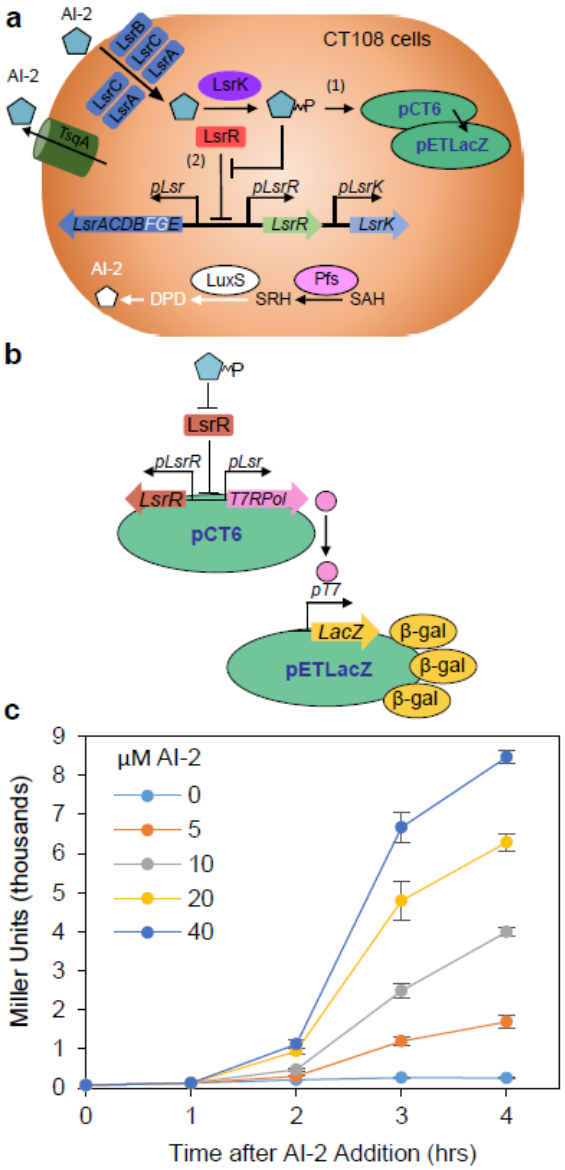

Figure 3.2: AI-2 biosensor characterization. a, The biosensing scheme for a cell producing β-gal as a response to added AI-2. **b,** The synthetic construct, in which the Lsr promoter activation induces β-gal production through a two-plasmid system. Plasmid pCT6 responds to AI-2 by producing T7 polymerase and activating the T7 promoter on pETLacZ, which results in β-gal overexpression. **c,** A time-course response to different added AI-2 concentrations of the above construct, CT108 cells with pCT6 and pETLacZ plasmids. Averages are from 3 samples and error bars indicate S.D.

Real-time electrochemical vs. spectrophotometric measurement of β-gal activity

To establish the electrochemical measurement using our electrodes, we first used purchased β-gal as a reference material. In Figure 3.3, we characterized β-gal activity using both spectrophotometric and electrochemical methods, re-suspending the enzyme in either the Miller assay's Z-buffer or 40 mM Tris-HCl, respectively. These experiments provided a basis for quantifying enzyme (g/L) relative to its activity using both methods and for estimating β-gal concentration within biosensor cells.

The spectrophotometric technique (Fig. 3.3 b) allows measurements that are rapid, sensitive, and linear at low β-gal concentrations. However, we can also see that it takes less than a minute for the highest β-gal concentration - 0.005 U/µl - to generate an amount of ONP that is no longer in the linear range on the spectrophotometer (>1 AU). Higher concentrations would need to be diluted for analysis in the linear range. The electrochemical technique, while also sensitive and linear, better differentiates between higher concentrations of β-gal (Fig. 3.3 c); after 20 minutes of reaction, 0.005 U/µl of β-gal yields a signal still in the linear range. In both cases, rates of product generation were higher with increasing enzyme concentration (as expected), and the two measurements showed a linear correlation with each other (Fig. 3.3 d). Also in Fig. 3.3 d, we can see that the rate of PAP detection is ~5 fold slower than the rate of ONP detection.

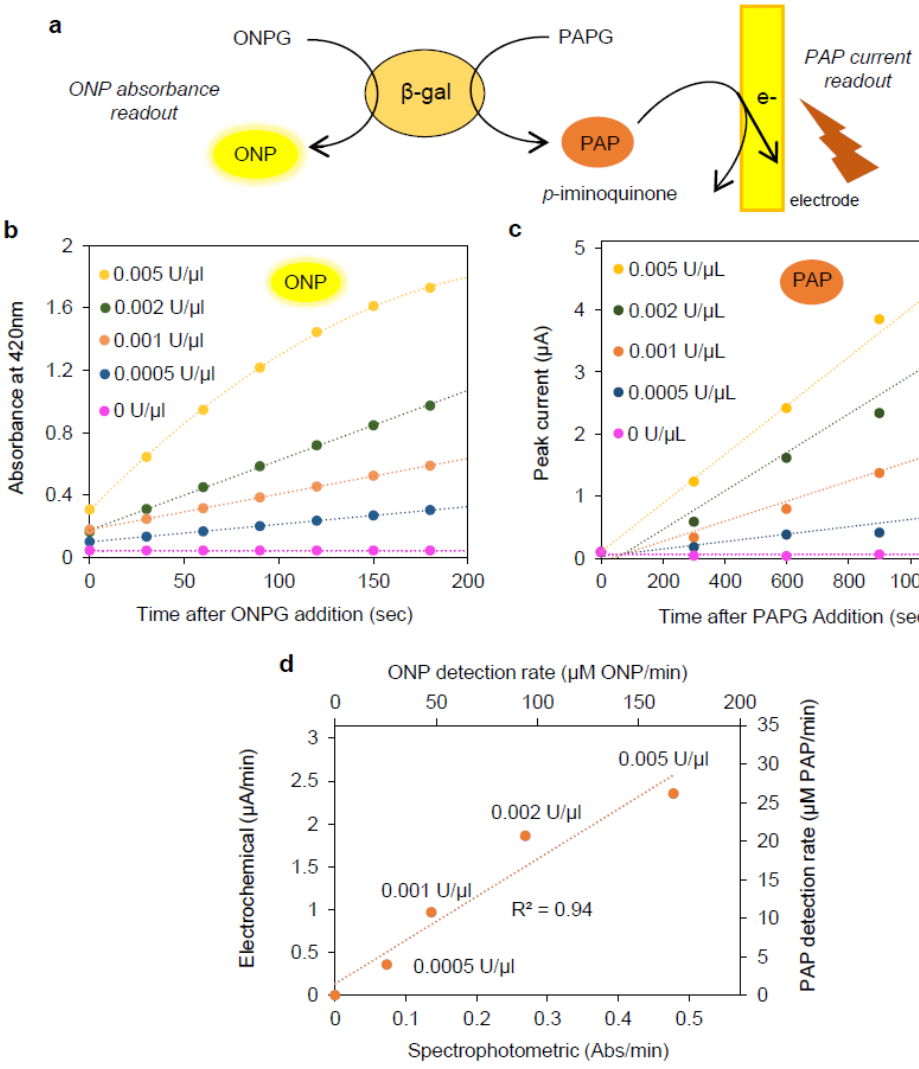

Figure 3.3: β-galactosidase activity detection. a, Scheme of real-time electrochemical and spectrophotometric detection of PAP or ONP produced by β-gal cleavage of PAPG or ONPG. **b,** Spectrophotometric ONP measurement from reactions of various concentrations of β-gal with ONPG over time. **c,** The same β-gal concentrations and conditions as in **b**, where the activity was instead measured by electrochemical detection of PAPG cleavage to PAP. **d,** Correlation between electrochemical measurement rate of PAP detection to spectrophotometric measurement rate of ONP detection from data in **b** and **c**, as well as the same data converted to the same units of µM/min of measured PAP or ONP. All lines in B-D

indicate linear trendlines except for 0.005 U/µl in **b**, which indicates a best fit 2nd order polynomial trendline.

Electrochemical response of AI-2 biosensor cells

We then moved on to electrochemically characterizing the response of our biosensor cells, in which we used cell samples after a 3 hour AI-2 induction. Since the Miller assay requires cell lysis, we first investigated the electrochemical response of lysed cells. The schematic in Figure 3.4 a depicts the relationships between all of the system components. PAP current was measured at 0, 5, 10, and 15 minutes after the addition of PAPG. As can be seen from Figure 3.4 b, the current rose as a function of both time and initial AI-2 concentration. The Miller assay was also performed on the same cells at the 0 time point, and in Figure 3.4 c, we found a linear correlation between the Miller Units and the rate of PAP detection from the same cells.

This allows us to correlate the electrochemical measurement to the Miller Units. To our knowledge this correlation has never been reported for β-gal expressed in any cell type. These data provide direct correlation for the two measurements and demonstrate, at least for this synthetic biology application with *E. coli*, that the assays are easily employed for typical experimental ranges. Finally, these data can be used to approximate the amount of intracellular β-gal in the host cells (Supplementary Figure S3.2).

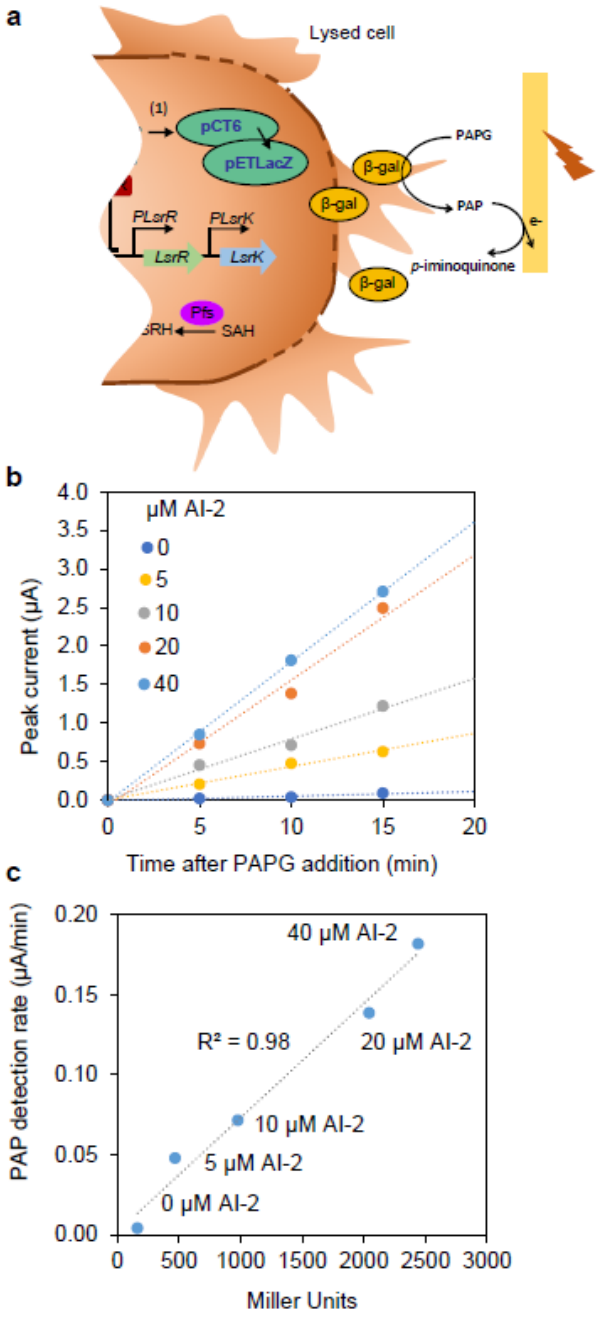

Figure 3.4: Lysed cell electrochemical PAP measurement. a, Scheme of detection of AI-2 by electrochemical measurement of PAP production by lysed biosensor cells. **b,** Detection of PAP from cells induced with the indicated AI-2 concentrations for 3 hours and lysed prior to PAPG incubation for the indicated time. **c,** Comparison of the rate of PAP

detection from the samples in **b** to the Miller units measured from the same samples, indicating a linear relationship and low background. Dotted lines indicate linear trendlines.

In Figure 3.5, we continued our studies with whole live cells. PAP current was measured at the 0, 1, and 2 hour time points after addition of PAPG. Recall that whole cell measurements are not possible via the Miller protocol, which lyses cells. In order to perform measurements in live cells, PAPG and PAP diffusion through the cell membrane is required, which can be quantified using electrochemical techniques. As seen in Figure 3.5 b, the current response correlates with the initial amount of AI-2 added, as was the case with the lysed cells. Multiple experiments are shown which were performed on different days. A more informative representation of our results is shown in Figure 3.5 c, where each point represents both the rate of PAP detection at 2 hours (as in Figure 3.5 b) and the corresponding Miller results of the same cell samples. It is important to note that during those two hours following PAPG addition, the quantity of β-gal within the cells did not vary significantly. Figure 3.5 c shows correlation ($R^2 = 0.97$, with $R^2 = 0.92$ for all points between the Miller Units and the electrochemical response up to about 2000 Miller units. The limit tested for the lysed cells was also in this range, and although above 2000 Miller units we noted larger deviation linearity was still preserved. We also note that the current-generation rate was much lower in whole cells than in lysed cells (Fig. 3.4). The current obtained in the 40 μM case for the whole cells reached 1.5 μA after 2 hours, but the same output was obtained within ~7 min for the lysed cells. Clearly, the intact cells represent a

barrier to PAPG and/or PAP transport, in addition to unknown factors that affect the molecule's concentrations or reactions.

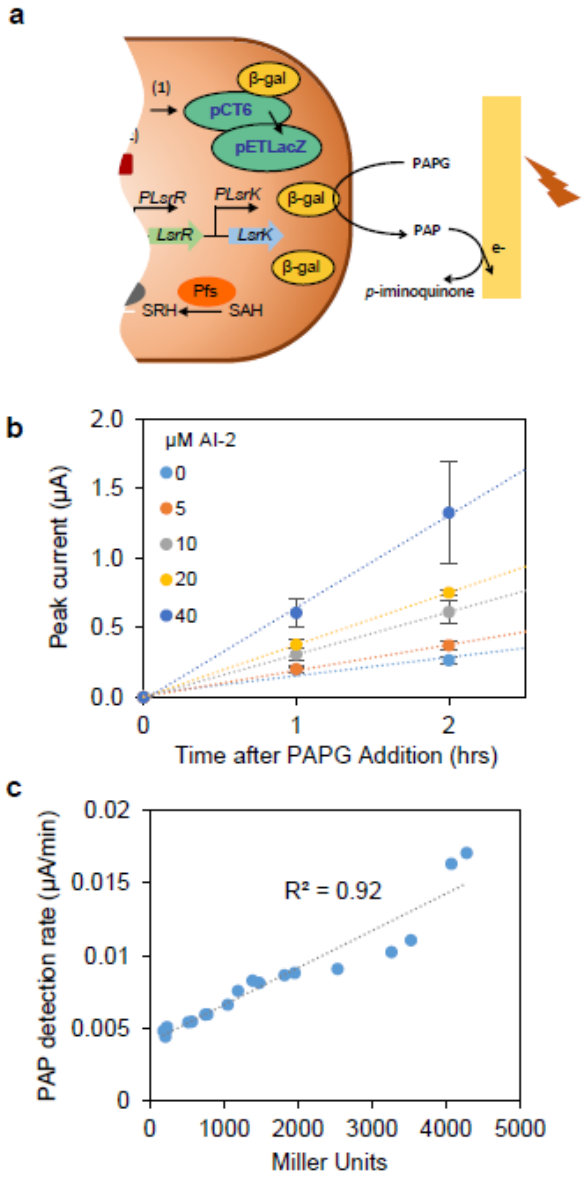

Figure 3.5: PAP measurement from live cells. a, Scheme of detection of AI-2 by electrochemical measurement of PAP production by whole biosensor cells. **b,** PAP detection from whole cells after incubation with the given AI-2 concentrations for 3 hours and then PAPG for the indicated time. Averages are from 3-4 replicates on separate days and error bars show S.D. **c,** The calculated rates of PAP detection over the two hour period versus the

Miller Units of the same cell samples shows a linear relationship. Dotted lines indicate trendlines.

In Figure 3.6 a, we show a comparison between the lysed and whole cell electrochemical response rates, dependent on the corresponding Miller Unit measurements. This allows a prediction of the current for either lysed or whole cells based on Miller assay results. Again, while the whole cell assay was slower, in both cases, linearity was demonstrated. The linear relationships from Figures 3.4 c & 3.5 c were used to construct a line in Figure 3.6 b (see Methods for further information and calculations), which relates the lysed cell assay to the intact cell assay, both measured via electrochemical means. It is evident from the graphs that lysed cell measurements are more than an order of magnitude faster than whole cell measurements for conditions with similar Miller Unit results. Nonetheless, the fact that the detection rates are linear at even low levels of β-gal suggests that relatively rapid analysis of gene expression is possible using this method, especially if more sensitive electrodes are used. Potentially, a normalized unit comparable to the Miller Unit could be calculated from the electrochemical measurements (we present our calculations in the Supplementary Information and Supplementary Figure S3.8). Additionally, we performed similar preliminary experiments using constructs with single plasmids and different promoters and were able to confirm similar trends.

One aspect that is not obvious from the plot is that the amount of background signal for whole cells (~0.005 μA/min, Fig. 3.6 b) was similar to that for lysed cells (~0.004 μA/min, Fig. 3.6 a). This background could be due to a combination of

factors: physical PAPG degradation to PAP or other uncharacterized cell processes resulting in PAPG cleavage, rather than due to reaction by β-gal. We note, however, that experiments without the addition of PAPG resulted in near zero background (Supplementary Figure S3.3), indicating that the cells are not producing additional electrochemical species that overlap with the signal of PAP.

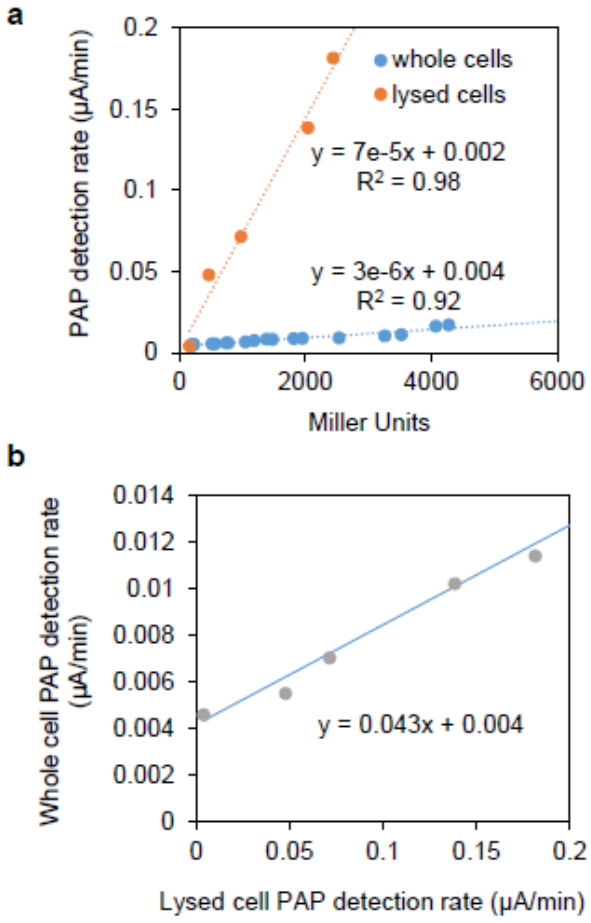

Figure 3.6: Lysed vs. whole cell response. a, Comparison of the rates of PAP detection from whole versus lysed CT108 pCT6/pETLacZ sensor cells based on measured Miller Units in response to different AI-2 concentrations. **b,** The line indicating the relationship/conversion of PAP detection rate from lysed cells directly to whole cells. The

points on the line indicate calculated whole-cell rates for lysed cells with specific Miller Units. Dotted lines indicate trendlines.

The two-compartment mathematical model

We constructed a simple computational model that generates β-gal levels and PAP concentrations in response to PAPG and AI-2 addition to cells with respect to time. In order to build this model, compartments (ie. sub-models) were constructed separately (Figure 3.7 a). The first compartment modeled cell behavior (LacZ expression) in response to AI-2. The second compartment modeled the production of PAP via the substrate PAPG and its response to the enzyme, β-gal. The two sub-models (Figure 3.7 a, 3.7 b) were combined into one final model that was then compared to the lysed cell data. Figure 3.7 c shows that there exists a good correlation between the model predictions and the PAP measurements (see also Supplementary Figures S3.5-3.7). That is, we have divided the model into two compartments so that the latter compartment could be an electrochemical "plug in" to the first compartment, which in turn, would be constructed for any generic construct wherein the first principles reactions could be conceptualized. In our case, the first compartment models the AI-2 – mediated expression of β-gal.

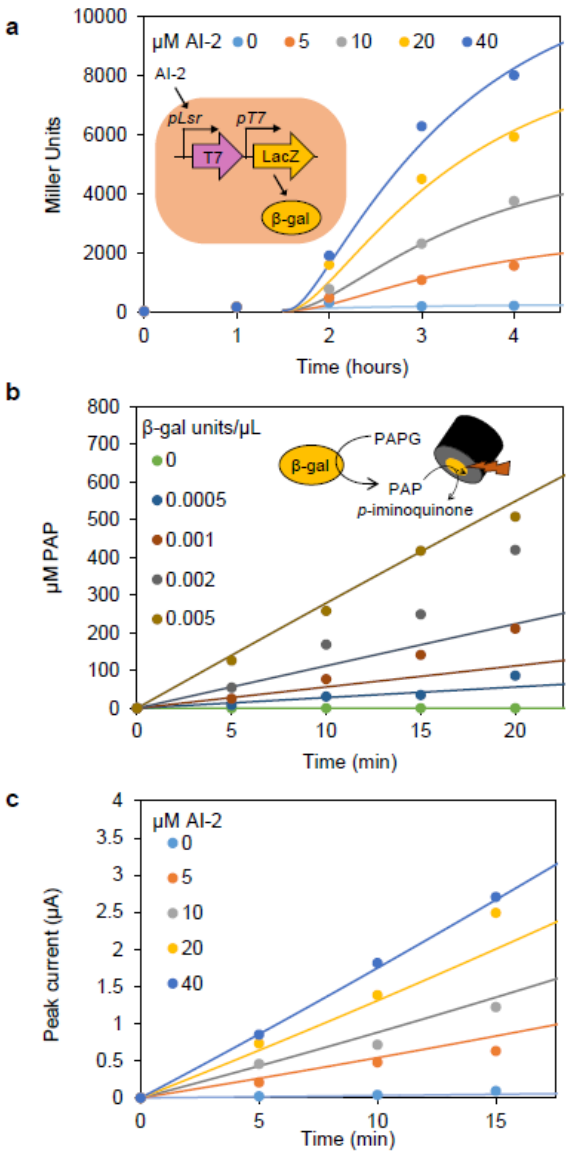

Figure 3.7: Model comparison with experimental results. a, Model results of cell production of β-gal depending on AI-2 induction, converted to Miller Units and overlaid with experimental data. Insert indicates modeled processes. **b,** Model results of β-gal conversion rate of PAPG to PAP overlaid with experimental results. Inserted scheme indicates modeled processes. **c,** Model results of lysed-cell production of β-gal and PAP production converted to current (combination of two modeled compartments in **a** and **b**) and overlaid with experimental results.

Conclusions

In this work, we report the first in-depth comparison of the electrochemical method for measuring β-gal activity in both lysed and intact cells to the gold-standard Miller assay. Our results indicate that the electrochemical method is a feasible alternative that enables added versatility for analysis of synthetic biology constructs, especially in applications exploiting lab-on-a-chip devices or real-time measurements. We demonstrated this by developing a biosensor bacterium that converts the signaling function of quorum sensing molecule AI-2 to electronic signals through a genetic (β-gal) and chemical (PAPG) transducer system. Our results showed that the electronic current measured was proportional to Miller Units from the same samples, and can be used to approximate gene expression in a multi-component synthetic circuit. Such electrochemical measurements would allow for *in situ* analyte detection as they integrate seamlessly into electronic systems, and could therefore provide for programmable measurements of synthetic biology constructs. Additionally, we created a two-compartment model that can be used to predict PAP (and thus electrochemical) output from our construct, and can be modified to accommodate other systems driving *LacZ* expression. We believe this work connects, for the first time, the work of the biosensor community in enzymatic reporter detection, with the standard optical measurement techniques biologists use for the same purpose. A better link between synthetic biologists and biochip / microelectronics designers enables parallel use of each other's' tools and advances the potential for synergistic outcomes.

Acknowledgements

We would like to acknowledge the following grants for funding our work: National Science Foundation (CBET-1435957); the Department of Defense, and Defense Threat Reduction Agency (HDTRA1-13-1-0037).

Supporting Information

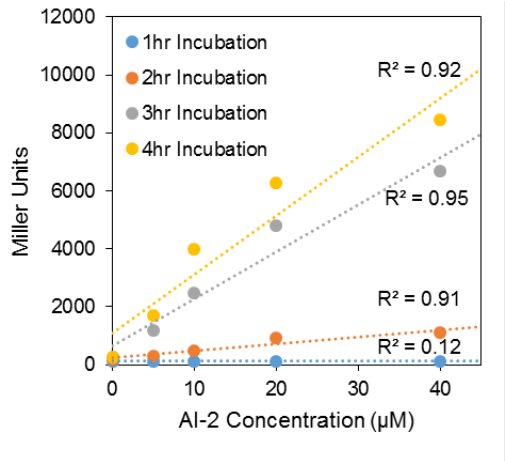

Supplementary Figure S3.1: Biosensor cell response over time. Correlation between the concentration of AI-2 used to induce the biosensor cells and the Miller Units, based on the time after induction (incubation).

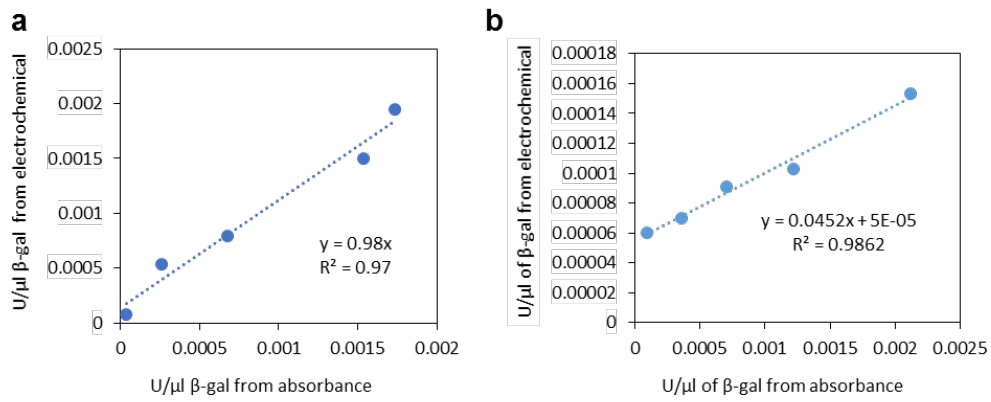

Supplementary Figure S3.2: Spectrophotometric and electrochemical measurement comparisons. a, The linear correlation between the enzyme units calculated from absorbance or electrochemical measurements for lysed cells. **b,** Similar results as in **a** but with electrochemical measurements coming from whole cells.

Calculations: In order to convert absorbance (Abs/min) or electrochemical (µA/min) measurements to β -gal (U/µl), the following equations were used, respectively: $x = (y - 0.0016)/134$ and $x = (y + 0.035)/94.8$ (x is the U/µl and y the measurement in either Abs/min or µA/min). Both equations were calculated from the data in Figure 3.3, where for each β-gal amount a calculated rate (Abs/min or µA/min) was found using Excel's LINEST function. For the absorbance data, the highest enzyme concentration's data was omitted as it was not in the linear range.

We can see that in Supplementary Figure S3.2 a, the rates correlate in almost a 1-to-1 ratio since in both cases the cells are lysed. In Supplementary Figure S3.2 b, however, the electrochemical measurements show a much lower apparent enzyme amount compared to the absorbance measurements. This is because although the absorbance measurements (as part of the Miller assay) were done on lysed cells, the

electrochemical measurements were done on whole cells. The relationship allows us to calculate the underestimation of the electrochemical whole-cell measurement.

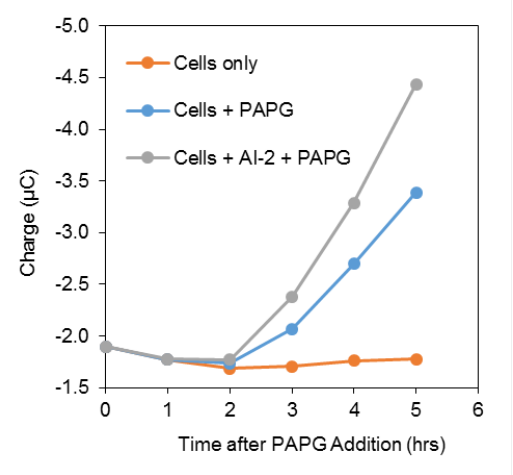

Supplementary Figure S3.3: Control experiments. Performed with biosensor cells different than ones used in the main paper, but which behaved similarly. PAPG concentrations were 0.5 mg/ml and AI-2 was 40 µM. Procedure was similar to that in the paper, and charge measurements were recorded instead of current, but represent similar data.

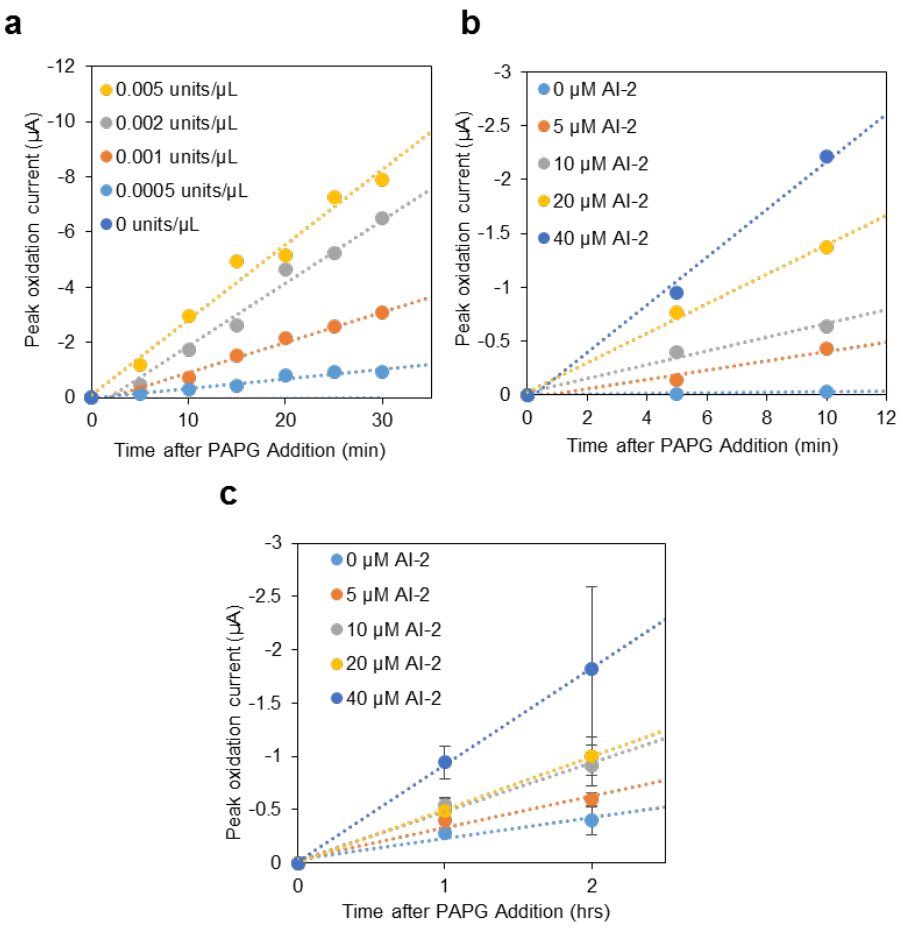

Supplementary Figure S3.4: PAP measurement. a, Oxidation currents of PAP generated by various β-gal concentrations, same as in Figure 3.3 c. **b,** Oxidation current of PAP generated by lysed cells induced with the indicated concentrations of AI-2, same as in Figure 3.4 b. **c,** Oxidation current of PAP generated by whole cells induced with the indicated concentrations of AI-2, same as in Figure 3.5 b.

Calculations for line in Figure 3.6 b

The line was-calculated by equating the x's of the two equations of the lines in 3.4 c and 3.5 c, representative of the Miller Units, and rearranging the combined equation so that the current for whole cells (y1) depended on the current for lysed

cells (y2). This allowed for direct conversion of lysed-cell rate to whole-cell rate for samples with the same Miller Units. The points on the graph indicate lysed-cell points [(x,y) being Miller, current] whose Miller Units were taken and plugged into the whole-cell equation to calculate what the whole-cell current would be for cells with the same Miller Units (x's). The results were used as the y's for the points on the graphs, with the x's being the experimentally-measured lysed cell currents.

The Two-Compartment model

The model for tracking β-gal activity is a two-compartment model. That is, the main model is a construction of two sub-models. The first sub-model is a system of 3 differential equations that model β-gal activity expressed in cells exposed to different levels of AI-2. The known parameter values are taken from literature and the rest are fitted to the data. The second sub-model uses the two Michaelis-Menten differential equations to model PAP production at various concentrations of β-gal. The Michaelis constant (K_{m1}) is taken from the literature. The turnover rate (k_{cat1}) is fitted to the data. The two sub-models are combined to create a model that predicts PAP concentrations at various levels of AI-2 added. To observe the quality of our predictions, the model output is compared to data collected from the lysed cells.

The First Compartment

Data Conversion

In order to fit the sub-model, data was converted from Miller units to μM of β-gal. Using Beers Law, with extinction coefficient e = 4800 and length = 1 cm, we

converted the absorbance at 420nm into μM concentration of ONP. In order to convert μM ONP into μM β-gal, we use the following Michaelis-Menten equations:

$$\frac{d(ONP)}{dt} = \frac{k_{cat_1} E_{o_1} (ONPG)}{K_{m_1} + ONPG} \tag{1}$$

$$\frac{d(ONPG)}{dt} = -\frac{k_{cat_1} E_{o_1} (ONPG)}{K_{m_1} + ONPG} \tag{2}$$

with known turnover rate k_{cat1} = 620/s and Michaelis constant K_{m1} = 120 μM[100,101]. E_{o1} denotes the β-gal concentration (μM). Assuming that K_{m1} << ONPG, the ONP differential equation simplifies to:

$$\frac{d(ONP)}{dt} = k_{cat_1} E_{o_1} \tag{3}$$

The slope is estimated by least squares regression, so E_{o1} can be solved at each time point to extract the β-gal concentration (μM).

Model Fitting

$$\text{AI-2}_{\text{out}} \xrightarrow{k_{\text{AI-2}}} \text{AI-2}_{\text{in}} \tag{4}$$

$$C_R + \text{AI-2}_{\text{in}} \xrightarrow{k_2} \text{DNA} \tag{5}$$

$$4R + \text{DNA} \xrightarrow{k_3} C_R \tag{6}$$

$$\text{DNA} \xrightarrow{k_4} \text{DNA} + \beta + R \tag{7}$$

For this model, we assume a first order reaction for the influx of AI-2 from the outside. We have simplified the intracellular dynamics and provide equations 8-10 (below) which describe the β-gal enzyme concentration, the LsrR repressor concentration, and the amount of LsrR bound to DNA[102]. These equations base β-gal expression on the interplay between LsrR bound as a repressor and its freely dissociated form. LsrR repression is known to result from the formation of an LsrR

tetramer bound between two distal looped strands of DNA comprising the intergenic region of the lsr regulon[103]. While a significant simplification of the known biochemistry, the topology of the expression kinetics agrees well with our experimental observations. For example, we do not include the phosphorylation of AI-2 by LsrK. We generalize the transcriptions on the pCT6 and pETLacZ into one equation that codes for LacZ and LsrR. Hence, we call k_2 a generalized rate as it takes into account these factors. The law of mass action is used to translate these reactions into differential equations. The constraint C_R + DNA = D_{total}, in which D_{total} is a constant, simplifies the system of differential equations into:

$$\frac{d\beta}{dt} = k_4(D_{total} - C_R) - k_{d_2}\beta \tag{8}$$

$$\frac{dC_R}{dt} = k_3R^4(D_{total} - C_R) - k_2C_R\left(C_{\text{AI-2}}\left(1 - e^{-k_{\text{AI-2}}(t-1.5)}\right)\right) - k_{d_3}R \tag{9}$$

$$\frac{dR}{dt} = k_4(D_{total} - C_R) - 4k_3R^4(D_{total} - C_R) - k_{d_3}R \tag{10}$$

Table 1: Variable/Parameter Descriptions

Name	Description
C_R	LsrR repressor bound to operon (ie acts as a cap over the DNA to block transcription)
AI-2_{out}	Extracellular AI-2
AI-2_{in}	Intracellular AI-2
DNA	represents DNA that codes for β and LsrR
R	LsrR repressor
β	Beta-galactosidase enzyme
$k_{\text{AI-2}}$	rate at which AI-2 enters cell
k_2	generalized rate of de-repression by AI-2
k_3	rate at which LsrR binds to operon
k_4	transcription rate
$C_{\text{AI-2}}$	initial AI-2 concentration
k_{d_2}	LacZ degradation rate
k_{d_3}	LsrR degradation rate

The application of this constraint is explained in Alon[104]. However, in our equations we did not apply the assumption that $\frac{dC_R}{dt} = 0$ (steady state amount of bound repressor).

We induced the synthesis of LacZ by the addition of AI-2; typically aiming for an initial OD of 0.2. To facilitate errors in dynamic lag associated with altered OD's for induction and to account for variability in initial growth kinetics, we have set the initial condition so that the initial appearance of β-gal in the zero AI-2 control culture matched with the simulation at that point. This meant that the simulations commenced at t =1 .5 hrs, or about a half hour before the initial β-gal measurement. The rest of the initial conditions are $C_R(1.5) = D_{total} - 1.175 \times 10^{-6}$ μM and $R(1.5) = 1.692 \times 10^{-5}$ μM. The differential equations were solved using MATLAB.

Table 2: Parameter values and source

Parameter Value	Source
$k_{\text{AI-2}} = 1.7/\text{hr}$	Li et al. (2006)
$k_2 = 0.73/(\mu M\text{-hr})$	fitted to data
$k_3 = 1.055 \times 10^{20}\ /(\mu M^4\text{-hr})$	fitted to data
$k_4 = (1/83.324)/\text{s}$	Fuerst et al. (1986), Bremer/Dennis (1996), Iost et al.(1991), Kanehisa et al.(2000, 2014)
$D_{total} = 13.1 \times 10^{-5} \mu M$	fitted to data
$k_{d_2} = 0.6/\text{hr}$	Santillan et al. (2007)
$k_{d_3} = 0.6/\text{hr}$	assumed (same as LacZ degradation rate)

Table 2 shows the parameter values used in the model. Note that for k_4 (the transcription rate of LsrR and LacZ), we take into account the rate at which the endogenous RNA polymerase transcribes the T7RNA polymerase (2.65 kbp at 39 nt/s)[105,106] as well as the rate at which the T7RNA polymerase transcribes LacZ (3.075 kbp at 200 nt/s)[107-109]. Supplementary Figure S3.5 shows the resulting first sub-model.

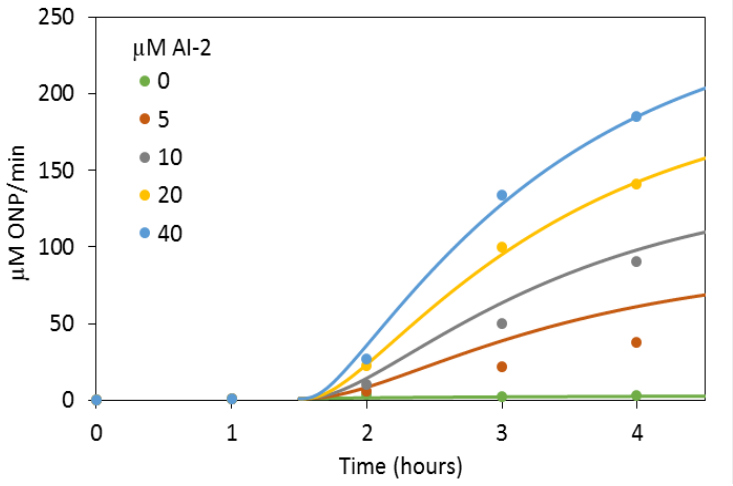

Supplementary Figure S3.5. Cell model and data overlay of experimental data.

Converting µM ONP/min data from model to Miller Units for Figure 3.7 a

In order to convert the data outputted by the model, in µM ONP/min, Miller Units were calculated as follows:

$$\text{Miller Unit} = \frac{1000 \times (OD_{420} - 1.75 \times OD_{550})}{(\text{volume} \times \text{reaction time} \times OD_{600})}$$

To convert the model's output to an absorbance value at 420 nm (OD_{420}) we used Beer's Law as described above. Since the model data was not actual data from cells, we used values for OD_{550}, volume, reaction time, and OD_{600} that were similar to those from the experimental data.

For the OD_{550}, since the experimental values were all almost identical, we used the overall mean for all conversions. The volume and time stayed the same as in the experimental data. The OD_{600}, indicative of the amount of cells present, was averaged for all samples treated with the same AI-2 concentration. These values were

then used to calculate the corresponding Miller Units for the model data and plotted along with the experimental data in Figure 3.7 a.

The Second Compartment

Data Conversion

First, the data were converted into μM. The data describe concentrations of PAP in response to different levels of β-gal. We generated a standard curve that converts current (μA) to μM of PAP. Then, we convert to units of β-gal. To convert units of purchased and powdered β-gal into μM of β-gal, we introduced a factor of ¼ (ie ¼ gram of β-gal for every 1 gram of powdered β-gal). This factor can also compensate for the differences between cell-generated β-gal activity and store-bought β-gal activity. After fitting the model (explained below), the resulting turnover rate, $k_{cat,}$ is closer (103.26/s) to the value stated in literature, (90/s)[110].

Model Fitting

Michaelis-Menten equations were again used for the PAPG substrate and β-gal enzyme. However, the parameter values (turnover rate k_{cat} and Michaelis constant K_m) were not documented as well as the ONPG substrate. Viratelle and Yon[110] provided values of k_{cat} = 90/s and K_m = 330 μM. Since these values, nor any combination of k_{cat} and K_m, do not produce a reasonable fit that encompasses all our data, we fixed K_m and searched for the k_{cat} that minimized the distance between the model and the data points. Overall, the values we found were within expected variances based on our experience, k_{cat} = 103.26/s and K_m = 330 μM.

Similar to above in which μM of ONPG was converted into μM of β-gal, we invoked a similar assumption that K_m << PAPG (excess PAPG). The PAP differential equation of Michaelis-Menten then simplified to:

$$\frac{d(PAP)}{dt} = k_{cat} E_o \tag{11}$$

Since we had PAP (μM) at 5 time points for 4 nonzero levels of β-gal, the slopes were estimated by resolving a linear fit of each of the four datasets. The slopes were applied to the above equation for each level of enzyme to obtain 4 k_{cat} values. This provided a range of k_{cat} values that was used to find the best fit k_{cat} by calculating the least squares fit of the first four time points (as the fifth time point of one of the datasets seemed noisy). The resulting turnover rate was k_{cat} = 103.26/s. In this way, we used the average k_{cat} = 103.26/s and the literature value of K_m (330 μM) for our Michaelis-Menten model, shown below. We used this model to describe PAP activity after the addition of PAPG to β-gal (E_o).

$$\frac{d(PAP)}{dt} = \frac{k_{cat} E_o (PAPG)}{K_m + PAPG} \tag{12}$$

$$\frac{d(PAPG)}{dt} = -\frac{k_{cat} E_o (PAPG)}{K_m + PAPG} \tag{13}$$

The model output is shown in Supplementary Figure S3.6 and there is reasonable agreement, particularly at both limits.

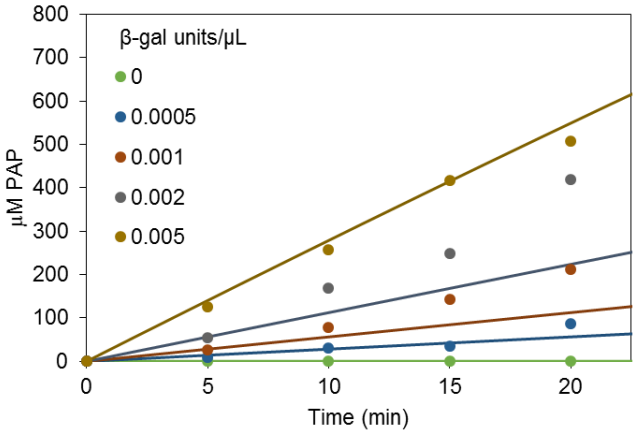

Supplementary Figure S3.6. PAP model and overlay of experimental data.

The Combined Model

The above models (equations 8-10 and 12-13) were then combined into one system of differential equations. The output of the combined model was compared to the data collected from the lysed cells in which AI-2 was added to the cells and the levels of PAP were measured. (Note that cell lysate was used so our results would not include any time lag associated with transport of small molecules (AI-2) or proteins (β-gal) passing through the membrane.)

The data collected represents the PAPG that was added to the cell extracts after hour 3, with the PAP levels measured in the subsequent 15 minutes, at 5 minute intervals. The model was run accordingly and the predictions are shown in Figure S3.3 along with the data points. The data support well, the Michaelis-Menten assumptions and constants evaluated here and reported by others[105-108,111,112].

Again, there is reasonable agreement between the models and the corresponding data, suggesting the mechanisms underpinning the system of ODEs represents a reasonable representation of the actual system. We do not, however,

claim that because the model simulations and the data match, the mechanistic bases are validated. Instead, we suggest that the mechanistic basis for the *in vitro* electrochemical reactions can be faithfully represented by Michaelis-Menten kinetics, largely supported by constants obtained by previous researchers, and that the simplified cell based model describing the kinetics of β-gal expression is sufficiently accurate so that any future cell-based model describing LacZ kinetics could be added to sub-model 2 described here. While this is conjecture at this time, it is the primary motivation for partitioning the model as described and for including here.

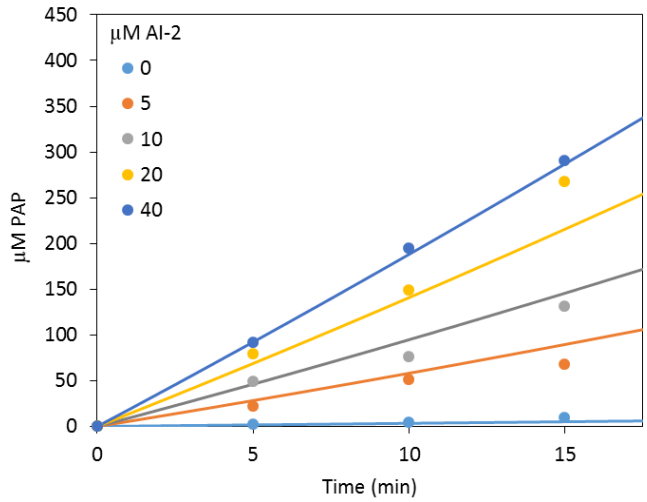

Supplementary Figure S3.7. Final model predictions and lysed cell overlay of experimental data.

Determination of a unit for electrochemical measurements analogous to the Miller Unit:

A unit analogous to the Miller Unit would ideally be developed for normalizing electrochemical PAP measurements. Below we use our data to demonstrate the concept. Here lysed cells will be used since those measurements are

most similar to the way the spectrophotometric measurements are done to get the Miller Units.

$$\text{Miller Unit} = \frac{1000 \times (OD_{420} - 1.75 \times OD_{550})}{(\text{volume} \times \text{reaction time} \times OD_{600})}$$

In the Miller Unit the OD_{420} indicates the resulting ONP generated in a volume of cells (of OD_{600}) after the indicated reaction time. The OD_{550} indicates the scatter from cell debris, and when multiplied by 1.75 approximates the scatter at 420nm.

$$\text{Electrochemical Unit} = \frac{\text{current}}{(\text{volume} \times \text{reaction time} \times OD_{600})}$$

Our analogous unit would take into account the current (in µA) measured after the indicated time (min) of a specific volume (mL) of cells of a certain OD_{600}.

In order to further develop and standardize the electrochemically-measured unit, measurements would need to be performed with various cell amounts and volumes and using different electrode materials, sizes, and setups (the units would likely be different based on the electrodes used). Additionally, any background interference between the cell lysate and the electrode surface would need to be studied and taken into account, especially for smaller electrodes. Below are our sample calculations for lysed cell measurements from Figure 3.4:

Table 3: Calculation of Electrochemical units

AI-2 concentration (µM)	Peak current (at end)(µA)	Time (min)	Volume (mL)	Cell OD600	Electrochemical Units
0	0.093	15	1	2	0.003
5	0.631	15	1	2	0.021
10	1.220	15	1	2	0.041
20	2.490	15	1	2	0.083
40	2.710	15	1	2	0.090

When plotted against the Miller Units from Figure 3.4 c, there is a very good correlation (Supplementary Figure S3.8 below), though again, to standardize this unit much more data would have to be analyzed.

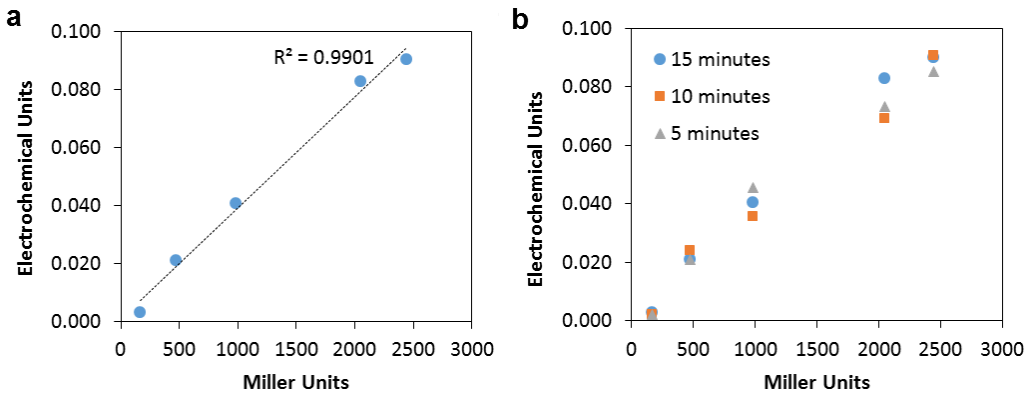

Supplementary Figure S3.8. Normalized Electrochemical Unit vs. Miller Units of lysed cells. a, Linear relationship between the Miller Units measure from the lysed cells in Figure 3.4 c and the electrochemical units calculated as described above from the same cells. **b,** Linear relationship is also maintained with the 5, and 10 minute measurements.

Chapter 4: Electronic control of bacterial gene expression through redox-driven transcriptional activation

This chapter will be turned into a manuscript after some additional work is done and submitted by the end of 2015.

Chapter abstract

The engineering of directional, efficient, and programmable communication between living and nonliving systems has immense potential to harness the distinctive features of each for a variety of applications in both clinical and research settings. However, living cells use small molecules, ions, and protein assemblies to send signals, while electronics utilizes electrons. Here we present the novel use of redox molecules to shuttle information from electronics to *Escherichia coli* (*E. coli*) cells. In our original method, electronic control of the state of the redox molecules pyocyanin and ferricyanide, to which the cells have been engineered to respond with the use of a single promoter, allows for electronic gene control. We show that the signal output (cell response) is dependent on the amplitude and frequency of signal input (electronic charge), allowing for a tunable response. The biological and metabolic underpinnings and effects of the method are also characterized. This work shows for the first time the use of redox mediators to control genetic expression in a reversible and programmable manner, and furthers technologies that aim to combine living and nonliving systems.

Introduction

Communication and information transfer between biology and electronics is a highly sought-after functionality with many applications in both clinical and research settings. If we are to make the best predictions and analyses of diseases as well as study and manipulate the biological environment, we need to grant cells the ability to interpret electric signals into specific pre-programmed functions, which would allow us to manipulate and study cellular behavior with an unprecedented degree of precision. Moreover, gaining electronic control of cell functions would advance bio-hybrid device development, which could lead to a variety of technologies – including implantable bio-hybrid organs and devices as well as remote bio-hybrid robots. Despite this potential, electro-genetic control has not garnered popular attention, with previous such work relying mainly on non-specific effects on the entire *E. coli* transcriptome [113] and a mammalian electro-genetic control circuit (which will be described below) [114].

Existing "bio-electronic communication"

There is, of course, a significant body of literature that concerns itself with electron transport in cells. This includes transport of electrons between cells and between cells and external electrodes or other electro-active species. The articles sometimes have titles or descriptions of the advancements use the words "bio-electronic communication"[115,116]. Below we make the distinction between previous such research and ours.

Electron transport between living (cells) and non-living sources is a topic that can fall under various areas of study. One such area that is also relevant to our research is that of microbial fuel cells (MFCs)[117], where external electrodes are used to accept electrons from cells, thus driving an electric circuit and accomplishing some other goal. The goal is typically either the consumption of waste, the generation of useful chemicals or electricity by the cells, or the measurement of some metabolic or redox status of the cell that can be deduced from the current[118-123]. The electrons reach the electrodes through diffusible mediators (such as in our case), nanowires, or surface bound proteins[124,125]. Although wildtype bacteria are typically used, some have been engineered to enhance the process or to give more-easily-engineered *E.coli* additional functionality[116,126]. The main concerns in these technologies are the ability of the cells to store, transfer, and donate electrons (usually the species of bacteria used and its' electron transfer mechanisms), the method of this interaction, power generation, and the stability of the electrodes and system over time, among others. Typically, genetic responses of the cells to the current or the various redox interactions are not investigated.

In our work, since we utilize ferricyanide as an electron shuttle that interacts with the electron transport chain, we use some of the research principles, setups, and have some similar concerns as those of MFC studies, especially when investigating the metabolic effects of our system. An additional similarity with some of the above research lies in that essentially what we are doing is also drawing out electrons from the cells using the electrode, even though our goal is to put "information" into the cells. However, the big difference between this previously-mentioned research and

ours is that we are not concerned with power, product, or current generation. We are concerned with using electronic control of redox molecules to activate a specific promoter sequence and elicit specific gene expression. In this, our method has more in common with research developing novel methods for precise spatio-temporal gene control such as discussed below.

State of the art of externally-mediated biological gene control

Typical cellular genetic control by an external inducer involves the addition of the inducing chemical to the cell culture media. Varying concentration and time of exposure can result in different cellular responses. Washing the cells, i.e. pelleting and re-suspending in inducer-free media, is one way to determine behavior related to a "burst" of induction. Another avenue that has been pursued for quickly varying and pulsing the concentration of inducer molecules is through the use of microfluidics. A variety of geometries has been implemented in order to allow alternating fluid flows with different inducer concentrations[127-130]. This, however, requires a lot of setup planning and equipment for pumping and controlling the fluid flow and making the channels and devices. Below, we summarize some additional methods that explore the use of stimuli that can be more easily regulated.

The past decade or so has seen a great push towards getting cells to recognize non-biological or non-native signals which can then be used to functionally or genetically control the cells. There are several benefits to this, including faster and more precise (both in terms of location and in terms of genetic elements) control, low background response, and less unintended side-effects. Both application-driven and

basic research have been the end goals. Figure 4.1 shows some examples of using stimuli of non-native origin to control gene transcription. Light waves have been used in a variety of setups- one example being that which is described in Figure 4.1 a, where a light-controlled photo-caging group is released upon light illumination from a molecule, which can then bind to and de-repress a repressor, resulting in gene transcription [131]. More commonly, light-responsive proteins expressed inside cells have been shown by many to induce gene expression or cellular behaviors in programmable temporal patterns and in a variety formats, including in live mice [132-137]. Protein engineering has been also used and has yielded cells that respond to light and produce NO to communicate to electrodes[138]. Light-driven genetic and behavioral control has grown into the field of optogenetics, and has even been used to wirelessly translate human thoughts to gene expression in mice[139].

In addition to light-mediated communication, in Figure 4.1 b is an example of an electrically-driven mammalian genetic circuit where the electrochemical oxidation of ethanol to acetaldehyde drives the production of the enzyme SEAP, whose product *p*-nitrophenolate can be optically detected [114]. In Figure 4.1 c, we can see an example of a remote radio-controlled heating of nanoparticles resulting in calcium influx into the cell, which then results in the gene expression of insulin [140]. Electronic control has also resulted in the influx of calcium in neurons[141]. These are just some example of such innovative genetic control systems.

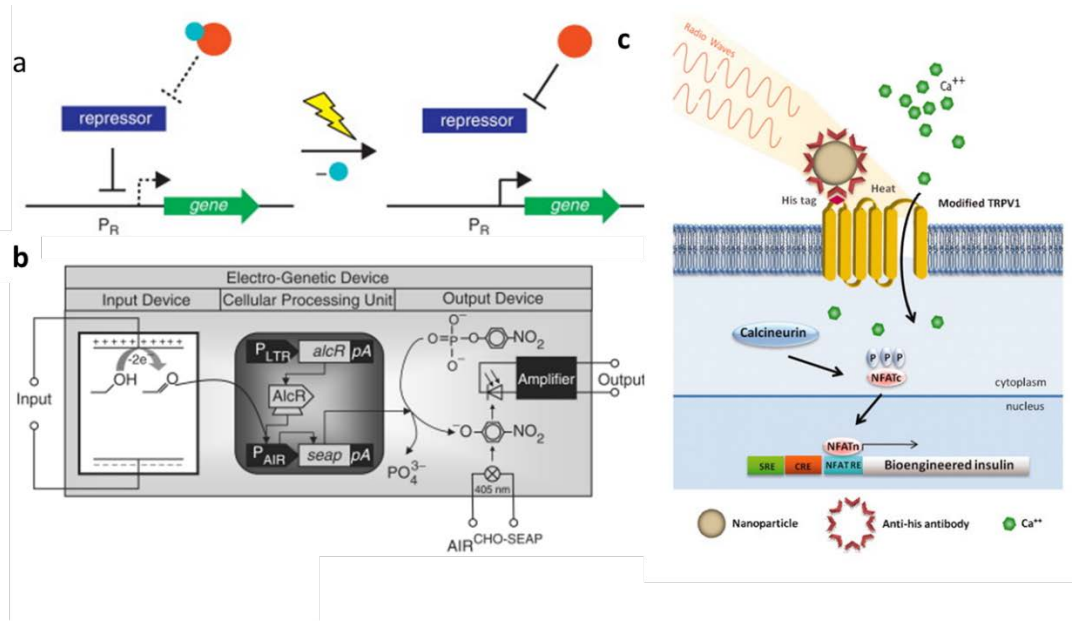

Figure 4.1: **Novel modalities of gene control. a,** Control over gene expression with photocaged small molecule inducers of transcription. The photocaging group is represented by a blue sphere and the small molecule inducer is represented by a red sphere. When the small molecule is caged, the repressor protein will bind the promoter P_R. After UV irradiation the caging group is removed and the small molecule will bind the repressor, which releases P_R, and allows for transcription to occur [131]. **b,** Diagram of the mammalian electro-genetic device. DC applied to the input device results in the electrochemical conversion of ethanol into acetaldehyde, which enables the acetaldehyde-dependent activator AlcR to bind and induce transcription from the promoter P_{AIR}, which triggers transcription of SEAP. SEAP subsequently catalyzes the production of colored *p*-nitrophenolate, which is quantified photometrically at 405 nm by a photodiode and converted into an electric output signal[114]. **c,** Schematic of nanoparticle-induced cell activation and gene expression. Antibody-coated ferrous oxide nanoparticles bind to an epitope, His × 6, in the extracellular loop of the temperature-sensitive TRPV1 channel. Exposure to an RF field induces local nanoparticle heating, which opens the TRPV1 channels. Calcium entry triggers downstream pathways, such as activation of calcineurin, leading to de-phosphorylation of NFAT and its

translocation to the nucleus. There NFAT binds to upstream response elements to initiate gene expression of a bioengineered human insulin gene[140].

All of the above-mentioned stimuli originate from electronic devices whose signals we are able to easily control. The hope is to have more precise, localized, and remotely-activated stimulus control. These ingenious methods have either repurposed naturally-responsive proteins and wired them to behave in a novel way or implemented a combination of nanotechnology and genetic engineering to accomplish their goals. All methods are interesting and have roles in a variety of applications. As can be seem from the above, there has been some interest in using a more direct electronic stimulus, but finding the best method or intermediaries to use has proved challenging. Below we describe how redox molecules could be used to accomplish this goal.

Redox reactions in the cellular context

Cells are continually bombarded by a variety of redox-active molecules both from the external environment and those endogenously produced. There are many biologically-relevant molecules that have redox properties. Some, such as those that are part of the electron transport chain in cells, have very specific locations in the cell and standard potentials tailored to accomplish their tasks. They are well localized and their interactions are thusly contained. Other molecules are diffusible and more promiscuous in their interactions– superoxide, hydrogen peroxide and secreted redox mediators such as pyocyanin are good examples.

There is a biologically-relevant class of redox molecules known as reactive oxygen species, or ROS. These molecules are often generated as byproducts of normal cellular metabolism or as a sign of a diseased state, and can be highly reactive. Because these molecules are often strong oxidants, they can wreak havoc on the cell by "stealing" electrons from a variety of components – damaging proteins, lipids, and DNA[142]. Since these molecules can result in oxidative stress, cells have evolved intricate mechanisms to combat it and bring the conditions back to normal. The OxyR and SoxR proteins, for example, are both part of *E.coli'*s natural oxidative stress response network[143]. They react with damaging redox molecules, such as H_2O_2 and redox cycling drugs, and act to modulate cell genetic responses to mediate the damage and return to homeostatis. Our aim is to hijack one of these redox-responsive proteins to activate engineered genes and control desired cellular behavior.

Pyocyanin and its genetic effects

One redox molecule we propose to use for electrically-driven genetic control is pyocyanin (sometimes indicated as Pyo in figures in this chapter), whose structure can be seen in Figure 4.2 a below. Pyocyanin is a well-studied redox-cycling molecule that is secreted by *P. aeruginosa* and has a number of effects on the metabolism, community organization, and behavior of a number of bacteria[144,145]. Another important effect that pyocyanin has on many prokaryotic and eukaryotic cells is that of oxidative stress generation[146]. Although a complete model of the actions of pyocyanin still has to be elucidated, there is evidence that it enters non-pyocyanin-producing cells in the oxidized form and acts as an oxidant on a variety of

reduced flavins or metal centers of proteins[147,148]. If re-oxidized, it can generate superoxide radicals and hydrogen peroxide and continue its cycling behavior to increase oxidative stress inside the cell[147].

Although high concentrations of pyocyanin are toxic due to the oxidative stress they create, the molecule has also been shown to act as an extracellular electron shuttle in cases of oxygen limitation and in microbial fuel cells[149]. Additionally, our work with pyocyanin has shown that it is reduced by *E.coli* cells in growth media and in anaerobic conditions extracellular pyocyanin remains in the reduced form until re-oxidized either by oxygen or an electrode[150].

To use pyocyanin as a gene activator, we used the specific regulon system that responds to it, the SoxRS regulon[144,151,152]. It is one of the best characterized redox-responsive systems in bacteria, and its workings and effects can be seen in Figure 4.2 b. In *E.coli*, it consists of the SoxR and SoxS proteins. SoxR is an iron-sulfur cluster protein that is usually maintained in an inactive form while its clusters are in the reduced state. Upon the oxidation of the clusters through the actions of redox-cycling drugs, SoxR changes its conformation. This results in the transcription of the SoxS protein from the *soxS* promoter[151].

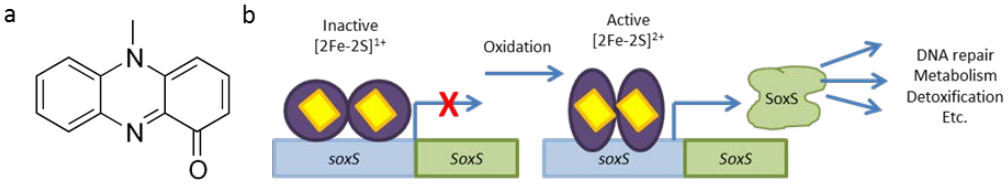

Figure 4.2: Pyocyanin and SoxRS operon. a, The chemical structure of pyocyanin. **b,** The SoxRS regulon in *E. coli*. When the inactive iron-sulfur cluster of SoxR is activated by

oxidation, the *SoxS* gene is transcribed from the *soxS* promoter. SoxS then starts the transcription of a variety of genes involved in DNA repair, metabolism, and detoxification.

The SoxS protein then activates the transcription of a few dozen genes, including those involved in DNA repair, detoxification, central metabolism, and maintaining cellular reducing power[153]. It has previously been hypothesized that redox-cycling drugs, such as pyocyanin, activate SoxR indirectly by first reacting with oxygen and producing the superoxide radicals that then activated SoxR[154]. Recently, Gu and Imlay have shown convincingly that it is not superoxide but rather the redox cycling drugs themselves that directly cause the activating conformational change of SoxR. Menadione, phenazine methosulfate, methyl vialogen (paraquat) and pyocyanin are examples of drugs that were shown to have this effect on the SoxRS system[155]. The role of oxygen in the activation is that of recycling the drugs to the oxidized state either directly or through the electron transport machinery. Once the drug is cleared, the SoxRS system returns to its inactive state through the action of NADPH-dependent reductases which reduce SoxR[156]. Thus the SoxRS regulon, activated by pyocyanin, presented us with a genetic element to implement in our system.

Initially, our thought was to use only pyocyanin as a redox mediator and to control its oxidative form with an external electrode and thus control expression from the *soxS* promoter. Since it has been shown in literature [157] as well as in our work[150] that oxidized pyocyanin can be electrochemically reduced and re-oxidized, the process theoretically allows us to control the specific amounts and timing of oxidized pyocyanin at an electrode. The electrically-oxidized pyocyanin would interact with

SoxR and activate reporter genes under the *soxS* promoter. Using pyocyanin to shuttle electrons from the electrode to the cell and to the SoxR protein to activate transcription in this way would allow us to explore this strategy as a possible spatio-temporally precise way for controlling genetic switches. Many of our initial experiments showed, however, that the pyocyanin-only induction from the *soxS* promoter was not consistently and significantly high enough at low-enough concentrations anaerobically. The reasons for this and the additional components we introduced to the system are described below.

Anaerobic respiration in *E. coli*

One of the most important processes where electron transfer plays a major role inside the cell is during metabolism in the electron transport chain[158]. In both aerobic and anaerobic conditions, *E.coli* cells express proteins and enzymes depending to the electron donors (fuel) and acceptors present[159]. Although we do not present an exhaustive review of *E.coli* metabolism here, this section will explain briefly the processes that are relevant to our studies.

E.coli are facultative anaerobes – meaning they prefer to grow with oxygen but can do so without it by expressing different proteins to take advantage of available alternative electron acceptors. The substrate-dependencies, machineries and pathways are well-documented for *E.coli*, a representation of which can be seen in Figure 4.3 below.

In most studies that describe the use of *E. coli* for applied processes, sugars are used as a carbon and therefore an electron source. They are imported and

phosphorylated using different mechanisms, depending on the sugar. Here we will use glucose as an example. The glycolysis pathway, located in the cytosol, processes the phosphorylated glucose into two molecules of pyruvate, which is accompanied by the release of a net of two ATP and two NADH molecules.

Under aerobic conditions, pyruvate is then converted to acetyl-CoA and carbon dioxide. Acetyl-CoA is further processed within the TCA cycle, which produces more ATP and NADH. The NADH is then used in the respiratory machinery to create a proton gradient, which drives the production of more ATP through ATP synthase. Aerobic electron transport chains contain a dehydrogenase enzyme, which oxidizes an electron donor such as NADH, and a cytochrome oxidase that reduces O_2 to H_2O with the electrons from the donor. Ubiquinone acts as the electron carrier between the enzymes. Cytochrome oxidases can be made with different affinities for O_2, ability to pump protons, cytochrome content, and gene expression profiles. Each of the cytochrome oxidases can receive electrons from various alternative electron-donating dehydrogenases. This allows *E. coli* to grow under aerobic and microaerophilic conditions. It is important to note that both aerobic and anaerobic respiratory chains are modular, with different enzymes produced depending on the conditions or donors/acceptors present.

When oxygen is not present, cells switch into anaerobic respiration or fermentation mode depending on whether and which electron acceptor molecule is present. Electron acceptors include nitrate, nitrite, DMSO, TMAO, and fumarate, among others[160,161] (we discuss below that ferricyanide has been shown to act as an electron acceptor in *E.coli*). Additionally, the enzymes of the TCA cycle are down-

regulated, which leads to an incomplete oxidation of the sugars. Different dehydrogenase and reductase enzymes (used here instead of the oxidase enzymes) are expressed to allow electrons from the available donors to reach the available acceptors (see inset table in Fig. 4.3 below). Here menaquinone is typically used instead of ubiquinone to transport electrons. Depending on available acceptors the number of electrons transferred differs and the cell is able to gain a specific number of ATP molecules through the respiratory processes resulting from the proton gradient or substrate level phosphorylation/fermentation.

When suitable electron acceptors are unavailable in anaerobic conditions, *E.coli* uses fermentation to produce the ATP it needs to function. It is known that acetate accumulates during anaerobic respiration[162] but under fermentative conditions, a mixture of various metabolites such as succinate, formate, acetate, lactate, carbon dioxide, hydrogen, and ethanol are produced to maintain redox balance[163]. After glucose is broken down to pyruvate via glycolysis and ATP and NADH are released, the NADH must be re-oxidized to NAD+ to support further glucose metabolism by the cell. These oxidation steps are accomplished by reducing several of the intermediates (such as pyruvate or a derivative product), which results in the formation of the “mixed acid” fermentation products.

In our experiments, we grew cells in mostly anaerobic conditions, though some aerobic experiments were also performed. The availability and type of fuel, of course, also determines the rates of growth of the bacteria, the movement of electrons, and the production of proteins, including reporter proteins. Additionally, it is important to note that the phenomenon of metabolic burden – the reduction of growth

of cells producing significant amounts of recombinant protein – affected the growth of our cells[79].

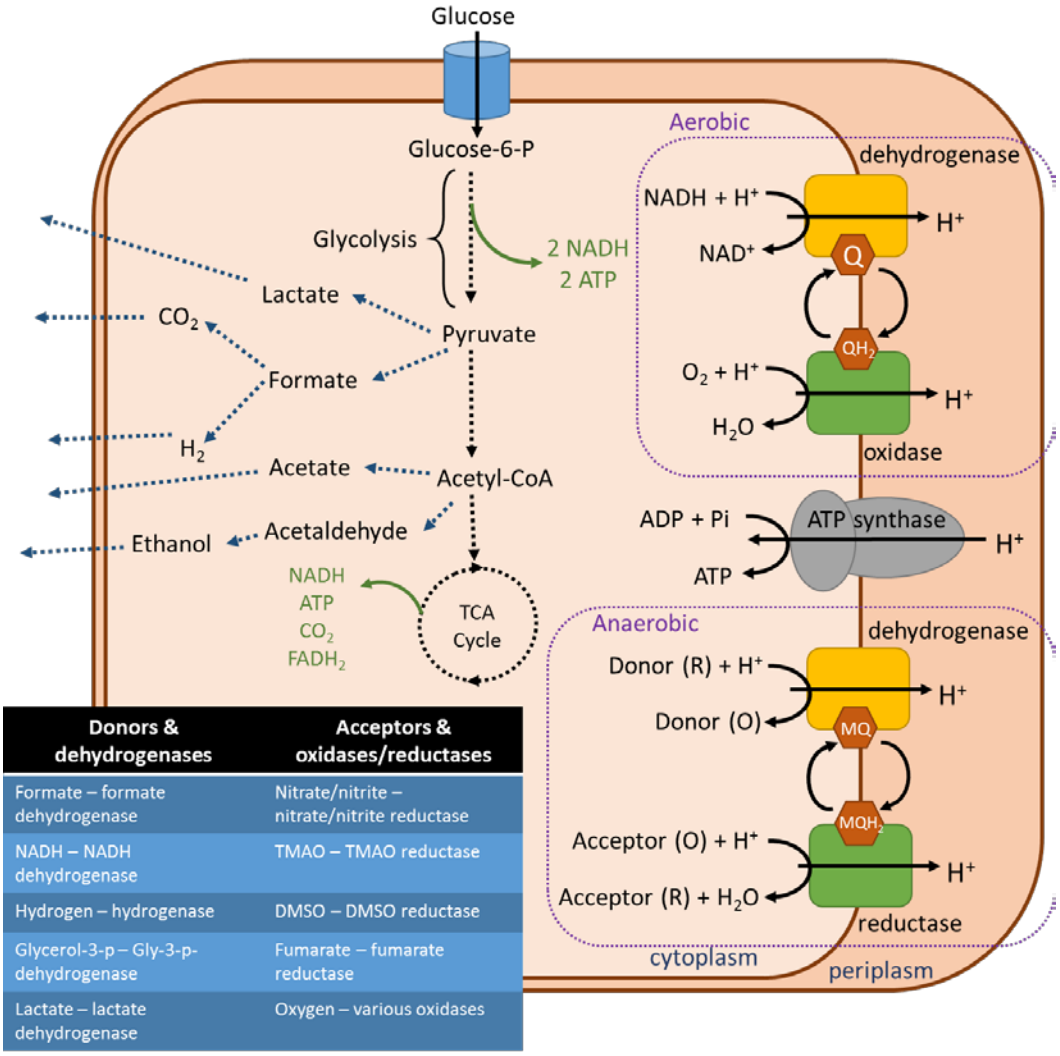

Donors & dehydrogenases	Acceptors & oxidases/reductases
Formate – formate dehydrogenase	Nitrate/nitrite – nitrate/nitrite reductase
NADH – NADH dehydrogenase	TMAO – TMAO reductase
Hydrogen – hydrogenase	DMSO – DMSO reductase
Glycerol-3-p – Gly-3-p-dehydrogenase	Fumarate – fumarate reductase
Lactate – lactate dehydrogenase	Oxygen – various oxidases

Figure 4.3: Schematic overview of metabolism and respiration in *E.coli*.

Schematic showing the metabolic reactions involving glucose – glycolysis, TCA cycle, and mixed acid fermentation (dark blue dashed arrows). If the appropriate electron donors and acceptors are available (insert table) then either aerobic or anaerobic respiration can take place (purple dashed boxes). Some of the ATP synthesis through substrate-level phosphorylation is indicated in green text, along with NADH and other products. ATP synthesis through ATP synthase occurs when hydrogen is pumped back into the cell.

Ferricyanide as an electron acceptor

Ferricyanide and ferrocyanide, oxidized and reduced forms of the same molecule (sometimes indicated as FCN3 and FCN2 in figures in this chapter), are used as a common reference redox couple in electrochemical experiments. The standard potential of the couple is about +0.25 V in the buffered system that we employed[164]. The molecule has been commonly used in biochemical oxygen demand (BOD) and toxicity[165] testing of microbial cultures, as ferricyanide can act as an electron acceptor by interacting with the electron transport chain (Figure 4.4) [166-169]. Upon accepting electrons, the reduced ferrocyanide exits the cell and can be quantified, either spectrophotometrically or electrochemically. The rate of ferricyanide reduction is then used to calculate the metabolic activity of the culture or toxicity of any chemicals tested. The molecule is said to not enter the cytosol of the bacteria or interact with any genetic or cytosolic elements. It has also been used as an electron shuttle in microbial fuel cells[170] and as an indicator for internal redox activity[121], as it "samples" the electron transport chain without being toxic.

Although there has been use of ferricyanide as a microbial electron acceptor, there is still not a great amount of evidence as to which elements of the electron transport chain it interacts with. Some studies indicated that ferricyanide interacts with members of the nitrate respiratory system[171] while others suggest that thiol groups in general play a role[172]. Studies have also shown that ferricyanide promotes ATP generation in *E.coli* through substrate level phosphorylation[173] instead of through the electron transport chain since it may interact with NADH directly instead

of electron carriers in the chain. In Figure 4.4 c we show the standard potentials of various dehydrogenases, reductases, oxidases, and the quinones of the *E.coli* electron transport system. Pyocyanin and ferri/ferrocyanide are also included to demonstrate which components they are most likely to interact with.

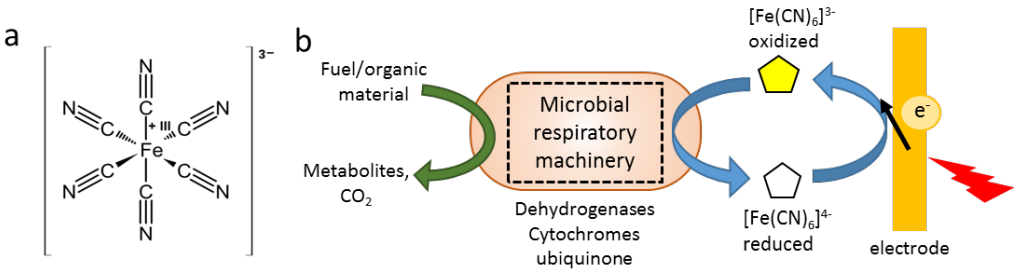

c

Dehydrogenase enzymes	E'$_m$ (V)
Formate DH_N,DH_O	-0.43
Hydrogenase 1,2	-0.42
NADH DH I, DH II	-0.32
Glycerol-3-P DH_N,DH_O	-0.19
D-Lactate DH, L-lactate DH	-0.19
Glucose DH	-0.14
Succinate DH	+0.03

Quinones	E'$_m$ (V)
Ubiquinone	+0.11
Demethylmenaquinone	+0.04
Menaquinone	-0.08

Pyocyanin -0.032

Reductases and oxidases	E'$_m$ (V)
Fumarate reductase	+0.03
TMAO reductase	+0.13
DMSO reductase	+0.16
Nitrite reductase	+0.36
Nitrate reductase A, Z	+0.42
Quinol oxidase III, *bo_3*, *bd*	+0.82

Ferri/ferrocyanide +0.36

Figure 4.4: Standard potentials of electron transport machinery. a, Chemical structure of ferricyanide. **b,** A schematic representation of the interactions between oxidized

ferricyanide and the respiratory chain of microorganisms. The reduced ferricyanide can then be recycled back to the oxidized form at an electrode. **c,** The standard potential of the majority of *E.coli* dehydrogenases, reductases, oxidases, and quinones. Pyocyanin and ferri/ferrocyanide are also included to demonstrate the potential for redox interactions with the enzymes. Data is mostly from Unden and Bongaerts.

Ferricyanide addition to anaerobic cultures has been shown to increase growth rate, which is proportional to the amount of reduced ferricyanide[174,175]. The more recent application-driven research utilizing ferricyanide as an electron acceptor do not postulate on or present specific sites where it may be reduced. Although locating the site of ferricyanide interaction was not part of our research goals, we did investigate the metabolic and growth effects of both ferricyanide and pyocyanin on our cells in order to shed more light on the functioning of the system.

Ferricyanide effect on redox cycling drugs and SoxR

Gu and Imlay[144] showed that adding ferricyanide to an anaerobic culture of bacteria sensitizes them to the effect of redox cycling drugs, of which pyocyanin is an example. Specifically, they saw that SoxR-driven β-galactosidase production was greatly increased in the presence of ferricyanide and phenazine methosulfate (PMS) than with PMS only. They hypothesized that the ferricyanide acted as an electron acceptor and drew electrons through the electron transport chain. The PMS interacted with SoxR, oxidizing it and becoming reduced itself, and then donated electrons into the electron transport chain, becoming re-oxidized, and continuing to oxidize SoxR and drive expression of the β-galactosidase. In this way, ferricyanide increased this

PMS-electron-transport-chain cycling and amplified gene expression. In this paper, Gu and Imlay put forth that oxygen's role in amplifying the response to redox cycling drugs is to cause re-oxidation of the drug internally and that ferricyanide was acting in a similar manner. Based on this data, and after performing our own preliminary studies, we decided to utilize this mechanism to use electrochemical control of ferricyanide form to drive pyocyanin-induced gene expression in anaerobic conditions.

phiLOV- an anaerobic fluorescent protein

Anaerobically-respiring *E.coli* grow slower than when oxygen is present, and produce any oxygen-dependent proteins much slower or not at all. This unfortunately includes many of the commonly-used fluorescent reporter proteins such as GFP, for which oxygen is needed for the fluorophore to mature[176]. Thus for our experiments, without oxygen, an anaerobic reporter was needed to track the response of the cells. We use an engineered anaerobic fluorescent protein with an FMN cofactor that does not require oxygen to produce fluorescence. The protein is called phiLOV [177], and is a genetically-enhanced iLOV fluorescent protein taken from *Arabidopsis thaliana* phototropin 2. Additional benefits of phiLOV include its pH stability (4-9)[178], and small size (112 bp). A degradation tag was put on the protein to allow it to degrade in the absence of the inducing signal (or in the absence of enough inducing signal). This allowed us to use time-variable induction and measure the correlated responses. Additionally, this would allow us to balance inducing with non-inducing forces in order to hone in on a desired protein production rate and total amount.

Dynamic reporter engineering

In order to achieve quick protein degradation and subsequent oscillations a small amino-acid tag, called an ssRA tag, is often used to mark the protein for degradation. Naturally, ssRA tagging occurs when a ribosome encounters and gets stuck on a broken mRNA. Without the normal termination codon, the ribosome then cannot separate from the malfunctioning mRNA. A special type of RNA known as ssRA (small stable RNA A) saves the ribosome by the addition of an eleven-codon degradation tag followed by the stop codon. This allows the ribosome to break free and continue its normal job. The tagged, incomplete protein then gets degraded by the proteases ClpXP or ClpAP. The original ssRA tag had the sequence AANDENYALAA[179], but additional tags have been engineered which result in different half-lives of the proteins[180]. Several recent studies have used this degradation tag on fluorescent or regulatory proteins and have achieved numerous complete oscillations of the fluorescent proteins with one to two-hour cycles [13,181,182]. Here we utilize the ssRA tag AANDENYADAS for fast degradation of a number of proteins, as stated in the text, to achieve dynamic response.

Materials and Methods

Chemicals and Biocomponents

Potassium ferricyanide (III), potassium hexacyanoferrate (II) trihydrate, parafolmaldehyde powder, propidium iodide, pyocyanin ready-made solution from *Pseudomonas aeruginosa*, D-(+)-glucose, sodium nitrite, sodium nitrate, MOPS, and

phosphate buffered saline tablets were from Sigma Aldrich. LB broth, Miller, Agar, KCl, and casamino acids were from Fischer scientific. M9 medium consisted of 1 x M9 salts, 0.4 % glucose, 0.2 % casamino acids, 2 mM $MgSO_4$, and 0.1 mM $CaCl_2$. For *in situ* electrochemical control 100 mM MOPS was also added. M9 salts were made according to common recipes from components purchased from Fischer scientific.

Electrodes and Electrochemical Setup

For bulk electrolysis we used 50 cm-long gold electrodes from Alfa Aesar (0.5 mm diameter, 99.95 % metal basis) wound to increase surface area. Ag/AgCl reference electrode was from BASi. For measurement purposes, an Au working electrode with 2 mm diameter, CH Instruments, Inc. was used. A CHI 600-series potentiostat was used for all electrochemical experiments.

Agar salt bridges were made by bending a 6 inch –long 1.2 mm OD, 0.9 mm ID glass capillary tube (from World Precision Instruments, Inc.) using a Bunsen burner. A 3 % agar solution with 1M KCl was heated and added into the u-shaped capillary tube. This was then cooled by immediately immersing in a 3 M KCl solution. The bridges were stored in 3 M KCl in 4 °C.

For bulk electrolysis, oxidation in this chapter indicates a constant application of +0.5 to +0.51 V and reduction -0.3 to -0.29 V. Typical electrochemical setup for bulk electrolysis and *in situ* experiments was as following: Working electrode and reference electrode in one vial with 3mL of solution and/or cells (about 1/3-way

filled). In a separate similar vial was the counter electrode with another 3mL of solution. Two salt bridges linked the two chambers. A mini magnetic stirrer from Fischer Scientific with a 7 mm stir bar was used to facilitate mixing and accelerate electrochemical conversion in both vials.

Establishment of Anaerobic Conditions

A Coy anaerobic chamber was used in order to maintain anaerobic conditions. It was set up as per manufacturer's instructions and Nitrogen + $CO_2/H_2/N_2$ mix was used to maintain anaerobic conditions.

Cell Strains

The majority of the experiments used the *E.coli* cell line DJ901 (Δ lacU169 rpsL ΔsoxRS90) [183] or GC4468 (Δ lacU169 rpsL) [184]. For cloning the cell lines NEB5α (New England Biosciences) and Top10 Chemically Competent (ThermoFisher Scientific) were used.

Cell Culture

Before beginning of experiments, cells were grown in LB media in 37C in aerobic conditions with 250 rpm shaking until early or mid-log phase (OD600 0.25 – 0.5). For anaerobic experiments the cells were spun down and re-suspended in M9 glucose casamino acids media, unless otherwise stated, and then taken into and grown in a 37 °C mini-incubator inside the Coy chamber.

Bacterial Cloning

E.coli cloning was done according to standard molecular techniques [185]. The SoxR-*soxS* DNA region was amplified from the *E.coli* MG1665 genome using the primers indicated in Table S4.Z and ligated into the TOPO plasmid. The *SoxR-soxS* fragment was then digested out with the BamHI and HindIII enzymes and ligated into a similarly-digested pBR322 vector. The phiLOV protein was produced as a gBlock by IDT (sequence in Table S4.1). The pBR322-SoxR-*soxS*-phiLOVand phiLOV-LAA plasmids were assembled using the Gibson Assembly method [186] by PCR-ing both the phiLOV protein (with or without the tag) and the pBR322-SoxR-*soxS* constructs with the appropriate overlaps using the primers in Table S4.1. The DAS tag was added to the phiLOV protein in the assembled plasmid by PCR-ing the whole plasmid with the LAA tag with the primers in Table S4.1, treating the PCR with T4 polynucleotide kinase and ligating with T4 ligase. The relevant genetic element sequences can be found in Table S4.2.

In all cases DNA was extracted from cells using either a Qiagen or a Zymo Research Miniprep kit according to manufacturer's instructions. Polymerase chain reaction (PCR) was used to amplify genes or DNA of interest using Q5 DNA Polymerase (New England Biolabs, NEB). Primers were ordered from Integrated DNA Technologies (IDT). NEB restriction enzymes such as BamHI and HindIII were used to generate restriction digests of desired PCR products or plasmids. Agarose gel electrophoresis was used to separate DNA fragments based on size and the gel bands (as visualized with SYBR Safe, Invitrogen) as well as DNA sequencing at the IBBR

DNA Sequencing Facility was used to verify the constructs. Digested fragments were ligated using either NEB Quick Ligase or NEB T4 Ligase. Gibson Assembly was performed with NEB's Gibson Master Mix according to manufacturer's instructions. Electro- or chemically-competent cells (either from NEB, Invitrogen or made competent with Zymo Research's Z-Competent *E.coli* Transformation Kit) were used for transformation.

Cell Fixing

Cells were washed and re-suspended in 0.1M Phosphate Buffered Saline (PBS) of pH 7.1 (from tablets). The cells were then fixed with an equal volume of chilled 4% parafolmaldehyde in PBS (pH 7.1) for 30 min at room temperature.

Spectrophotometric Reading

An M2 spectrophotometer was used. To detect absorbance of ferricyanide a 420 nm wavelength was used. To detect cell OD, a 600 nm wavelength was used. In a 96-well plate, volumes varied between 100 – 200 µl, but all compared samples were of the same volume. The OD600 was then converted to a cuvette-equivalent using the spectrophotometer manufacturer's suggested conversion and measured standards.

Flow Cytometry

Flow cytometry was performed by a BD Biosciences FACS Canto with the BD FACSDiva software. Fixed cells were added to 5mL polystyrene tubes, and

measured with the flow cytometer. To ensure sample consistency, 50,000 cells were collected for each sample and consistently gated by forward scatter (FSC) and side scatter (SSC). The mean green fluorescence levels (set to measure FITC fluorescence) are based on the means from the number of indicated samples, and analysis of the cell population was done in FACSDiva and Excel.

Propidium Iodide Staining

Propidium Iodide was used to stain dead bacteria. After the treatment, cells were washed in 10mM MgSO4 (pH 6.5), then PBS, and finally re-suspended in PBS with 5 µg/ml of PI added. The cells were incubated at RT while covered with foil. Afterwards, they were resuspended in PBS and measured with FACS as above, except the excitation and emission were set for DsRed measurement.

Glucose Measurement

Glucose measurements in the media were done using a YSI 2700 bioanalyzer. A standard dextrose membrane and a 2.5g/L standard solution were used. Measurements were done according to manufacturer's instruction.

Results and Discussion

Pyocyanin and ferricyanide-dependent gene induction from the *soxS* promoter

We first investigated the induction of the phiLOV fluorescent protein from the *soxS* promoter in response to the addition of pyocyanin and ferricyanide. Our hypothesis is that pyocyanin interacts with the SoxR protein and oxidizes it, which results in phiLOV protein production (Box 2 in Figure 4.5). Ferricyanide interacts with the cell by acting as an electron acceptor for one or more parts of the electron transport machinery (Box 1 in Figure 4.5). Ferricyanide can be re-oxidized from ferrocyanide by an extracellular electrode. Together, pyocyanin and ferricyanide added to cells amplify the response from the *soxS* promoter through the interaction of pyocyanin with the electron transport chain as it donates electrons into the chain. Ferricyanide allows this process to amplify as it provides an electron sink. These processes work anaerobically since oxygen interacts both with the electron transport chain and with pyocyanin (by oxidizing it).

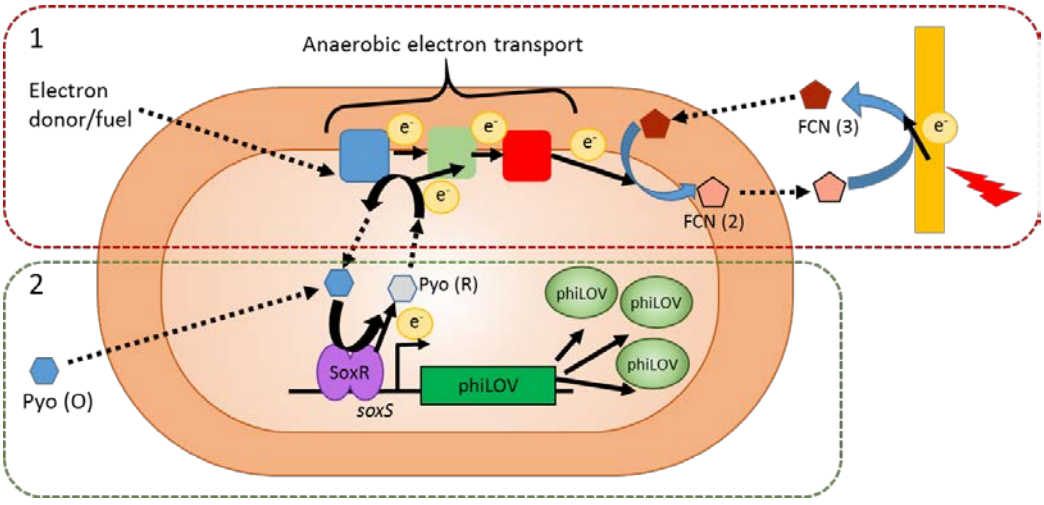

Figure 4.5: Schematic of ferricyanide-driven amplification of pyocyanin-mediated production of philov protein from the SoxS promoter. Box 1 represents

the components that allow ferricyanide to interact with the electron transport machinery (general representation by colored rounded squares) of *E.coli* as an electron acceptor. Electronic recycling of the oxidized FCN3 form allows this process to be controlled. Box 2 represents the oxidation of the SoxR protein by pyocyanin and the subsequent protein production. The functioning respiratory chain (with the electronically-controlled ferricyanide as the acceptor) works to re-oxidize the pyocyanin and amplify the response from the s*oxS* promoter.

We began testing our hypothesis by growing DJ901 cell containing the pBR322 SoxR-*soxS*-phiLOV plasmid anaerobically in M9 glucose media in the Coy Chamber. Increasing concentrations of pyocyanin added to the culture resulted in higher phiLOV production as measured by FACS (Fig. 4.6 a insert). The addition of 5 mM of ferricyanide amplified protein production to a much higher degree than just increasing pyocyanin concentration (up to 17-fold in the case of 5 µM of pyocyanin) (Fig. 4.6 a). Varying the concentration of ferricyanide also changed the amount of protein produced (Figure 4.6 b), and when the degradation tag –DAS was put onto phiLOV and protein production was measured over time, increasing ferricyanide resulted in a higher protein amount over a longer period of time (Figure 4.6 c and d, pyocyanin was 5 µM of pyocyanin). Negative controls of ferrocyanide or ferricyanide only were also tested, and as can be seen from Figure 4.6 b, did not result in an increase of protein. Therefore, we concluded that pyocyanin and ferricyanide are both necessary for the increased protein production from the *soxS* promoter, with pyocyanin initiating the protein production, and ferricyanide amplifying it.

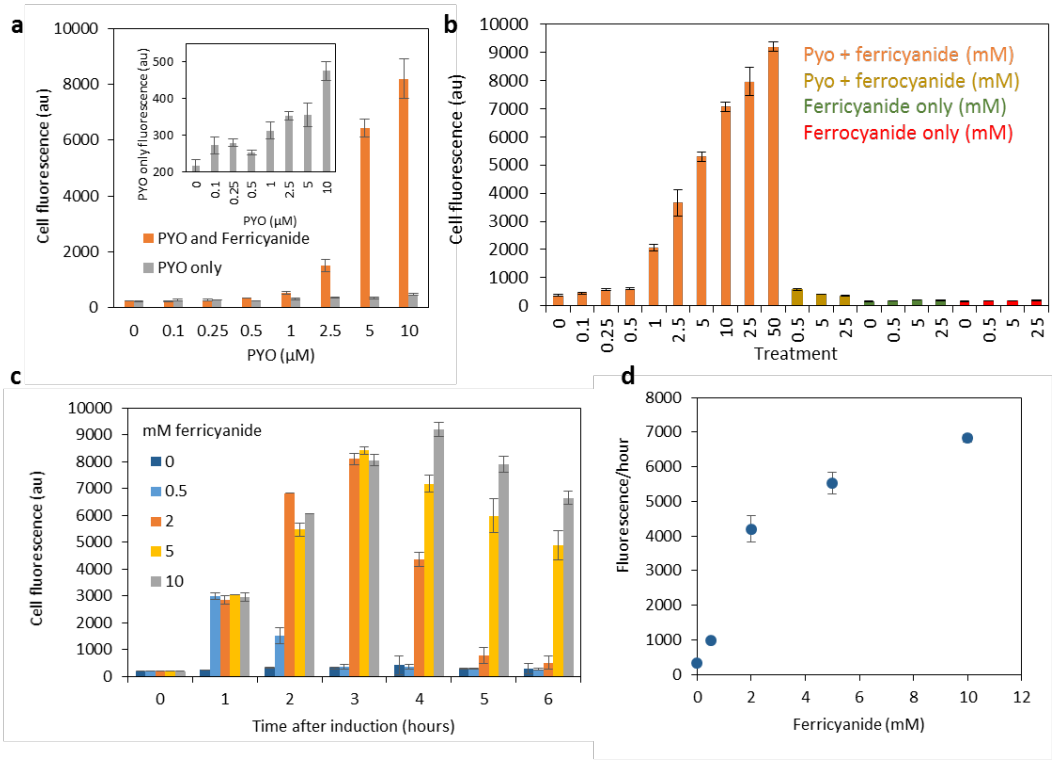

Figure 4.6: Pyocyanin and ferricyanide effect on fluorescent protein production from *soxS* promoter. a, Fluorescent protein production due to pyocyanin and amplification with the addition of 5 mM ferricyanide. **b,** Cell fluorescent response is concentration-dependent on ferricyanide that is added to 5 µM pyocyanin and is not affected by ferrocyanide or ferricyanide alone. **c,** Fluorescent protein time profile with the same pyocanin (5 µM) but different ferriycanide additions. Ferricyanide oxidation by cells results in fluorescence drop. **d,** Data from c averaged over time for each ferricyanide concentration. This takes the amount of protein produced and degraded over the experiment.

We are able to measure ferricyanide reduction by cells to ferrocyanide spectrophotometrically at 420 nm (420 nm absorbance correlates with ferricyanide concentration, Supplementary Figure S4.1). A higher concentration of ferricyanide results in faster reduction rates (Supplementary Fig. S4.2 a, b), as does a higher cell

OD when used with the same ferricyanide concentration (Supplementary Fig. S4.2 d). Additionally, higher cell OD's resulted in lower cell fluorescence (phiLOV production) than lower cell OD's induced with the same pyocyanin and ferricyanide concentration (Supplementary Fig. S4.2 c), indicating that perhaps the diffusion and partitioning of the molecules is dependent on cell amount. For our further experiments we induced cells with starting OD's between 0.2 and 0.4.

In order to test the dynamics of the system we induced the same cells periodically with pyocyanin and ferricyanide for 1 hour and then with pyocyanin and ferrocyanide. We did this by spinning the cells down and re-suspending them in fresh media + inducers. As can be seen in Figure 4.7, when ferricyanide was present, protein production increased, and when ferrocyanide was present it decreased, presumably from the –DAS-driven degradation of the protein. This showed us that the switch of ferricyanide to ferrocyanide and back is enough to turn protein balance in the positive (ON) or negative (OFF). Additionally, cells exposed to the cyclical treatment over time were still able to respond by producing protein.

We further tested the timing of the system by varying the ON and OFF times from 15 to 90 minutes each. Figure 4.7 b shows that a variety of ON/OFF times can be used. The minimum to see a complete ON/OFF cycle seems to lie somewhere between 15 and 30 minutes, as that is how long is needed to switch the cells from mostly protein production to mostly protein degradation states. This can be seen from the fact that the 15 minutes of OFF does not seem to decrease the protein amount, though it does slow down production, whereas 30 minutes results in significant

protein degradation. Additionally, this showed us that a 15 minute lag-time in response is expected in this *in situ* system.

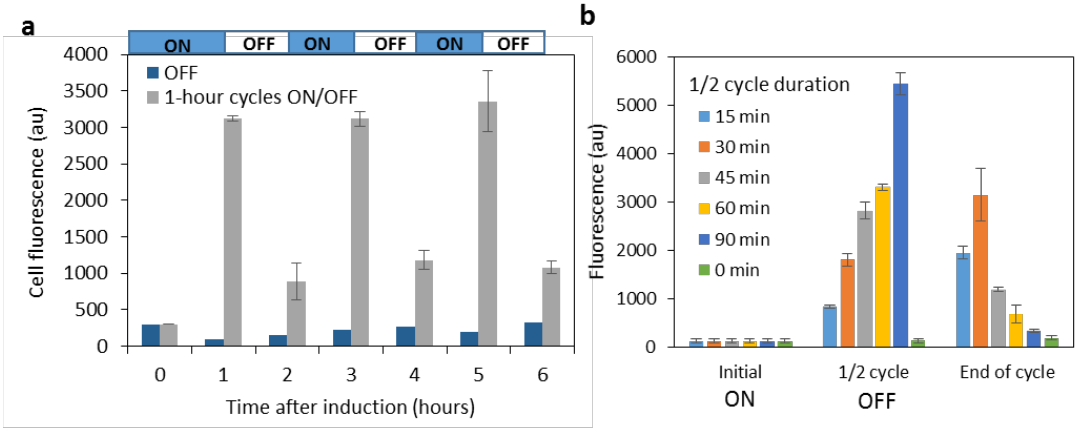

Figure 4.7: Ferricyanide/ferrocyanide cycling effect on cell response. a, Cycling of ferricyanide and ferrocyanide alone results in either increase or decrease of fluorescence, respectively. **b.** Cycling of ferricyanide and ferrocyanide for different lengths of time allows tuning of amplitude of response. After the ½ cycle measurement, cells were re-suspended in the "OFF' solution of ferrocyanide and pyocyanin for the rest of the cycle.

Growth and metabolic effects of ferricyanide and pyocyanin

Since ferricyanide acts as an electron acceptor in anaerobic conditions, and pyocyanin can be toxic to cells, we wanted to check the metabolic and toxicity effects of our treatments. This included the measurement of cell growth, the reduction of ferricyanide (which indicates cell respiratory health), glucose consumption and propidium iodide staining of treated cells. To tease apart metabolic effects of our treatments vs. those due to protein production, we used both the DJ901 cells with our plasmid, and those without any plasmid. Additionally, the GC6648 cells, which are the parent cells of DJ901 (ie. without the SoxR mutation), were also used.

As can be seen in Figures 4.8 and 4.9 below, we first grew cells with various treatments over 8 hours in a 96 well plate and took both OD600 (cell growth) and OD420 (ferricyanide) measurements. Cells without plasmid show a slight decrease in growth rate with added ferricyanide, but a higher growth when both pyocyanin and ferricyanide are added. The same can be seen with the GC4468 cells.

Cells with the plasmid show a slight growth decrease with ferricyanide as well, but due to high protein production with both pyocyanin and ferricyanide, show a marked decrease in growth rate when both are added – with the DJ901 cells showing a much more pronounced decrease than GC4468. The GC4468 cells do not have the genomic SoxR mutation that DJ901 do, and therefore have a higher native/starting defense against pyocyanin, showing a lower anaerobic fluorescent protein production than DJ901 (Supplementary Figure S4.4 b).

The most interesting effects were that cells both with and without the plasmid show a higher ferricyanide reduction rate when pyocyanin is present than when it is not, even though the cells with the reporter grew slower. This is evident for both the DJ901 and GC4468 cells (Figures 4.8 b and 4.9 b). This is a consistent trend we saw throughout our experiments.

The above could be due to the enhanced cycling of pyocyanin inside the cell due to ferricyanide, which further increases ferricyanide reduction. The recycled pyocyanin inside the cell oxidizes SoxR and drives further phiLOV production, or, in the case of cells without the plasmid, oxidation of other cellular components. The GC4468 have a slower rate of ferricyanide reduction, presumably because of their already-active SoxRS regulon and higher defenses against pyocyanin (including

higher rate of its export from the cell). This is a phenomenon which we intend to investigate further prior to publishing the data.

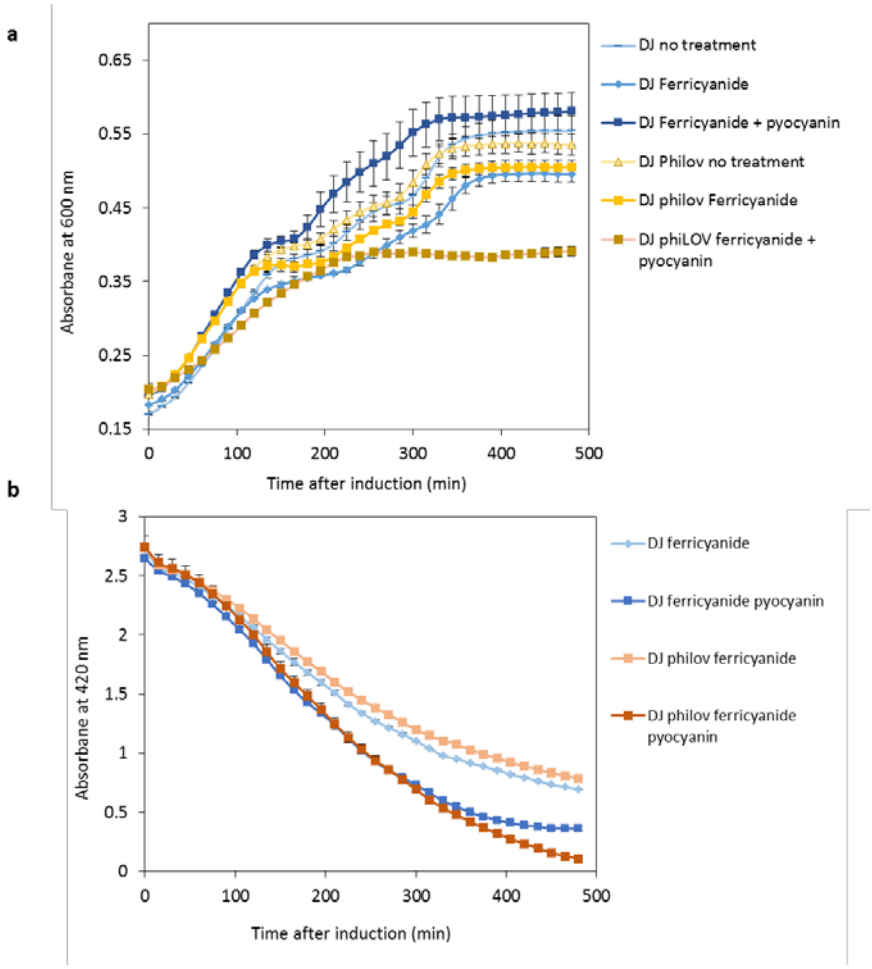

Figure 4.8: DJ901 cell growth and ferricyanide reduction. **a,** Growth of DJ901 cells, with or without the pyocyanin-induced phiLOV fluorescent protein, is affected by the addition of ferricyanide and pyocyanin. **b,**. The reduction of added 5 mM ferricyanide or 5 mM ferriycanide and 5 µM pyocyanin by DJ901 cells with or without the pyocyanin-induced phiLOV protein, as measured by decrease in 420 nm absorbance.

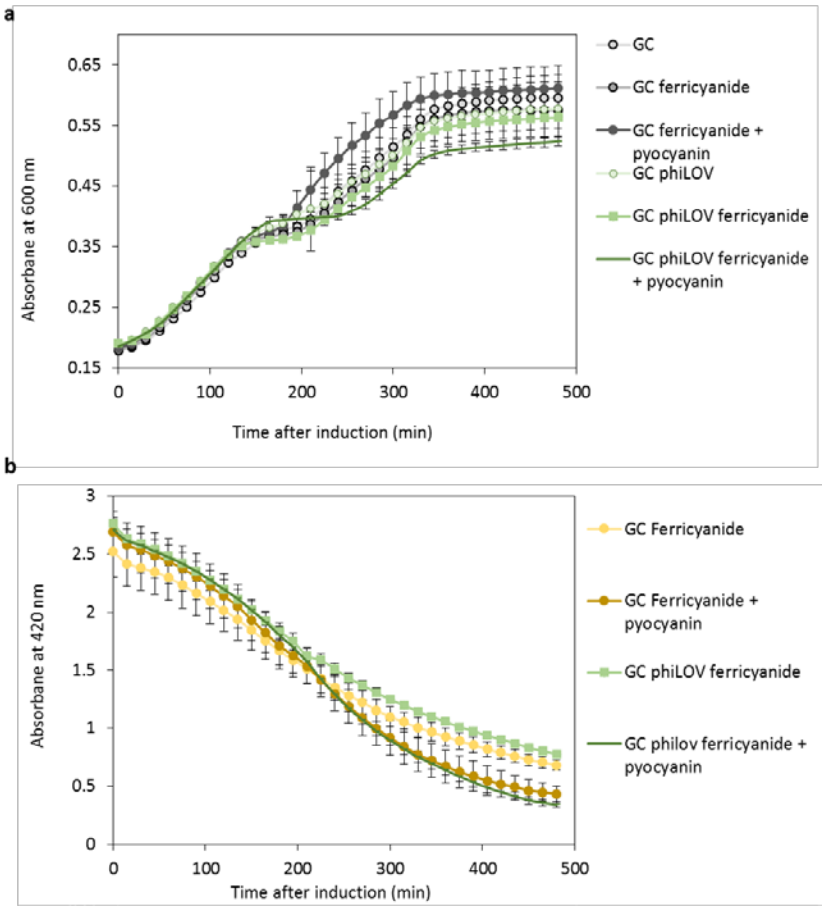

Figure 4.9: GC4468 cell growth and ferricyanide reduction. **a,** Growth of GC4468 cells, with or without the pyocyanin-induced phiLOV fluorescent protein, is affected by the addition of ferricyanide and pyocyanin. **b,**. The reduction of added 5 mM ferricyanide or 5 mM ferriycanide and 5 µM pyocyanin by GC4468 cells with or without the pyocyanin-induced phiLOV protein, as measured by decrease in 420 nm absorbance.

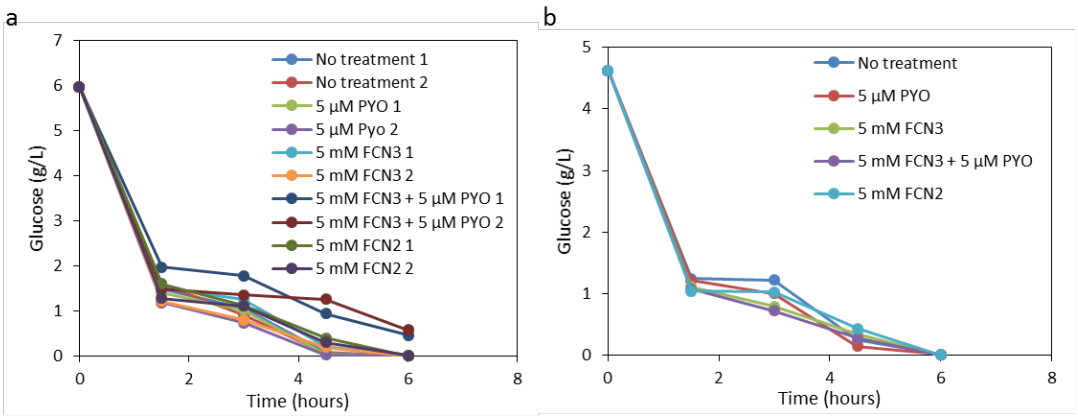

Figure 4.10: Effect of ferricyanide and pyocyanin on glucose consumption. a, Glucose measurements from DJ901 cells with the pBR322-SoxR-*soxS*-phiLOV plasmid grown with the indicated treatments starting at OD600 = 0.25. **b,** Glucose measurements from DJ901 cells without plasmid grown with the indicated treatments starting at OD600 = 0.25.

We measured the anaerobic consumption of glucose due to various treatments of both DJ901 cells with and without the plasmid. M9 media supplemented with 0.4% glucose and 0.2% casamino acids was used. As can be seen from preliminary data in Figure 4.10 a above, when the plasmid for phiLOV-DAS production is present, glucose consumption is slowed with the addition of both pyocyanin and ferricyanide, but not in the presence of one or the other alone. This could be due to the slowed growth of the cells as protein production is greatly increased (higher metabolic burden). This is corroborated by the fact that when the plasmid isn't present, glucose consumption does not seem to depend on the added mediators.

DJ910 cells with the philov-DAS plasmid were grown and induced with ferricyanide and pyocyanin in media with different glucose percentages, and not surprisingly, higher glucose percentage resulted in a higher fluorescence

(Supplementary Figure S4.3 a). Additionally, cells grown in the same media aneaerobically were induced with pyocyanin and ferricyanide for an hour at various points of growth (and therefore after higher amounts of glucose were consumed) (Figure S4.3 b). Again, cells that were grown for shorter amounts of time in the same media responded with higher fluorescence, presumably due to cell amount, glucose left, pH, and other metabolites present. Finally, re-suspending the same pyocyanin and ferricyanide-induced cells with fresh media + mediators resulted in a linear increase of response, whereas keeping cells in the same media resulted in eventual protein degradation.

An interesting trend can be seen when looking at both glucose consumption in Figure 4.10 above and cell growth in Figure 4.8 above. The cells start out growing relatively at a steady rate, then slow down around the 2 hour mark, and pick up growth again at a steady rate around 3 hours mark. Although the experiments in Figures 4.10 and 4.8 were done with different starting cell OD's (those in 4.8 were lower at the start than those in 4.10) and slightly differing conditions (plate format vs tubes, and microaerobic vs anaerobic), we hypothesize that it is due to the consumption of most of the glucose present around 2 hours that the cells' growth slows down. Before this, the cells would secrete various other more reduced compounds such as acetate or other mixed acid fermentation by-products. The end of the glucose supply would signal to the cells to switch their metabolism and utilize these more reduced compounds.

As stated in the introduction, previous studies have suggested that growth of *E.coli* anaerobically with ferricyanide as the electron acceptor results in a higher

production of acetate, which is a reduced compound and a result of fermentation. In these cases, it is among other products which signify higher energy production through substrate level phosphorylation rather than by respiration.

We have recently started the above experiments and plan on further investigating cellular production of acetate and other metabolic intermediates and products such as ATP in cells treated like those above. We hope to shed more light on the metabolic effect of the pyocyanin + ferricyanide combination and included the preliminary results above to demonstrate its importance. This would allow us to better tailor the experimental conditions (specifically, media composition) to achieve our desired result and responses from the cells.

Next, to further verify that it is because ferricyanide is acting as an electron acceptor that it amplifies the production of pyocyanin-induced protein, we used an alternative electron acceptor in a similar experiment with pyocyanin. As can be seen in Figure 4.11 below, nitrate, a common anaerobic electron acceptor, also results in an increase in phiLOV production when pyocynin is added. Nitrite, however, does not result in as high an increase in protein production, as it is the reduced form of nitrate.

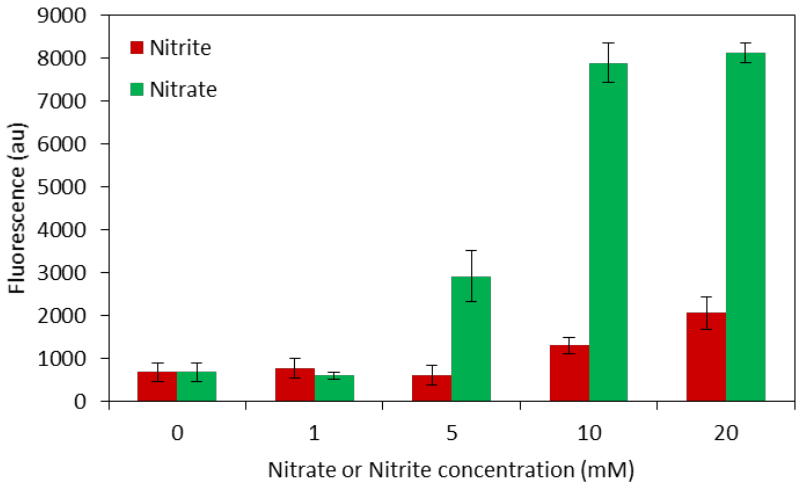

Figure 4.11: Effect of nitrate and nitrite, electron acceptors, on cell response to pyocyanin treatment. Fluorescence of cells producing the phiLOV protein in response to 5 µM added pyocyanin and the indicated concentrations of either nitrate or nitrite. 5 µM Na Myolobdate was added to all samples.

Our system is concentration-dependent on both pyocyanin and ferricyanide anaerobically, but when oxygen is present, as can be seen in Supplementary Figure S4.4, it is not. When any pyocyanin is present, oxygen amplifies the response in both GC4468 and DJ901 cells, and the concentration of ferricyanide (or even its presence as opposed to that of ferrocyanide) does not influence the amount of phiLOV. This is not to say that ferricyanide is not reduced by cells even when oxygen is present or doesn't act in part as an electron acceptor, but it is probably that the protein production machinery is maxed-out in this state and/or oxygen is favored as the electron acceptor. In Supplementary Figure S4.4 b we can see that GC4468 cells respond with a lower amount of fluorescence when in anaerobic but not aerobic conditions. This response also corroborates with the explanations given above.

Electrochemical control of ferricyanide and pyocyanin redox state

To introduce electronic control of gene expression we needed to be able to have good control of the electrochemical state of the ferricyanide/ferrocyanide couple, as this would result in either an ON or OFF state of protein production. Using a three-electrode setup and a potentiostat we were able to easily perform cyclic voltammetry and chronoamperometry measurements to both determine the concentration and the redox state of the molecules (Supplementary Figure S4.5). Using bulk electrolysis and a salt bridge, as described in the Methods section, we were able to start with ferrocyanide in the working-electrode-compartment and ferricyanide in the counter and switch the redox state of both back and forth over several cycles without degrading the molecules or generating any interfering species (Figure 4.12). This confirmed to us that we would be able to oxidize and reduce the molecules back and forth successfully in media and that they may retain their effects on the cells and phiLOV production.

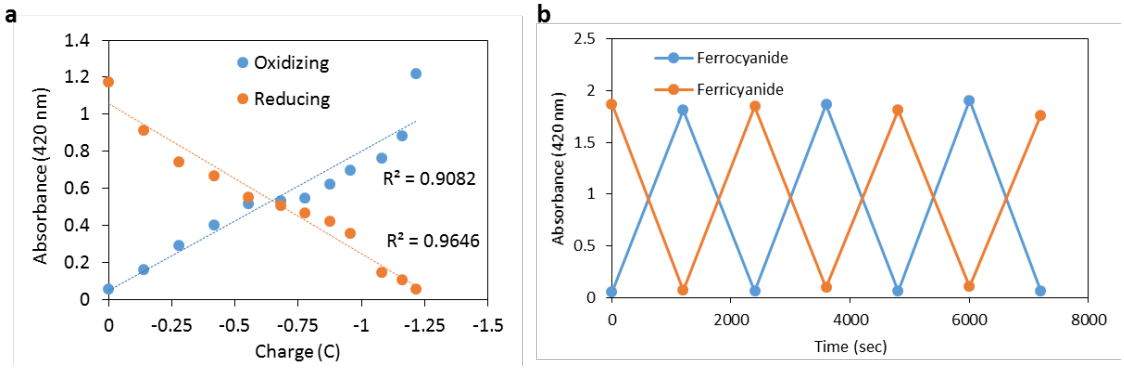

Figure 4.12: Continuous oxidation and reduction of ferro/ferricyanide. a, Absorbance increase and decrease as ferrocyanide is oxidized to ferricyanide and vice versa,

in the working and counter chambers. Higher charge indicates a longer time of oxidation or reduction. **b,** cycling of the reduced/oxidized form of the ferro/ferricyanide couple in the same chamber shows no destruction of the electrochemical or absorption properties.

To test this, we repeatedly oxidized and then reduced the same solution of media + mediators and saved these in aliquots on ice. At the end of the cycling, we added the saved media + either oxidized or reduced mediators to spun down DJ901 pBR322 SoxR s*oxS* phiLOV-DAS cells for 1.5 hours before fixing and measuring fluorescence with FACS. Figure 4.13 below shows that the cells responded in a predictable way, generating higher amount of protein when ferricyanide was present and less when ferrocyanide was present, even after the molecules were redox-cycled several times. These results allowed us to be confident that in further experiments, which would involve *in situ* ferricyanide reduction and oxidation, the redox cycling would have the desired effect on the cells.

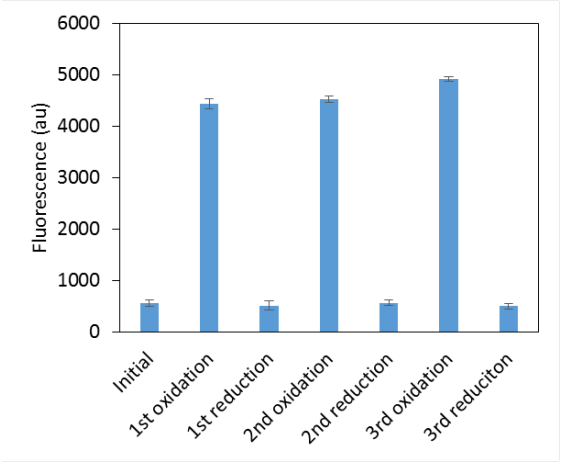

Figure 4.13: Cell response to electrochemically-oxidized or reduced mediators. Fluorescence of phiLOV produced by cells treated with media and supplements, 5 µM

pyocyanin, and 5 mM ferrocyanide that was either fully oxidized or reduced the indicated number of times.

It's important to note that we did not observe any chemical or electrochemical interactions between pyocyanin and ferricyanide, in either redox form. Though it is possible that one may oxidize or reduce the other, these interactions did not have any effect on our experimental results. When a ferricyanide + pyocyanin solution is reduced, we presume that the pyocyanin is reduced as well. However, reduced pyocyanin inside the cell can be re-oxidized somewhat even without ferricyanide, as we showed earlier. Therefore, we concluded that reduction of ferricyanide + pyocyanin solution and its effect in reducing protein production is largely due to the reduction of ferricyanide rather than pyocyanin.

Electronic *In situ* control of protein amount

After confirming that the electrochemically-cycled ferricyanide/ferrocyanide result in different rates of protein production, we decided to test an *in situ* system, with the cells already in the media with the redox molecules (5 µM pyocyanin and 5 mM ferrocyanide) . Our first experiments involved turning the system "ON" with various potentials, to confirm that a specific oxidizing voltage is required. We applied the indicated potentials all for 15 minutes. As can be seen below in Figure 4.14, potentials between -0.3 and +0.6 were used. The grey CV in the background of Figure 4.14 a is that of ferricyanide, with the reduction and oxidation peaks labeled at R and O, respectively. The reducing peak current was at -0.14 V and the oxidizing peak

current was at +0.22 V. We can see from Figure 4.14 a and b that applying voltages between -0.3 and 0 did not result in significant charge due to ferricyanide generation, and therefore cells did not fluoresce. Between 0 and +0.2V we see a steady increase in charge, absorbance of ferricyanide, and fluorescence of cells. This indicates that even though the potentials are not strictly oxidizing (not more positive than the oxidation peak), there is still some conversion of ferro to ferricyanide, and therefore an increased response from the cells. Potentials more positive than the E_0 resulted in similar conversions of ferro to ferricyanide and therefore similarly high/maximum average fluorescence. These results confirmed to us that indeed there is a particular voltage that fully turns the cells "ON" (+0.22 V and higher), and another voltage that turns them partially "ON" (+0.05 V and higher).

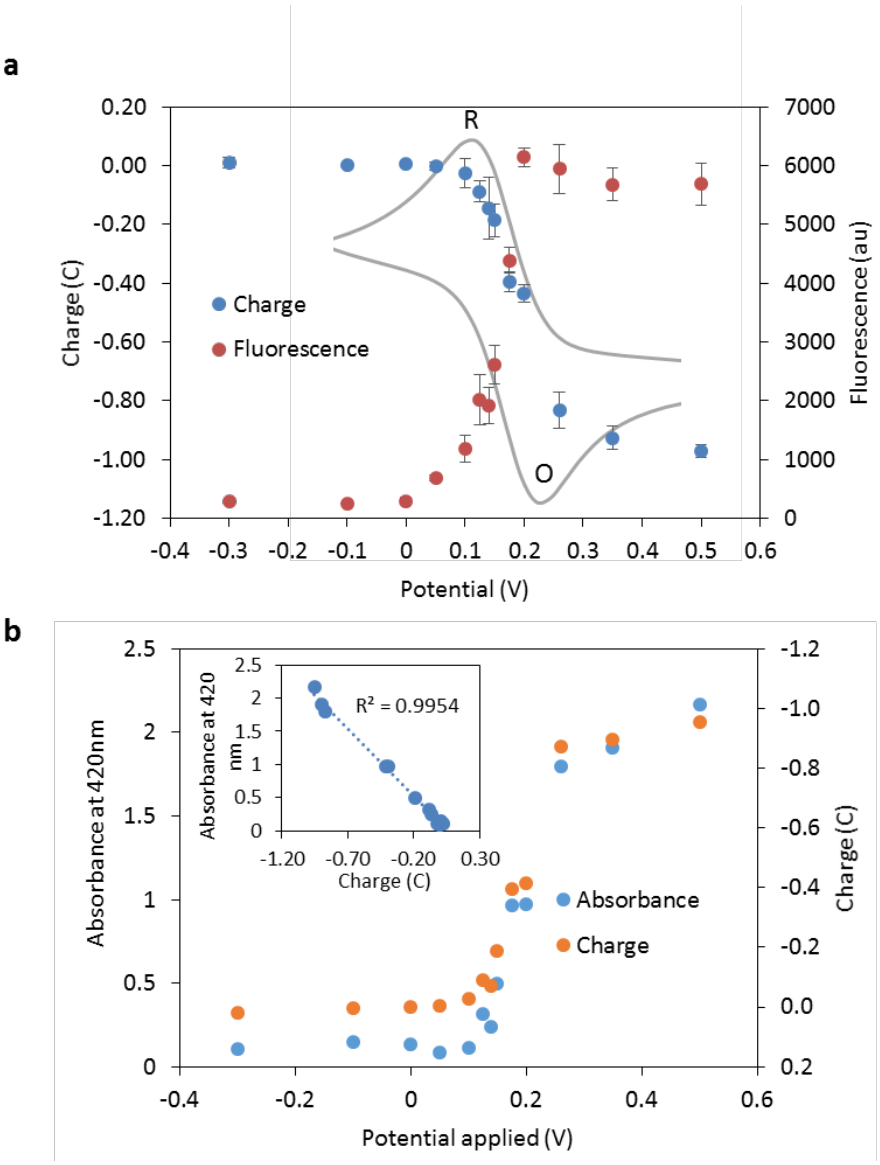

Figure 4.14: Potential step-up and control of gene expression. a. Various potentials (x-axis) were applied for 15 minutes to cells with 5 µM pyocyanin and 5 mM ferrocyanide. The indicated charge was measured/observed. Cells were then incubated for 3 hours, over which the indicated average fluorescence was measured at one hour intervals. The grey CV in the background indicates the reduction(R) and oxidation (O) peaks of ferricyanide. **b.** The resulting charge (also from a) as compared to the absorbance of the resulting ferricyanide generated (420nm). Insert shows the linear correlation between the two.

We picked a potential (+0.5 V) that was much more positive than the oxidation peak, since it is possible that the peaks may drift over the course of the experiment (we've observed this before, and it is based on the pH of the media), and applied various charges, ie. by electrochemically oxidizing 5 mM ferrocyanide and 5 µM pyocyanin for various lengths of time, and therefore turning only portions of it to the ferricyanide form. As can be seen in Figure 4.15 a, the resulting average fluorescence is proportional to the charge of the oxidation reaction. The fluorescence is an average of several measurements taken over time, all of which can be seen in Figure 4.15 b. These results corresponded well with the trends seen when different concentrations of ferricyanide were added previously in Figure 4.6.

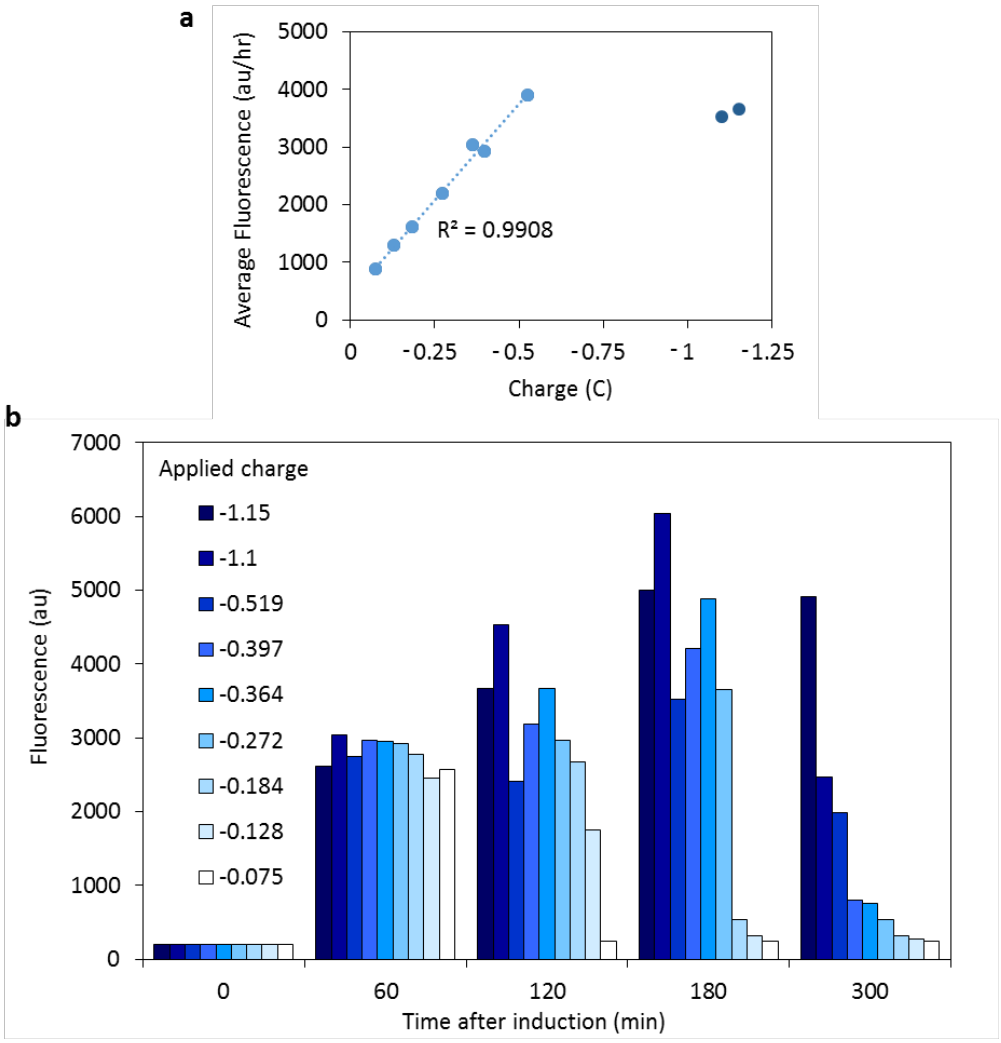

Figure 4.15: Fluorescent response to various charges. a, Average cell fluorescence, phiLOV-DAS produced in response to the indicated charge, which turned part of the 5mM ferrocyanide + pyocyanin from reduced to oxidized form. **b,** A subset of the actual fluorescence FACS measurements from cells activated with the indicated charge, over time. Lower charges resulted in less conversion of ferro to ferricyanide and therefore lower response over time and quicker degradation. 5 µM pyocyanin is used for all samples.

Additionally, we performed negative controls where the oxidizing and reducing currents themselves, without mediators, were applied, and the oxidizing

current was run with the oxidized molecules and the reducing current with the reduced molecules. This was done to rule out any genetic response to the current itself or other electrochemically-related unknown factors. Supplementary Figure S4.6 shows that there was no response unless ferricyanide and pyocyanin were present in the oxidized form, and no unanticipated response from the currents themselves occurred.

In situ response to ON/OFF cycling

Next, we investigated whether ON/OFF cycling can also be accomplished *in situ*. Our first experiments involved a similar idea to Figure 4.6 above, with the application of one ON and one OFF voltage for various amounts of time. As can be seen in Figure 4.16, we saw a similar response to when the ferri/ferrocyanide was changed in the media in Fig. 4.6. However, we do see a longer delay in the OFF part of the cycle, due to the fact that it takes about 15 minutes for the ferricyanide to completely turn into ferrocyanide, during which time the protein is still presumably made, at a higher rate than it would be if the media was just exchanged and the concentration of ferricyanide gone to zero almost immediately.

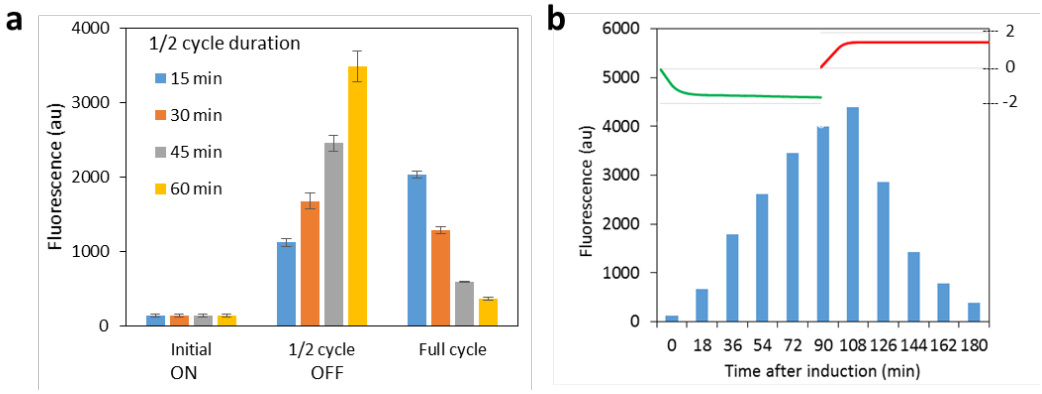

Figure 4.16: *In situ* electrochemical cycling effect on response. a, Electrochemical actuation – 1/2 cycle of ON and then OFF. Cells were initially in the OFF state, and turned ON at time zero. After the ½ cycle measuremnt, the voltage was turned from ON back to OFF, electrochemically. Each half of the cycle was of the indicated time length. **b,** The 90-minute series shown here with the charge traces. The green and red curves represent accumulated charge. Green is during the ON phase (oxidizing +0.5 V applied) and red is during the OFF phase (reducing -0.3 V applied).

In order to apply multiple cycles to the same cells, we chose 1 hour for each part of the cycle (ON 1 hour, OFF 1 hour), which would allow for sufficient protein production and degradation. Complete oxidation and reduction of the 5 mM ferrocyanide was accomplished within about 15-30 minutes. As can be seen in Figure 4.17, we were indeed able to see increases and decreases in overall protein based on whether the ferrocyanide was oxidized or reduced previously. The actual charge traces can be seem above the graph in Figure 4.17 as green (ON) or red (OFF) lines. These show that the first 15 minutes have a linear oxidation/reduction and much higher slope than the remainder, as in Figure 4.16 b.

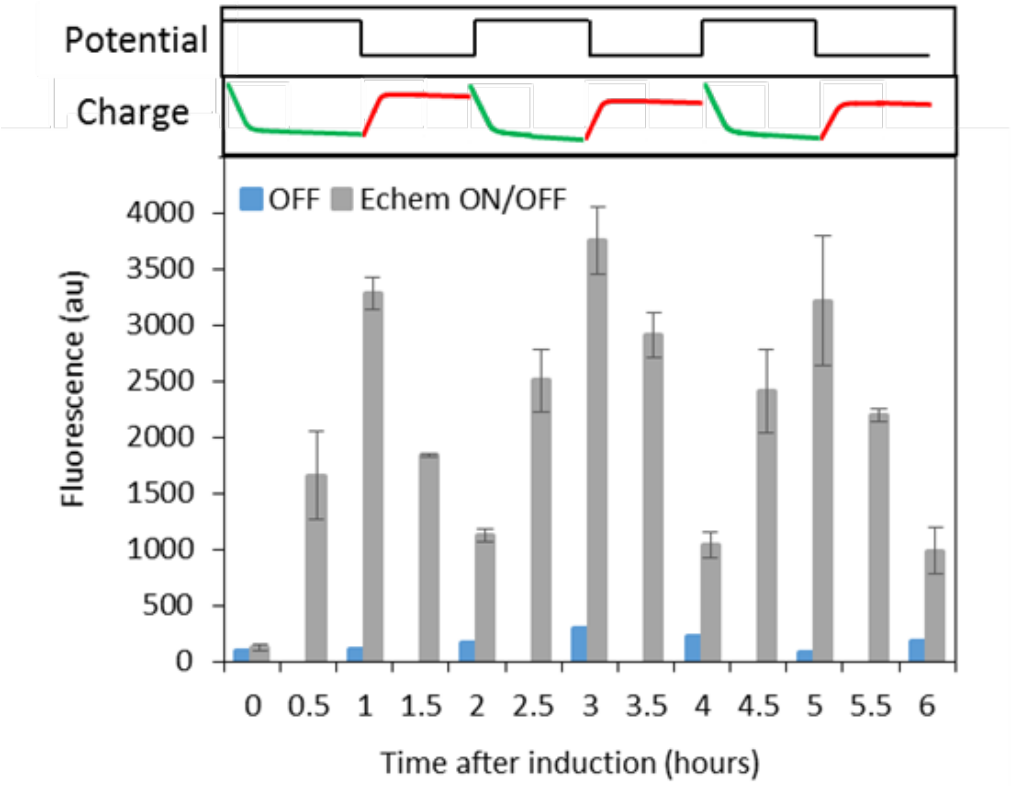

Figure 4.17. Electrochemical ON/OFF cycling. Cell fluorescence as measured by FACS in response to cyclic ON/OFF electrochemical signals. The applied potential was either 0.5V (high, oxidizing, ON) or -0.3 (low, reducing, OFF). The green and red traces above indicate the resulting charge from the applied potential. Charge axes are 0 to -2 for ON (green) and 0 to 2 for OFF, similarly to Figure 4.16 above. Error bars represent standard deviation.

In situ reactions over periods of time longer than about 6 hours, however, resulted in general fluorescence decrease and the inability of the cells to produce as much of a response as in the earlier timepoints. This is because over time, the growth of the cells, the metabolic products, the change in pH, and consumption of substrate

all affected the ability of the cells to respond. Starting with a lower cell OD, and adding LB media with MOPS buffer instead of M9 media alleviated the problem of seeing consistent responses up to 6 hours, but for longer periods of time media exchange or some limitation on growth would need to be implemented (cell dilution perhaps). This can be achieved with the immobilization of cells on electrodes within microfluidic devices, and is described further in the Future Work section in the next chapter. We are currently pursuing these alternatives.

Conclusions

In this chapter, we have shown for the first time the use of a reversible redox molecule to control gene expression in bacteria with temporal accuracy. Although we are currently continuing the work and foresee a lot of improvements to the system, the investigations outlined above show that it is a viable method for providing bio-electronic communication in the short term. The great benefits of our method are the direct translation of electronic to genetic signals (with a 15-30 minute lag time), the minimal additional genetic elements that need to be introduced to cells (SoxR protein and *soxS* promoter), the promising usefulness of the system in microelectronic-based lab-on-chip devices (location-specific response), and the low cost of the equipment needed to achieve electronic control. Overall this is a promising novel methodology that we envision has many applications mentioned in the introduction and motivation sections.

Acknowledgements

We would like to acknowledge funding provided for this work by the Defense Threat Reduction Agency (DTRA, HDTRA1-13-1-00037) and the National Science Foundation (CBET 1160005 and CBET 1264509, and EAPSI fellowship to T. Gordonov).

Supplementary Information

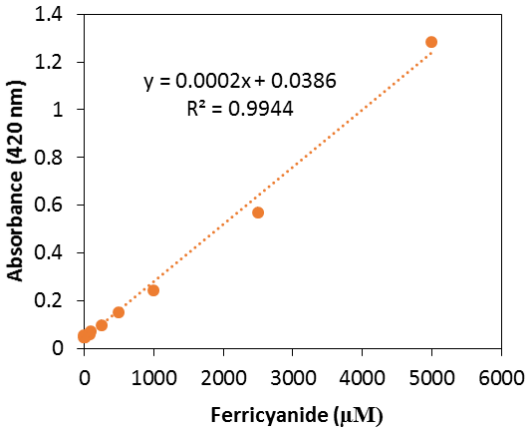

Supplementary Figure S4.1: Absorbance measurement of ferricyanide.

Absorbance at 420nm can be used to measure ferricyanide concentration in the ranges used in this chapter.

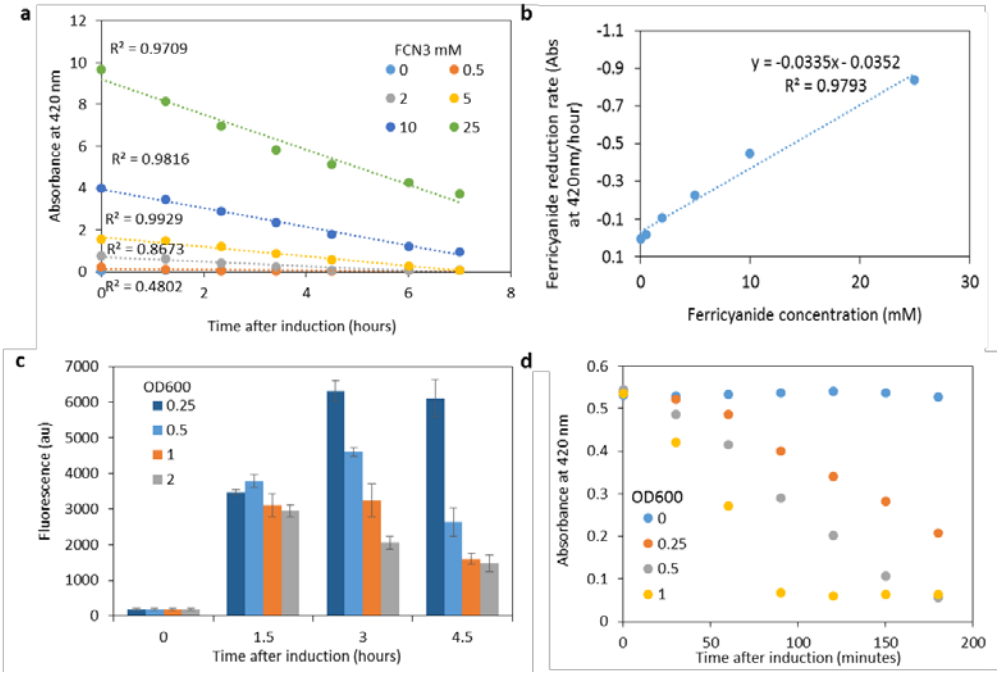

Supplementary Figure S4.2: Effect of cell OD and ferricyanide concentration on ferricyanide reduction and cell response. a, Ferricyanide reduction to ferrocyanide by cells results in absorbance decrease (measured at 420 nm, same starting cell OD) over time.

b, Ferricyanide reduction by cells (the slopes from a) is concentration-dependent. **c,** Different cell ODs are reacted with the same pyocyanin and ferricyanide concentrations. **d,** Increasing cell OD results in higher rate of reduction of the same ferricyanide concentration.

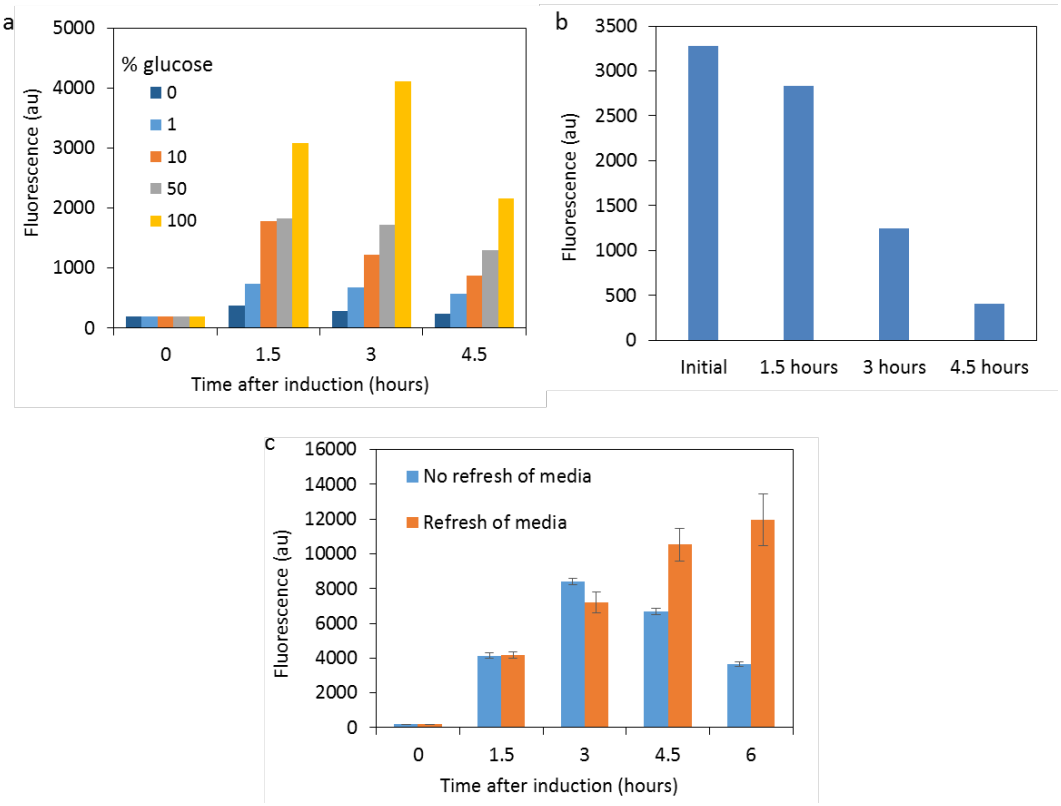

Supplementary Figure S4.3: Fluorescent protein production with different glucose amounts. a, DJ901 cells producing the phiLOV-DAS protein in response to 5 µM pyocyanin and 5 mM Ferricyanide in media with different glucose concentrations. 100% signifies M9 media with 0.4% glucose (w/v). **b,** Cells were grown anaerobically starting at OD600=0.25 in M9 glucose CA media. After the indicated amounts of time, 5 µM pyocyanin and 5 mM Ferricyanide were added, and after an hour cells were collected for fluorescence measurement. **c,** Production of fluorescent protein continues when used media + mediators are refreshed with new media + mediators.

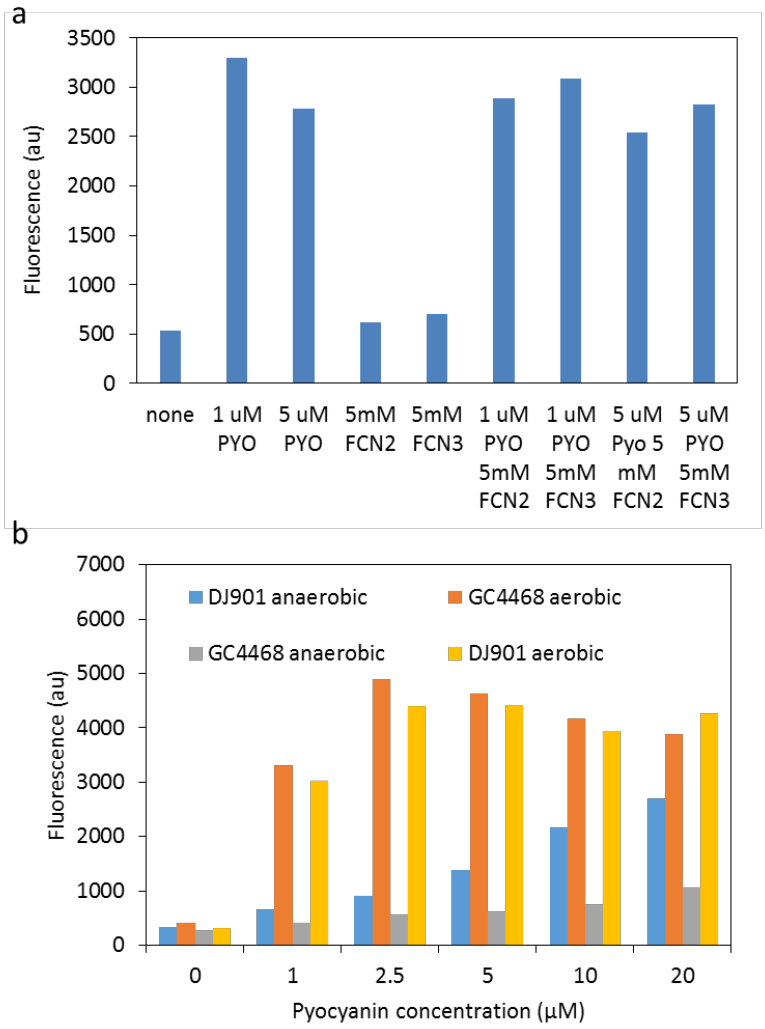

Supplementary Figure S4.4: Effect of aerobic conditions on ferricyanide and pyocyanin treatments. a, Fluorescence of cells producing phiLOV protein in response to the indicated treatments, aerobically. **b,** Fluorescence of DJ901 or GF4468 cell producing the phiLOV protein in response to different pyocyanin concentrations in either aerobic or anaerobic conditions.

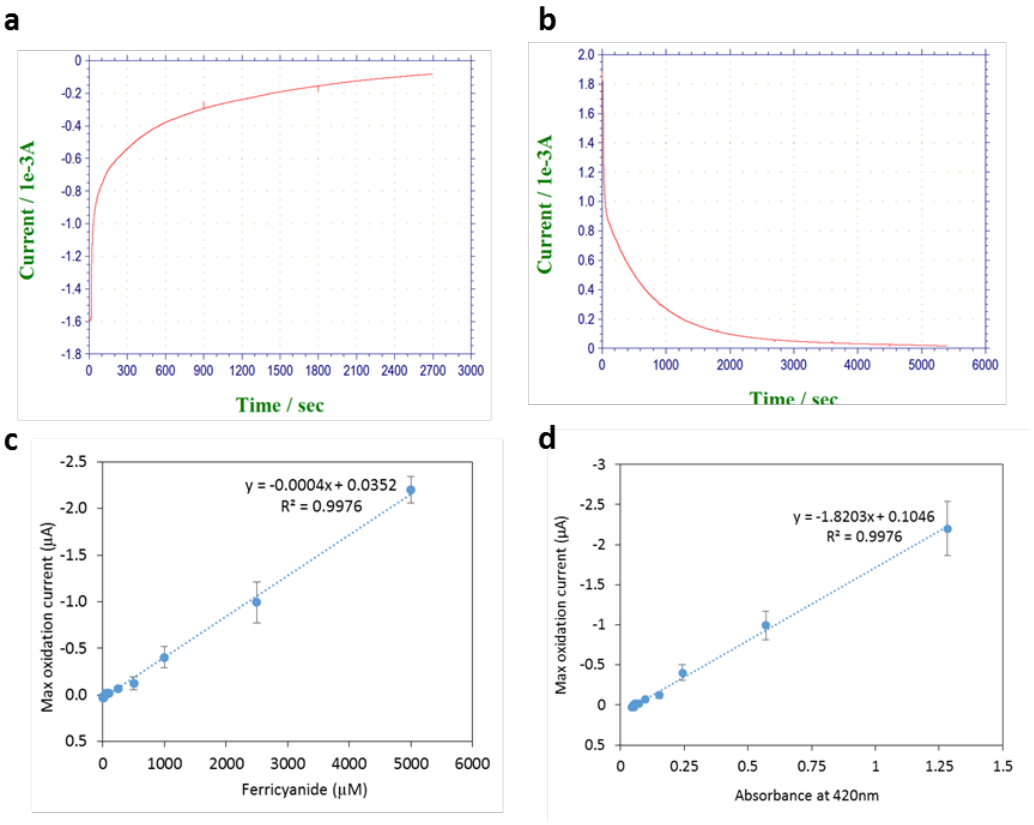

Supplementary Figure S4.5: Electrochemical ferri/ferrocyanide measurements and bulk electrolysis. a, Chronoamperometry of bulk oxidation of ferrocyanide to ferricyanide. **b,** Chronoamperometry of bulk reduction of ferricyanide to ferrocyanide. **c,** Maximum oxidation current measurements of various ferricyanide concentrations. **d,** Correlation between the 420nm absorbance and the maximum oxidation currents of various ferricyanide concentrations.

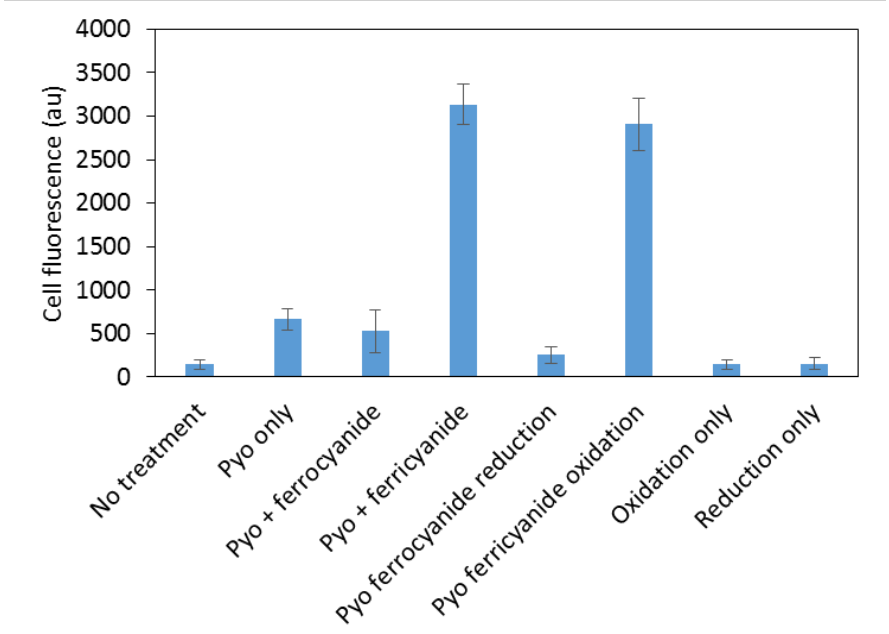

Supplementary Figure S4.6: Electrochemical negative controls. Cell fluorescence after 1 hour as measured by FACS (phiLOV-DAS) based on the indicated treatments. These are the electrochemical negative controls.

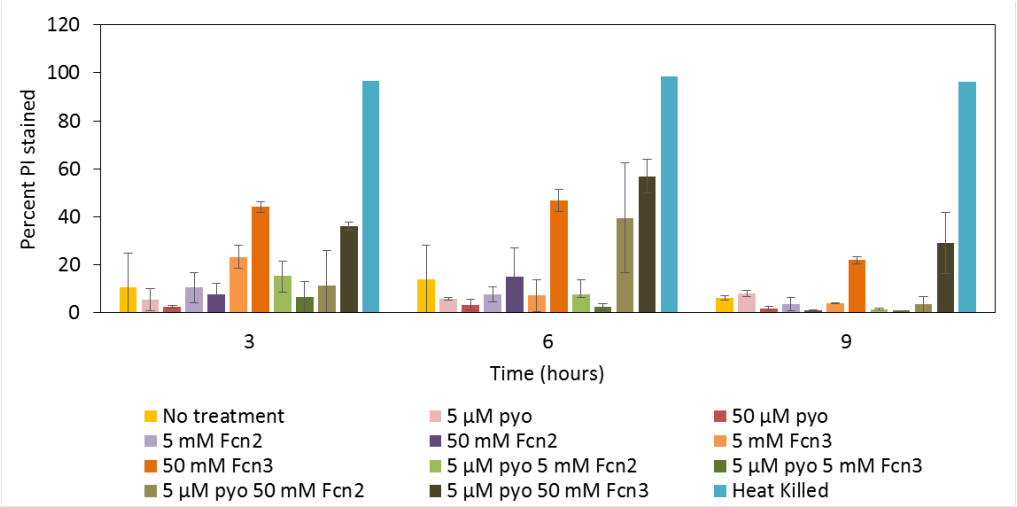

Supplementary Figure S4.7: Propidium iodide staining of cells. Cells were grown with the various treatments for the indicated amounts of time and stained with propidium iodide as stated in the Methods section.

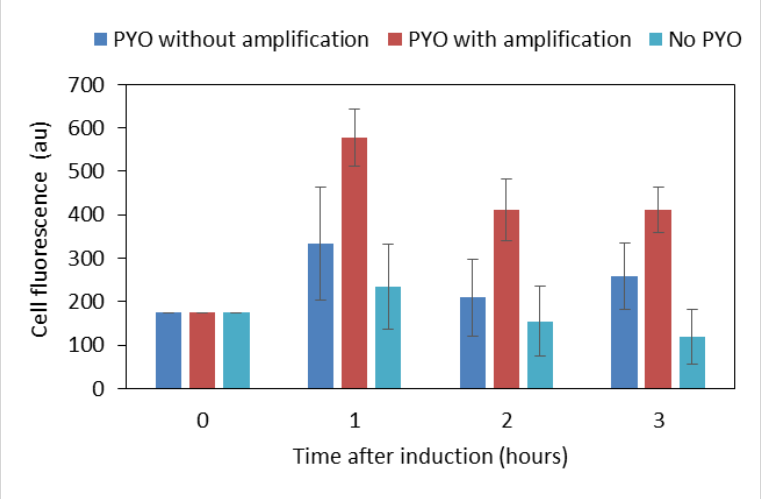

Supplementary Figure S4.8: Pyocyanin-only electrochemical oxidation.

Continuous oxidation of 5 µM pyocyanin in a slight but not significant increase in fluorescence.

Gene/construct	Primers
SoxR-*soxS* region from genome	F: GGA TTT GGA TCC TTA GTT TTG TTC ATC TTC CAG CAA G R: GAA CAC TGA AAA GAG GCA GAT TTA AGC TTA ATC
phiLOV for Gibson	F: GAC AGC TTA TCA TCG ATT TAT TAT TAC ACA TGA TCG CTG CC R: GAG GCA GAT TTA AGC TTA TGA TTG AAA AAA GCT TTG TGA TTA C
pBR322-SoxR-I for Gibson	F: AAG CTT AAA TCT GCC TCT TTT R: ATC GAT GAT AAG CTG TCA AA
phiLOV-LAA for Gibson	F: GAC AGC TTA TCA TCG ATT TAT TAT TAA GCA GCC AGA GC R: CCA GTG CAG GAG CTC TTA TTA TTA AGC AGC CAG AGC
DAS tag addition	F: TAG TTT TCG TCG TTA GCA GCC AC R: CGC TGA CGC TTC TTA ATA ATA ATA TCG ATG ATA AGC TGT CAA ACA TGA

Table S4.1: Primers used for creating pBR322-SoxR-*soxS*-phiLOV and –phiLOV-LAA and –phiLOV-DAS constructs.

Genetic element	Sequence
LAA degradation tag	GCT GCT AAC GAC GAA AAC TAC GCT CTG GCT GCT
DAS degradation tag	GCT GCT AAC GAC GAA AAC TAC GCT GAC GCT TCT
phiLOV2.1 anaerobic fluorescent protein (adapted from Christie et al.[177])	ATG ATT GAA AAA AGC TTT GTG ATT ACC GAT CCG CGC CTG CCG GAT TAT CCG ATT ATT TTT GCG AGC GAT GGC TTT CTG GAA CTG ACC GAA TAT AGC CGC GAA GAA ATT ATG GGC CGC AAC GCG CGC TTT CTG CAG GGC CCG GAA ACC GAT CAG GCG ACC GTG CAG AAA ATT CGC GAT GCG ATT CGC GAT CAG CGC GAA ACC ACC GTG CAG CTG ATT AAC TAT ACC AAA AGC GGC AAA AAA TTT TGG AAC CTG CTG CAT CTG CAG CCG GTG CGC GAT CGC AAA GGC GGC CTG CAG TAT TTT ATT GGC GTG CAG CTG GTG GGC AGC GAT CAT GTG TAA

Table S4.2. Relevant genetic element sequences.

Chapter 5: Summary, innovations, and future work

Summary

The dissertation presented here describes our work to facilitate bio-electronic communication. In Chapter 2 we showed that electronic signals can modulate the activity of the protein HLPT assembled on an electrode through the controlled oxidation of acetosyringone and the oxidation of residues on HLPT. To facilitate and explore electronic measurement of gene expression, we utilized the β-galactosidase reporter protein, whose reaction with the PAPG substrate yields the redox-active PAP molecule. In Chapter 3, we explored in-depth the relationship between this electrochemical method and the standard Miller assay – a first-time correlation which we hope will facilitate the use of the electrochemical measurement by synthetic biologists. Finally, in Chapter 4, we detailed the development of an electronic gene-control system with the use of pyocyanin-induced *soxS* promoter and the electrochemical control of the electron acceptor ferricyanide. Overall, our developments make great strides towards promoting meaningful and facile bi-directional communication between biology and electronics.

Our work has resulted in one published article, one article currently under review, and one in preparation. Additionally, the work has been presented at 5 international conferences.

Electronic modulation of biochemical signal generation

Innovation and contributions

The study described in Chapter 2 provides the first evidence that direct electronic control of a diffusible redox mediator at the surface of a gold electrode in the vicinity of an immobilized enzymatic pathway results in predictable protein oxidation, attenuation of activity, and biochemical signal generation. In addition to HLPT, we demonstrated similar electronic activity control of two other enzymes' activities (microbial transglutaminase and β-galactosidase). We also were able to use the redox couple Ir(III)/Ir(IV) with all three enzymes – further extending the utility of the technique. We envision that the novel suite of methodologies demonstrated here form the basis for targeting and controlling biochemical fluxes of other biohybrid devices.

Future work

In the work described, the electrode used, attenuation setup, and incubation system were all macroscale systems. We believe that all of our techniques and steps could be translated easily into a microfluidic system with integrated electrodes. Several such systems from our group could be adapted for the task. We have previously shown the deposition of a chitosan film and enzymatic assembly of functional enzymes on that film in a microfluidic channel[29,47]. A third electrode could be integrated for the use as a reference electrode for attenuation reactions as well as real-time measurement of Hcy generation[55]. In fact, a fluidic application with flow might be optimal. Options for which materials/metals to use include (but are not

limited to) (i) all gold or (ii) gold working and counter, with a silver reference. A variety of electrode geometries could also be used.

Electrochemical detection of synthetic biology constructs – in situ β-galactosidase detection in real time from whole cells

Innovation and contributions

Our results indicate for the first time that electrochemical measurement of β-gal activity (cleavage of PAPG to PAP) in both lysed and intact cells is feasible as an alternative method to the gold-standard Miller assay. It enables added versatility for analysis of synthetic biology constructs, such as those exploiting lab-on-a-chip and other methodologies that benefit from real-time measurement. We demonstrated this by developing a biosensor bacterium that converts the signaling function of quorum sensing molecule AI-2 to electronic signals through a genetic (β-gal) and chemical (PAPG) transducer system. Our results showed that the electronic current measured was proportional to Miller Units from the same samples, and can be used to approximate gene expression in a multi-component synthetic circuit. Such electrochemical measurements allow for *in situ* analyte detection as they integrate seamlessly into electronic systems, and could therefore allow for programmable measurements of synthetic biology constructs. Additionally, we created a two-compartment model that can be used to predict PAP (and thus electrochemical) output from our construct, and can be modified to accommodate other systems driving *LacZ* expression. We believe this work connects, for the first time, the work of the biosensor community in enzymatic reporter detection, with the standard optical

measurement techniques biologists use for the same purpose. A better link between synthetic biologists and biochip / microelectronics designers enables parallel use of each other's' tools and advances the potential for synergistic outcomes.

Future work

We believe that the work presented in Chapter 3 in general can be used by synthetic biologists to analyze genetic circuits by electrochemical means. Additionally, the electrochemical measurement of gene expression presented here can be combined with the electrochemical gene actuation in Chapter 4 to create an bio-hybrid system with both electronic inputs and outputs.

Electronic control of bacterial gene expression through redox-driven transcriptional activation

Innovation and contributions

The method described in Chapter 4 is the first to use a reversible redox molecule to control gene expression in bacteria with temporal accuracy. It adds to the suite of novel genetic control methods that aim to provide precise spatio-temporal control. We have shown that our method (with the mediators used) does not significantly damage the cells. Our results showed that by manipulating factors such as mediator concentrations, cell amount, and culture conditions, different responses can also be elicited – adding a degree of customizability. Additionally, our metabolic and growth studies shed some light on the effects and functioning of our design.

The great benefits of our method are the almost-direct translation of electronic to genetic signals, the minimal additional genetic elements that need to be introduced to cells, the promising usefulness of the system in microelectronic-based lab-on-chip devices (location-specific response), and the low cost of the equipment needed to achieve electronic control. Overall this is a promising novel methodology to translate electronic signals to genetic response that we intend to further develop and study.

Future work

In Chapter 4 is the first time our method has been described, and much work was put (and continues to be put) into validating the hypotheses of how the method works and what factors are important to elicit an optimal response. Some additional experiments will need to be performed in order to validate and strengthen our hypotheses and claims in the chapter, though we believe the data we presented is robust and convincing. We talk about those experiments throughout the results and discussion in Chapter 4. Here we present additional ideas that would expand on our method and utilize it in novel ways. We hope that much more can be done and demonstrated with our method, and some of this we have started working on.

The true potential of our method, we believe, can be realized with cells that are immobilized in the vicinity in the signaling electrodes in such a manner that allows easy media flow and exchange and faster diffusion of mediators between cells and electrodes. As one of our limitations in terms of eliciting a strong response was the growth and secretions of the cells *in situ*, we believe cell immobilization would allow us to not only regulate the communication quicker, but also allow us to perform longer experiments and retain cell responsiveness over time by limiting growth and

exchanging media easily. Depending on the reporters used, real-time responses could be measured, which would allow for a development of a closed-loop feedback-control system. We are currently working on developing a microfluidic platform that allows real-time detection of the fluorescent phiLOV response with a microscope from cells immobilized on gold electrodes within channels.

Showing a phenotypic change due to genes being turned on and off using our method is another avenue we are pursuing. Already, we started experiments that aim to turn on both bacterial motility (with the CheZ protein[187]) and bacterial cell-to-cell communication (using the LuxI and LuxR system of quorum sensing [QS][188]). The cell-to-cell communication will be especially beneficial as the "bio-electronics relay" cells, those producing LuxI and secreting the communication molecule in response to the electronic signals, will be the only ones that need to be in an anaerobic environment. Once the QS molecule is secreted, it can communicate the electronic signals to downstream sensor cells (those expressing LuxR) that can be in an aerobic environment. Additionally, an electrochemically-measured reporter, such as β-galactosidase from the previous chapter, can also be used to link electronic control to electronic reporting.

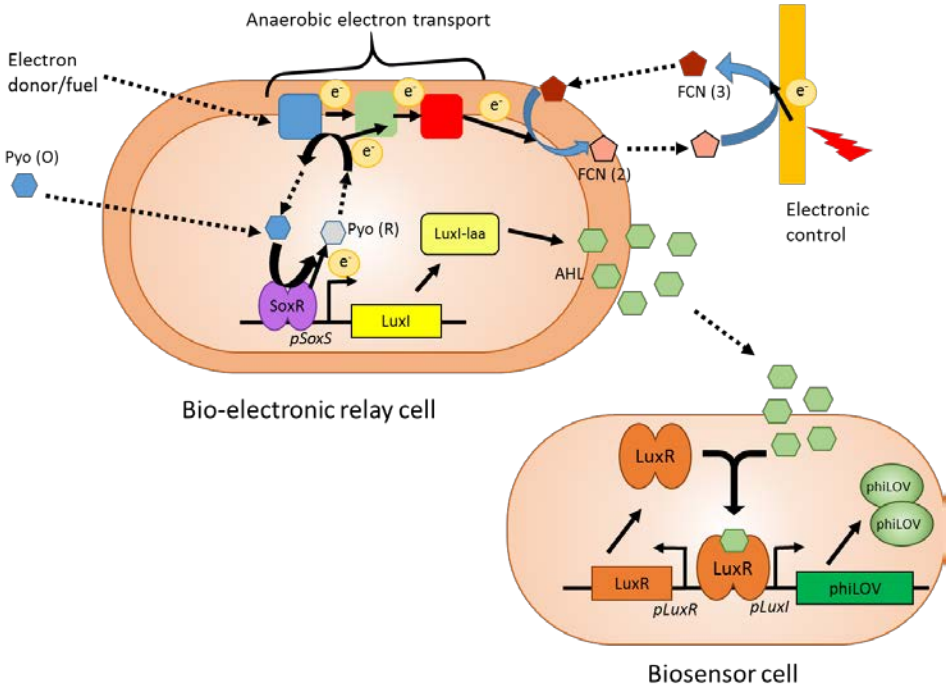

Figure 5.1: Schematic of bio-electronic cells. Cells are producing luxI and AHL in response to electronic signals. The AHL diffuses to biosensor cells, which respond by producing a reporter, such as phiLOV, from the LuxI promoter.

Additionally, in order to lessen the redox stress on the cells even further, the following can be implemented: To reduce the amount of pyocyanin and ferricyanide used, we can employ a genetic amplification mechanism (such as in Chapter 3) or an enzymatic reporter protein (including the above-mentioned LuxI and β-galactosidase). We can up-regulate redox-scavenging enzymes during the times when the protein of interest is not being produced. Additionally, we can employ a different redox mediator (other than pyocyanin) that perhaps has less of an impact on redox stress in the cells but still activates SoxR.

Bibliography

1 Green, J. & Paget, M. S. Bacterial redox sensors. *Nature reviews. Microbiology* **2**, 954-966, (2004).

2 Allen J. Bard, C. G. Z. *Electroanalytical Chemistry: A Series of Advances*. Vol. 24 (CRC Press, 2011).

3 Friedheim, E. & Michaelis, L. Potentiometric study of pyocyanine *Journal of Biological Chemistry* **91**, 355-368, (1931).

4 Peter T. Kissinger, W. R. H. *Laboratory Techniques in Electroanalytical Chemistry*. 2nd edn, (Marcel Dekker, 1996).

5 Ben-Yoav, H., Melamed, S., Freeman, A., Shacham-Diamand, Y. & Belkin, S. Whole-cell biochips for bio-sensing: integration of live cells and inanimate surfaces. *Critical reviews in biotechnology* **31**, 337-353, (2011).

6 Carlsen, R. W. & Sitti, M. Bio-Hybrid Cell-Based Actuators for Microsystems. *Small* **10**, 3831-3851, (2014).

7 Rusmini, F., Zhong, Z. & Feijen, J. Protein Immobilization Strategies for Protein Biochips. *Biomacromolecules* **8**, 1775-1789, (2007).

8 El-Ali, J., Sorger, P. K. & Jensen, K. F. Cells on chips. *Nature* **442**, 403-411, (2006).

9 Primiceri, E., Chiriaco, M. S., Rinaldi, R. & Maruccio, G. Cell chips as new tools for cell biology--results, perspectives and opportunities. *Lab Chip* **13**, 3789-3802, (2013).

10 Tigges, M., Marquez-Lago, T. T., Stelling, J. & Fussenegger, M. A tunable synthetic mammalian oscillator. *Nature* **457**, 309-312, (2009).

11 Markham, K. A. & Alper, H. S. Synthetic Biology for Specialty Chemicals. *Annual review of chemical and biomolecular engineering*, (2015).

12 Lu, T. K., Khalil, A. S. & Collins, J. J. Next-generation synthetic gene networks. *Nature biotechnology* **27**, 1139-1150, (2009).

13 Prindle, A. *et al.* A sensing array of radically coupled genetic /`biopixels/'. *Nature* **481**, 39-44, (2012).

14 Marchisio, M. A. & Rudolf, F. Synthetic biosensing systems. *The international journal of biochemistry & cell biology* **43**, 310-319, (2011).

15 Dueber, J. E. *et al.* Synthetic protein scaffolds provide modular control over metabolic flux. *Nature biotechnology* **27**, 753-759, (2009).

16 Tsai, C. S., Kwak, S., Turner, T. L. & Jin, Y. S. Yeast synthetic biology toolbox and applications for biofuel production. *FEMS yeast research*, (2014).

17 Jarboe, L. R. *et al.* Metabolic engineering for production of biorenewable fuels and chemicals: contributions of synthetic biology. *Journal of biomedicine & biotechnology* **2010**, 761042, (2010).

18 Weber, W. & Fussenegger, M. Emerging biomedical applications of synthetic biology. *Nat Rev Genet* **13**, 21-35, (2012).

19 Ruder, W. C., Lu, T. & Collins, J. J. Synthetic Biology Moving into the Clinic. *Science* **333**, 1248-1252, (2011).

20 Shankar, S. & Pillai, M. R. Translating cancer research by synthetic biology. *Molecular BioSystems* **7**, 1802-1810, (2011).

21 Sia, S. K., Gillette, B. M. & Yang, G. J. Synthetic tissue biology: tissue engineering meets synthetic biology. *Birth defects research. Part C, Embryo today : reviews* **81**, 354-361, (2007).
22 Paddon, C. J. & Keasling, J. D. Semi-synthetic artemisinin: a model for the use of synthetic biology in pharmaceutical development. *Nat Rev Micro* **12**, 355-367, (2014).
23 Courbet, A., Endy, D., Renard, E., Molina, F. & Bonnet, J. Detection of pathological biomarkers in human clinical samples via amplifying genetic switches and logic gates. **7**, 289ra283-289ra283, (2015).
24 Menezes, A. A., Cumbers, J., Hogan, J. A. & Arkin, A. P. Towards synthetic biological approaches to resource utilization on space missions. *Journal of The Royal Society Interface* **12**, (2014).
25 Gordonov, T. *et al.* Electronic modulation of biochemical signal generation. *Nat Nano* **9**, 605-610, (2014).
26 Nivala, J., Marks, D. B. & Akeson, M. Unfoldase-mediated protein translocation through an alpha-hemolysin nanopore. *Nature biotechnology* **31**, 247-250, (2013).
27 Moreau, C. J., Dupuis, J. P., Revilloud, J., Arumugam, K. & Vivaudou, M. Coupling ion channels to receptors for biomolecule sensing. *Nature nanotechnology* **3**, 620-625, (2008).
28 Mora-Pale, M., Sanchez-Rodriguez, S. P., Linhardt, R. J., Dordick, J. S. & Koffas, M. A. Metabolic engineering and in vitro biosynthesis of phytochemicals and non-natural analogues. *Plant science : an international journal of experimental plant biology* **210**, 10-24, (2013).
29 Luo, X. *et al.* Programmable assembly of a metabolic pathway enzyme in a pre-packaged reusable bioMEMS device. *Lab on a Chip* **8**, 420-430, (2008).
30 Jung, G. Y. & Stephanopoulos, G. A functional protein chip for pathway optimization and in vitro metabolic engineering. *Science* **304**, 428-431, (2004).
31 Lee, M. Y., Park, C. B., Dordick, J. S. & Clark, D. S. Metabolizing enzyme toxicology assay chip (MetaChip) for high-throughput microscale toxicity analyses. *Proceedings of the National Academy of Sciences of the United States of America* **102**, 983-987, (2005).
32 Fernandes, R., Roy, V., Wu, H. C. & Bentley, W. E. Engineered biological nanofactories trigger quorum sensing response in targeted bacteria. *Nature nanotechnology* **5**, 213-217, (2010).
33 Esch, M. B., King, T. L. & Shuler, M. L. The role of body-on-a-chip devices in drug and toxicity studies. *Annual review of biomedical engineering* **13**, 55-72, (2011).
34 Service, R. F. Bioengineering. Lung-on-a-chip breathes new life into drug discovery. *Science* **338**, 731, (2012).
35 Huh, D. *et al.* Reconstituting organ-level lung functions on a chip. *Science* **328**, 1662-1668, (2010).
36 Kim, E. *et al.* Redox-capacitor to connect electrochemistry to redox-biology. *Analyst*, (2014).

37 Wu, L. Q. & Payne, G. F. Biofabrication: using biological materials and biocatalysts to construct nanostructured assemblies. *Trends in biotechnology* **22**, 593-599, (2004).
38 Yi, H. *et al.* Biofabrication with chitosan. *Biomacromolecules* **6**, 2881-2894, (2005).
39 Schauder, S., Shokat, K., Surette, M. G. & Bassler, B. L. The LuxS family of bacterial autoinducers: biosynthesis of a novel quorum-sensing signal molecule. *Molecular microbiology* **41**, 463-476, (2001).
40 Hardie, K. R. & Heurlier, K. Establishing bacterial communities by 'word of mouth': LuxS and autoinducer 2 in biofilm development. *Nature Reviews: Microbiology* **6**, 635-643, (2008).
41 Li, J. *et al.* Quorum sensing in Escherichia coli is signaled by AI-2/LsrR: effects on small RNA and biofilm architecture. *Journal of bacteriology* **189**, 6011-6020, (2007).
42 Wu, H. C. *et al.* Biofabrication of antibodies and antigens via IgG-binding domain engineered with activatable pentatyrosine pro-tag. *Biotechnology and bioengineering* **103**, 231-240, (2009).
43 Lewandowski, A. T. *et al.* Protein assembly onto patterned microfabricated devices through enzymatic activation of fusion pro-tag. *Biotechnol Bioeng* **99**, 499-507, (2008).
44 Wu, L.-Q. *et al.* Spatially Selective Deposition of a Reactive Polysaccharide Layer onto a Patterned Template. *Langmuir* **19**, 519-524, (2003).
45 Cheng, Y. *et al.* In situ quantitative visualization and characterization of chitosan electrodeposition with paired sidewall electrodes. *Soft Matter* **6**, 3177-3183, (2010).
46 Wu, L.-Q. *et al.* Voltage-dependent assembly of the polysaccharide chitosan onto an electrode surface. *Langmuir* **18**, 8620-8625, (2002).
47 Fernandes, R. *et al.* Biological nanofactories facilitate spatially selective capture and manipulation of quorum sensing bacteria in a bioMEMS device. *Lab on a Chip* **10**, 1128-1134, (2010).
48 Tsao, C. Y., Hooshangi, S., Wu, H. C., Valdes, J. J. & Bentley, W. E. Autonomous induction of recombinant proteins by minimally rewiring native quorum sensing regulon of E. coli. *Metabolic Engineering* **12**, 291-297, (2010).
49 Ellman, G. L. Tissue sulfhydryl groups. *Archives of biochemistry and biophysics* **82**, 70-77, (1959).
50 Clement, J.-L., Gilbert, B. C., Rockenbauer, A. & Tordo, P. Radical damage to proteins studied by EPR spin-trapping techniques. *Journal of the Chemical Societ , Perkin Transactions 2* **0**, 1463-1470, (2001).
51 Baker, C. J. *et al.* Induction of redox sensitive extracellular phenolics during plant–bacterial interactions. *Physiological and Molecular Plant Pathology* **66**, 90-98, (2005).
52 Martorana, A. *et al.* A spectroscopic characterization of a phenolic natural mediator in the laccase biocatalytic reaction. *Journal of Molecular Catalysis B: Enzymatic* **97**, 203-208, (2013).

53 Hilgers, M. T. & Ludwig, M. L. Crystal structure of the quorum-sensing protein LuxS reveals a catalytic metal site. *Proceedings of the National Academy of Sciences* **98**, 11169-11174, (2001).
54 Lee, J. E., Cornell, K. A., Riscoe, M. K. & Howell, P. L. Structure of E. coli 5'-methylthioadenosine/S-adenosylhomocysteine nucleosidase reveals similarity to the purine nucleoside phosphorylases. *Structure (London, England : 1993)* **9**, 941-953, (2001).
55 Dykstra, P. H., Roy, V., Byrd, C., Bentley, W. E. & Ghodssi, R. Microfluidic electrochemical sensor array for characterizing protein interactions with various functionalized surfaces. *Analytical chemistry* **83**, 5920-5927, (2011).
56 Yung, C. W. *et al.* Transglutaminase crosslinked gelatin as a tissue engineering scaffold. *Journal of biomedical materials research. Part A* **83**, 1039-1046, (2007).
57 Liu, Y. *et al.* Biofabrication to build the biology-device interface. *Biofabrication* **2**, 022002, (2010).
58 Winterbourn, C. C. & Metodiewa, D. Reactivity of biologically important thiol compounds with superoxide and hydrogen peroxide. *Free Radical Biology and Medicine* **27**, 322-328, (1999).
59 Zhu, J. *et al.* S-Ribosylhomocysteinase (LuxS) Is a Mononuclear Iron Protein†. *Biochemistry* **42**, 4717-4726, (2003).
60 Oktyabrsky, O. N. & Smirnova, G. V. Redox regulation of cellular functions. *Biochemistry. Biokhimiia* **72**, 132-145, (2007).
61 Shacter, E. Quantification and significance of protein oxidation in biological samples. *Drug metabolism reviews* **32**, 307-326, (2000).
62 Craven, G. R., Steers, E., Jr. & Anfinsen, C. B. Purification, composition, and molecular weight of the beta-galactosidase of *Escherichia coli* K12. *The Journal of biological chemistry* **240**, 2468-2477, (1965).
63 Liba, B. D. *et al.* Biofabricated film with enzymatic and redox-capacitor functionalities to harvest and store electrons. *Biofabrication* **5**, 015008, (2013).
64 Wang, Y. *et al.* Coupling electrodeposition with layer-by-layer assembly to address proteins within microfluidic channels. *Advanced materials (Deerfield Beach, Fla.)* **23**, 5817-5821, (2011).
65 Meyer, W. L. *et al.* Chitosan-coated wires: conferring electrical properties to chitosan fibers. *Biomacromolecules* **10**, 858-864, (2009).
66 Stephanopoulos, G. Synthetic Biology and Metabolic Engineering. *ACS Synthetic Biology* **1**, 514-525, (2012).
67 Callura, J. M., Cantor, C. R. & Collins, J. J. Genetic switchboard for synthetic biology applications. *Proceedings of the National Academy of Sciences* **109**, 5850-5855, (2012).
68 Nandagopal, N. & Elowitz, M. B. Synthetic Biology: Integrated Gene Circuits. *Science* **333**, 1244-1248, (2011).
69 Rapp, M., Seppala, S., Granseth, E. & von Heijne, G. Emulating membrane protein evolution by rational design. *Science* **315**, 1282-1284, (2007).
70 Bridgham, J. T., Carroll, S. M. & Thornton, J. W. Evolution of hormone-receptor complexity by molecular exploitation. *Science* **312**, 97-101, (2006).

71 Sprinzak, D. & Elowitz, M. B. Reconstruction of genetic circuits. *Nature* **438**, 443-448, (2005).
72 Hooshangi, S. & Bentley, W. E. LsrR quorum sensing "switch" is revealed by a bottom-up approach. *PLoS computational biology* **7**, e1002172, (2011).
73 Rosenfeld, N., Young, J. W., Alon, U., Swain, P. S. & Elowitz, M. B. Gene Regulation at the Single-Cell Level. *Science* **307**, 1962-1965, (2005).
74 Tsai, T. Y. *et al.* Robust, tunable biological oscillations from interlinked positive and negative feedback loops. *Science* **321**, 126-129, (2008).
75 Chuang, J. S., Rivoire, O. & Leibler, S. Simpson's paradox in a synthetic microbial system. *Science* **323**, 272-275, (2009).
76 Hong, S. H. *et al.* Synthetic quorum-sensing circuit to control consortial biofilm formation and dispersal in a microfluidic device. *Nat Commun* **3**, 613, (2012).
77 You, L., Cox, R. S., 3rd, Weiss, R. & Arnold, F. H. Programmed population control by cell-cell communication and regulated killing. *Nature* **428**, 868-871, (2004).
78 Ghim, C. M., Lee, S. K., Takayama, S. & Mitchell, R. J. The art of reporter proteins in science: past, present and future applications. *BMB reports* **43**, 451-460, (2010).
79 Bentley, W. E., Mirjalili, N., Andersen, D. C., Davis, R. H. & Kompala, D. S. Plasmid-encoded protein: the principal factor in the "metabolic burden" associated with recombinant bacteria. *Biotechnol Bioeng* **35**, 668-681, (1990).
80 Miller, J. H. *Experiments in molecular genetics*. (Cold Spring Harbor Laboratory, 1972).
81 Moon, T. S., Lou, C., Tamsir, A., Stanton, B. C. & Voigt, C. A. Genetic programs constructed from layered logic gates in single cells. *Nature* **491**, 249-253, (2012).
82 Elowitz, M. B., Levine, A. J., Siggia, E. D. & Swain, P. S. Stochastic Gene Expression in a Single Cell. *Science* **297**, 1183-1186, (2002).
83 Baldrich, E., Munoz, F. X. & Garcia-Aljaro, C. Electrochemical detection of quorum sensing signaling molecules by dual signal confirmation at microelectrode arrays. *Analytical chemistry* **83**, 2097-2103, (2011).
84 Laczka, O. *et al.* Fast electrochemical detection of anti-HIV antibodies: coupling allosteric enzymes and disk microelectrode arrays. *Analytica chimica acta* **641**, 1-6, (2009).
85 Popovtzer, R. *et al.* Novel Integrated Electrochemical Nano-Biochip for Toxicity Detection in Water. *Nano Letters* **5**, 1023-1027, (2005).
86 Cortés-Salazar, F., Beggah, S., van der Meer, J. R. & Girault, H. H. Electrochemical As(III) whole-cell based biochip sensor. *Biosensors and Bioelectronics* **47**, 237-242, (2013).
87 Chen, I. J. & White, I. M. High-sensitivity electrochemical enzyme-linked assay on a microfluidic interdigitated microelectrode. *Biosensors & bioelectronics* **26**, 4375-4381, (2011).
88 Kaya, T. *et al.* On-chip electrochemical measurement of [small beta]-galactosidase expression using a microbial chip. *Chemical Communications*, 248-249, (2004).

89 Ko, F. H. & Monbouquette, H. G. Photometric and electrochemical enzyme-multiplied assay techniques using beta-galactosidase as reporter enzyme. *Biotechnology progress* **22**, 860-865, (2006).
90 Scott, D. L., Ramanathan, S., Shi, W., Rosen, B. P. & Daunert, S. Genetically engineered bacteria: electrochemical sensing systems for antimonite and arsenite. *Analytical chemistry* **69**, 16-20, (1997).
91 Biran, I., Klimentiy, L., Hengge-Aronis, R., Ron, E. Z. & Rishpon, J. On-line monitoring of gene expression. *Microbiology* **145**, 2129-2133, (1999).
92 Schauder, S., Shokat, K., Surette, M. G. & Bassler, B. L. The LuxS family of bacterial autoinducers: biosynthesis of a novel quorum-sensing signal molecule. *Molecular microbiology* **41**, 463-476, (2001).
93 Hardie, K. R. & Heurlier, K. Establishing bacterial communities by 'word of mouth': LuxS and autoinducer 2 in biofilm development. *Nat Rev Micro* **6**, 635-643, (2008).
94 Roy, V., Adams, B. L. & Bentley, W. E. Developing next generation antimicrobials by intercepting AI-2 mediated quorum sensing. *Enzyme and microbial technology* **49**, 113-123, (2011).
95 Hebert, C. G. *et al.* Biological nanofactories target and activate epithelial cell surfaces for modulating bacterial quorum sensing and interspecies signaling. *ACS nano* **4**, 6923-6931, (2010).
96 Connell, N., Han, Z., Moreno, F. & Kolter, R. An E. coli promoter induced by the cessation of growth. *Mol Microbiol* **1**, 195-201, (1987).
97 Datsenko, K. A. & Wanner, B. L. One-step inactivation of chromosomal genes in Escherichia coli K-12 using PCR products. *Proc Natl Acad Sci U S A* **97**, 6640-6645, (2000).
98 Wang, L., Hashimoto, Y., Tsao, C. Y., Valdes, J. J. & Bentley, W. E. Cyclic AMP (cAMP) and cAMP receptor protein influence both synthesis and uptake of extracellular autoinducer 2 in Escherichia coli. *Journal of bacteriology* **187**, 2066-2076, (2005).
99 Tsao, C.-Y., Hooshangi, S., Wu, H.-C., Valdes, J. J. & Bentley, W. E. Autonomous induction of recombinant proteins by minimally rewiring native quorum sensing regulon of E. coli. *Metabolic Engineering* **12**, 291-297, (2010).
100 Juers, D. H. *et al.* Direct and indirect roles of His-418 in metal binding and in the activity of beta-galactosidase (E. coli). *Protein science : a publication of the Protein Society* **18**, 1281-1292, (2009).
101 Lo, S. *et al.* Studies of Glu-416 variants of beta-galactosidase (E. coli) show that the active site Mg(2+) is not important for structure and indicate that the main role of Mg (2+) is to mediate optimization of active site chemistry. *The protein journal* **29**, 26-31, (2010).
102 Xue, T., Zhao, L., Sun, H., Zhou, X. & Sun, B. LsrR-binding site recognition and regulatory characteristics in Escherichia coli AI-2 quorum sensing. *Cell research* **19**, 1258-1268, (2009).
103 Ha, J. H. *et al.* Crystal structures of the LsrR proteins complexed with phospho-AI-2 and two signal-interrupting analogues reveal distinct

mechanisms for ligand recognition. *Journal of the American Chemical Society* **135**, 15526-15535, (2013).
104 Alon, U. *An Introduction to Systems Biology: Design Principles of Biological Circuits*. (Chapman and Hall/CRC, 2006).
105 Fuerst, T. R., Niles, E. G., Studier, F. W. & Moss, B. Eukaryotic transient-expression system based on recombinant vaccinia virus that synthesizes bacteriophage T7 RNA polymerase. *Proc Natl Acad Sci U S A* **83**, 8122-8126, (1986).
106 Bremer, H., Dennis, P. P. in *Escherichia coli and Salmonella typhimurium: Cellular and Molecular Biology* (ed et al. Neidhardt) Ch. 97, (ASM Press, 1996).
107 Kanehisa, M. *et al.* Data, information, knowledge and principle: back to metabolism in KEGG. *Nucleic acids research* **42**, D199-205, (2014).
108 Iost, I., Guillerez, J. & Dreyfus, M. Bacteriophage T7 RNA polymerase travels far ahead of ribosomes in vivo. *J Bacteriol* **174**, 619-622, (1992).
109 Kanehisa, M. & Goto, S. KEGG: kyoto encyclopedia of genes and genomes. *Nucleic acids research* **28**, 27-30, (2000).
110 Viratelle, O. M. & Yon, J. M. Nucleophilic competition in some -galactosidase-catalyzed reactions. *European journal of biochemistry / FEBS* **33**, 110-116, (1973).
111 Santillan, M., Mackey, M. C. & Zeron, E. S. Origin of bistability in the lac Operon. *Biophysical journal* **92**, 3830-3842, (2007).
112 Li, J. *et al.* A stochastic model of Escherichia coli AI-2 quorum signal circuit reveals alternative synthesis pathways. *Molecular systems biology* **2**, 67, (2006).
113 Simpson, M. L., Sayler, G. S., Fleming, J. T. & Applegate, B. Whole-cell biocomputing. *Trends Biotechnol* **19**, 317-323, (2001).
114 Weber, W. *et al.* A synthetic mammalian electro-genetic transcription circuit. *Nucleic acids research* **37**, e33, (2009).
115 Collier, J. H. & Mrksich, M. Engineering a biospecific communication pathway between cells and electrodes. *Proceedings of the National Academy of Sciences of the United States of America* **103**, 2021-2025, (2006).
116 Jensen, H. M. *et al.* Engineering of a synthetic electron conduit in living cells. *Proceedings of the National Academy of Sciences* **107**, 19213-19218, (2010).
117 Franks, A. E. & Nevin, K. P. Microbial Fuel Cells, A Current Review. *Energies* **3**, 899, (2010).
118 Richter, H. *et al.* Electricity generation by Geobacter sulfurreducens attached to gold electrodes. *Langmuir* **24**, 4376-4379, (2008).
119 Nevin, K. P. *et al.* Power output and columbic efficiencies from biofilms of Geobacter sulfurreducens comparable to mixed community microbial fuel cells. *Environmental microbiology* **10**, 2505-2514, (2008).
120 Logan, B. E. Exoelectrogenic bacteria that power microbial fuel cells. *Nature reviews. Microbiology* **7**, 375-381, (2009).
121 Rabinowitz, J. D., Vacchino, J. F., Beeson, C. & McConnell, H. M. Potentiometric Measurement of Intracellular Redox Activity. *Journal of the American Chemical Society* **120**, 2464-2473, (1998).

122 Rabaey, K. & Rozendal, R. A. Microbial electrosynthesis — revisiting the electrical route for microbial production. *Nat Rev Micro* **8**, 706-716, (2010).
123 Lovley, D. R. Bug juice: harvesting electricity with microorganisms. *Nat Rev Micro* **4**, 497-508, (2006).
124 Hernandez, M. E. & Newman, D. K. Extracellular electron transfer. *Cellular and molecular life sciences : CMLS* **58**, 1562-1571, (2001).
125 Gralnick, J. A. & Newman, D. K. Extracellular respiration. *Molecular microbiology* **65**, 1-11, (2007).
126 Alferov, S. *et al.* Electrical communication of cytochrome enriched Escherichia coli JM109 cells with graphite electrodes. *Electrochimica Acta* **54**, 4979-4984, (2009).
127 Bennett, M. R. & Hasty, J. Microfluidic devices for measuring gene network dynamics in single cells. *Nat Rev Genet* **10**, 628-638, (2009).
128 Bennett, M. R. *et al.* Metabolic gene regulation in a dynamically changing environment. *Nature* **454**, 1119-1122, (2008).
129 Mettetal, J. T., Muzzey, D., Gómez-Uribe, C. & van Oudenaarden, A. The Frequency Dependence of Osmo-Adaptation in Saccharomyces cerevisiae. *Science* **319**, 482-484, (2008).
130 Uhlendorf, J. *et al.* Long-term model predictive control of gene expression at the population and single-cell levels. *Proceedings of the National Academy of Sciences* **109**, 14271-14276, (2012).
131 Gardner, L. & Deiters, A. Light-controlled synthetic gene circuits. *Current Opinion in Chemical Biology* **16**, 292-299, (2012).
132 Milias-Argeitis, A. *et al.* In silico feedback for in vivo regulation of a gene expression circuit. *Nat Biotech* **29**, 1114-1116, (2011).
133 Olson, E. J., Hartsough, L. A., Landry, B. P., Shroff, R. & Tabor, J. J. Characterizing bacterial gene circuit dynamics with optically programmed gene expression signals. *Nat Meth* **11**, 449-455, (2014).
134 Wang, X., Chen, X. & Yang, Y. Spatiotemporal control of gene expression by a light-switchable transgene system. *Nat Meth* **9**, 266-269, (2012).
135 Ye, H., Baba, M. D.-E., Peng, R.-W. & Fussenegger, M. A Synthetic Optogenetic Transcription Device Enhances Blood-Glucose Homeostasis in Mice. *Science* **332**, 1565-1568, (2011).
136 Levskaya, A. *et al.* Synthetic biology: engineering Escherichia coli to see light. *Nature* **438**, 441-442, (2005).
137 Schmidl, S. R., Sheth, R. U., Wu, A. & Tabor, J. J. Refactoring and optimization of light-switchable escherichia coli two-component systems. *ACS Synth Biol* **3**, 820-831, (2014).
138 Yarkoni, O., Donlon, L. & Frankel, D. Creating a bio-hybrid signal transduction pathway: opening a new channel of communication between cells and machines. *Bioinspiration & Biomimetics* **7**, 046017, (2012).
139 Folcher, M. *et al.* Mind-controlled transgene expression by a wireless-powered optogenetic designer cell implant. *Nat Commun* **5**, (2014).
140 Stanley, S. A. *et al.* Radio-Wave Heating of Iron Oxide Nanoparticles Can Regulate Plasma Glucose in Mice. *Science* **336**, 604-608, (2012).

141 Isaksson, J. *et al.* Electronic control of Ca2+ signalling in neuronal cells using an organic electronic ion pump. *Nat Mater* **6**, 673-679, (2007).
142 Cabiscol, E., Tamarit, J. & Ros, J. Oxidative stress in bacteria and protein damage by reactive oxygen species. *International microbiology : the official journal of the Spanish Society for Microbiology* **3**, 3-8, (2000).
143 Pomposiello, P. J. & Demple, B. Redox-operated genetic switches: the SoxR and OxyR transcription factors. *Trends Biotechnol* **19**, 109-114, (2001).
144 Gu, M. & Imlay, J. A. The SoxRS response of Escherichia coli is directly activated by redox-cycling drugs rather than by superoxide. *Mol Microbiol* **79**, 1136-1150, (2011).
145 Price-Whelan, A., Dietrich, L. E. & Newman, D. K. Pyocyanin alters redox homeostasis and carbon flux through central metabolic pathways in Pseudomonas aeruginosa PA14. *J Bacteriol* **189**, 6372-6381, (2007).
146 Hassett, D. J., Charniga, L., Bean, K., Ohman, D. E. & Cohen, M. S. Response of Pseudomonas aeruginosa to pyocyanin: mechanisms of resistance, antioxidant defenses, and demonstration of a manganese-cofactored superoxide dismutase. *Infection and immunity* **60**, 328-336, (1992).
147 Hassan, H. M. & Fridovich, I. Mechanism of the antibiotic action pyocyanine. *Journal of bacteriology* **141**, 156-163, (1980).
148 Hassan, H. M. & Fridovich, I. Intracellular production of superoxide radical and of hydrogen peroxide by redox active compounds. *Arch Biochem Biophys* **196**, 385-395, (1979).
149 Rabaey, K., Boon, N., Hofte, M. & Verstraete, W. Microbial phenazine production enhances electron transfer in biofuel cells. *Environmental science & technology* **39**, 3401-3408, (2005).
150 Kim, E., Gordonov, T., Bentley, W. E. & Payne, G. F. Amplified and in situ detection of redox-active metabolite using a biobased redox capacitor. *Analytical chemistry* **85**, 2102-2108, (2013).
151 Demple, B., Ding, H. & Jorgensen, M. Escherichia coli SoxR protein: sensor/transducer of oxidative stress and nitric oxide. *Methods in enzymology* **348**, 355-364, (2002).
152 Hidalgo, E., Leautaud, V. & Demple, B. The redox-regulated SoxR protein acts from a single DNA site as a repressor and an allosteric activator. *The EMBO Journal* **17**, 2629-2636, (1998).
153 Pomposiello, P. J., Bennik, M. H. & Demple, B. Genome-wide transcriptional profiling of the Escherichia coli responses to superoxide stress and sodium salicylate. *J Bacteriol* **183**, 3890-3902, (2001).
154 Tsaneva, I. R. & Weiss, B. soxR, a locus governing a superoxide response regulon in Escherichia coli K-12. *J Bacteriol* **172**, 4197-4205, (1990).
155 Singh, A. K., Shin, J. H., Lee, K. L., Imlay, J. A. & Roe, J. H. Comparative study of SoxR activation by redox-active compounds. *Mol Microbiol* **90**, 983-996, (2013).
156 Koo, M. S. *et al.* A reducing system of the superoxide sensor SoxR in Escherichia coli. *EMBO J* **22**, 2614-2622, (2003).

157 Wang, Y. & Newman, D. K. Redox Reactions of Phenazine Antibiotics with Ferric (Hydr)oxides and Molecular Oxygen. *Environmental science & technology* **42**, 2380-2386, (2008).
158 Gunsalus, R. P. Control of electron flow in Escherichia coli: coordinated transcription of respiratory pathway genes. *Journal of bacteriology* **174**, 7069-7074, (1992).
159 Unden, G. & Bongaerts, J. Alternative respiratory pathways of Escherichia coli: energetics and transcriptional regulation in response to electron acceptors. *Biochimica et biophysica acta* **1320**, 217-234, (1997).
160 Ingledew, W. J. & Poole, R. K. The respiratory chains of Escherichia coli. *Microbiological reviews* **48**, 222-271, (1984).
161 Stewart, V. Nitrate regulation of anaerobic respiratory gene expression in Escherichia coli. *Mol Microbiol* **9**, 425-434, (1993).
162 Trotter, E. W. *et al.* Reprogramming of Escherichia coli K-12 metabolism during the initial phase of transition from an anaerobic to a micro-aerobic environment. *PloS one* **6**, e25501, (2011).
163 Clark, D. P. The fermentation pathways of Escherichia coli. *FEMS microbiology reviews* **5**, 223-234, (1989).
164 O'Reilly, J. E. Oxidation-reduction potential of the ferro-ferricyanide system in buffer solutions. *Biochimica et Biophysica Acta (BBA) - Bioenergetics* **292**, 509-515, (1973).
165 Liu, C., Yong, D., Yu, D. & Dong, S. Cell-based biosensor for measurement of phenol and nitrophenols toxicity. *Talanta* **84**, 766-770, (2011).
166 Morris, K., Zhao, H. & John, R. Ferricyanide-Mediated Microbial Reactions for Environmental Monitoring. *Australian Journal of Chemistry* **58**, 237-245, (2005).
167 Pasco, N., Baronian, K., Jeffries, C. & Hay, J. Biochemical mediator demand – a novel rapid alternative for measuring biochemical oxygen demand. *Appl Microbiol Biotechnol* **53**, 613-618, (2000).
168 Morris, K., Catterall, K., Zhao, H., Pasco, N. & John, R. Ferricyanide mediated biochemical oxygen demand – development of a rapid biochemical oxygen demand assay. *Analytica chimica acta* **442**, 129-139, (2001).
169 Catterall, K., Robertson, D., Teasdale, P. R., Welsh, D. T. & John, R. Evaluating use of ferricyanide-mediated respiration bioassays to quantify stimulatory and inhibitory effects on Escherichia coli populations. *Talanta* **80**, 1980-1985, (2010).
170 Du, Z., Li, H. & Gu, T. A state of the art review on microbial fuel cells: A promising technology for wastewater treatment and bioenergy. *Biotechnology Advances* **25**, 464-482, (2007).
171 Boonstra, J., Sips, H. J. & Konings, W. N. Active transport by membrane vesicles from anaerobically grown Escherichia coli energized by electron transfer to ferricyanide and chlorate. *European journal of biochemistry / FEBS* **69**, 35-44, (1976).

172 Oktyabrsky, O. N., Smirnova, G. V. & Kuznetsova, E. V. Ferricyanide reduction by Escherichia coli cells: Probable contribution of low molecular weight thiols. *Bioelectrochemistry and Bioenergetics* **32**, 267-275, (1993).
173 Hadjipetrou, L. P., Gray-Young, T. & Lilly, M. D. Effect of Ferricyanide on Energy Production by Escherichia coli. *Journal of General Microbiology* **45**, 479-488, (1966).
174 Emde, R., Swain, A. & Schink, B. Anaerobic oxidation of glycerol by Escherichia coli in an amperometric poised-potential culture system. *Appl Microbiol Biotechnol* **32**, 170-175, (1989).
175 Hadjipetrou, L., Lilly, M. D. & Kourounakis, P. Effect of ferricyanide onEscherichia coli. *Antonie van Leeuwenhoek* **36**, 531-540, (1970).
176 Tsien, R. Y. The green fluorescent protein. *Annual review of biochemistry* **67**, 509-544, (1998).
177 Christie, J. M. *et al.* Structural Tuning of the Fluorescent Protein iLOV for Improved Photostability. *The Journal of biological chemistry* **287**, 22295-22304, (2012).
178 Swartz, T. E. *et al.* The photocycle of a flavin-binding domain of the blue light photoreceptor phototropin. *The Journal of biological chemistry* **276**, 36493-36500, (2001).
179 Keiler, K. C., Waller, P. R. H. & Sauer, R. T. Role of a Peptide Tagging System in Degradation of Proteins Synthesized from Damaged Messenger RNA. *Science* **271**, 990-993, (1996).
180 Andersen, J. B. *et al.* New unstable variants of green fluorescent protein for studies of transient gene expression in bacteria. *Applied and environmental microbiology* **64**, 2240-2246, (1998).
181 Stricker, J. *et al.* A fast, robust and tunable synthetic gene oscillator. *Nature* **456**, 516-519, (2008).
182 Danino, T., Mondragon-Palomino, O., Tsimring, L. & Hasty, J. A synchronized quorum of genetic clocks. *Nature* **463**, 326-330, (2010).
183 Greenberg, J. T., Monach, P., Chou, J. H., Josephy, P. D. & Demple, B. Positive control of a global antioxidant defense regulon activated by superoxide-generating agents in Escherichia coli. *Proc Natl Acad Sci U S A* **87**, 6181-6185, (1990).
184 Farr, S. B., D'Ari, R. & Touati, D. Oxygen-dependent mutagenesis in Escherichia coli lacking superoxide dismutase. *Proceedings of the National Academy of Sciences of the United States of America* **83**, 8268-8272, (1986).
185 Sambrook J.C., F. E. F., Maniatis T. *Molecular Cloning: A Laboratory Manual*. (Cold Spring Harbor Laboratory Press, 2000).
186 Gibson, D. G. *et al.* Enzymatic assembly of DNA molecules up to several hundred kilobases. *Nature methods* **6**, 343-345, (2009).
187 Baker, M. D., Wolanin, P. M. & Stock, J. B. Signal transduction in bacterial chemotaxis. *BioEssays : news and reviews in molecular, cellular and developmental biology* **28**, 9-22, (2006).
188 Miller, M. B. & Bassler, B. L. Quorum sensing in bacteria. *Annual review of microbiology* **55**, 165-199, (2001).